
UNIVERSITATEA
MARITIMA
CONSTANTA

ISSN 1844-6116

ISSN (Print): 1844-6116
ISSN (Online): 2501-8795 http://www.cmu-edu.eu/jmte

Journal of Marine technology and Environment Year 2017, Vol.1

This Journal has been founded in 2008 as a biannual publication of
Constanta Maritime University/ROMANIA

TOPICS

- Marine Science and Engineering
- Marine Environmental Issues
- Marine Renewable Energy and Sustainability
- Maritime Safety
- Marine Chemistry
- Marine Corrosion and Material Science
- Ship Design, Building Technologies
- Ocean Engineering
- Advanced Technologies for MET
- Advances in numerical methods for marine engineering
- Algorithms for multidisciplinary problems in marine engineering
- Other related topics

JOURNAL ADDRESS
Journal of Marine Technology and Environment
Constanta Maritime University, 104, Mircea cel Batran Street, 900663, Constanta, Romania
Tel: +40 241 664 740/ 107
Fax: +40 241 617 260
E-mail: jmte@cmu-edu.eu
http://cmu-edu.eu/jmte/

EDITURA NAUTICA
Constanta Maritime University
CONSTANTA MARITIME UNIVERSITY, 104, MIRCEA CEL BATRAN STREET, 900663,

CONSTANTA, ROMANIA

CONTENTS

ISSN (Print): 1844-6116
ISSN (Online): 2501-8795 http://www.cmu-edu.eu/jmte

Journal of Marine technology and Environment Year 2017, Vol.1

ESTIMATED PROPULSION OF SMALL SCALE HYDROFOIL SHIPS

Beazit Ali[1], Adrian Popa[1], Gheorghe Ichimoaei[1] & Levent Ali[2]

[1]Marine Engineering and Naval Weapons Department, "Mircea cel Batan" Naval Academy, Constanţa, Romania, e-mail: ali.beazit@yahoo.com, [2]Bureau Veritas Romania Controle International, Romania

Abstract : This paper presents an original procedure for estimating the propulsion of small scale hydrofoil ships. This procedure has enabled the development of a computer program that can predict both those types of ship propulsion regime imposed at a quasi-stationary speed and the march regime on wings. The calculation software obtained may serve to design any type of hydrofoil ship. The input data are read in a network that has access throughout the development of the program. In the end, the program outlines for the two march regimes of the ship which the study has been carried on, the drag resistance curve depending on the speed.

Keywords: hydrofoil, propulsion, regime, scale, speed, wing.

1. MOVEMENT REGIMES OF HYDROFOIL SHIPS

Conventionally, ship movement on the wings is divided into the following regimes (Figure.1):
- the floating regime corresponding to the movement of the hull through the water when the wings' electromagnetic force is still reduced due to low speed. This regime continues up to speed v_1, where the fore of the ship comes out of the water;
- the quasi-stationary regime at imposed speed corresponding to the movement of the ship between speed and velocity v_1 and speed v_0 at which the hull detaches from the sea;
- the displacement system on the wings which corresponds to the movement of the ship at marching speeds greater than v_0 and it is characterized by the minimum drag resistance when the speed becomes maximum, v. The increase of speed is explained by the fact that the drag of the wing is smaller than the drag of the hull.

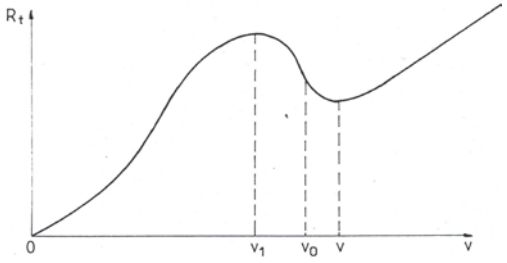

Figure 1 Conventionally ship movement on the wings

In the Figures below 2, 3 and 4, it has been represented the hull of the floating ship, the quasi-stationary regime on imposed speed and respectively the travel arrangements on wings.

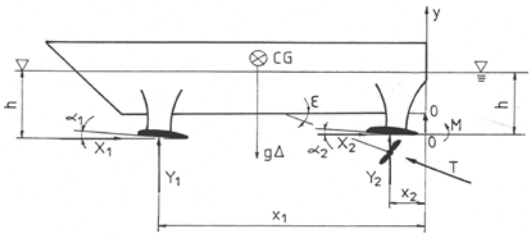

Figure 2 The hull of the floating ship

ISSN (Print): 1844-6116
ISSN (Online): 2501-8795
http://www.cmu-edu.eu/jmte

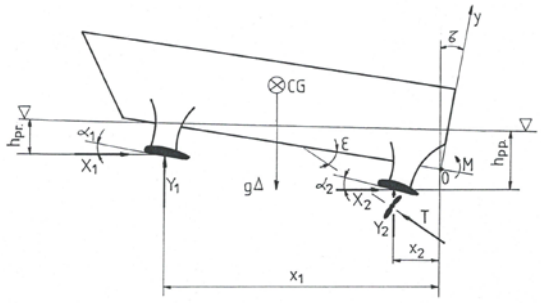

Figure 3 The quasi-stationary regime on imposed speed

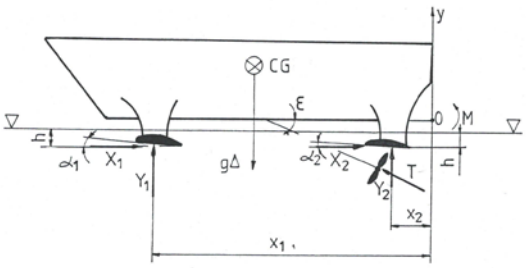

Figure 4 The travel arrangements on wings

In either of the travel arrangements of the ship, it is necessary to meet the balance of the equations:

$$\sum F_x = 0; \quad \sum F_y = 0 \; ; \quad \sum M_0 = 0 \; . \; (1); \; (2); \; (3)$$

2. ORIGINAL ASSUMPTIONS TO HYDROFOIL SHIP MODELLING MOVEMENTS

To modelling the hydrofoil ship movement, the following assumptions are made:

1 – The ship is proceeding in deep and calm water at a constant speed.

2 – The wave and current from the hydrofoil fore is calculated so that the correction $\Delta\alpha$ of the stern hydrofoil carrying capacity is neglected.

3 – The adherent mass of the ship and the depreciation are neglected, so that the movement of the ship on hydrofoil, the amount of the hydrofoil carrying capacity equals the weight of the ship.

4 – The bearing forces from the appendix (uprights) and of the shaft are neglected.

5 - The ship is equipped only with fore and aft carrying capacity of the wings thus not having stabilizing wings.

3. BALLANCE EQUATIONS

Following figures 2, 3 and 4, it appears that the balance of forces is achieved if the following three conditions (a, b and c) are met:

a) $\sum_1^6 F_x = 0$; the horizontally thrust projection of the propeller = drag resistance

$$T\cos(\tau+\varepsilon) = X_1 + X_2 + X_{apend}\,, \tag{4}$$

$$T\cos(\tau+\varepsilon) = \sum_1^6 \frac{1}{2}\cdot\rho\cdot v^2\cdot c_{xi}\cdot S_i\,; \tag{5}$$

where:

X_1 – drag resistance of a fore wing;

X_2 - drag resistance of a aft wing;

X_{apend} = X_3 + X_4 + X_5 + X_6 - the amount of drag resistance of uprights fore wings (X_3, X_4) and of uprights aft wings (X_5, X_6);

T – propeller thrust;

τ - longitudinal trim angle;

ε - the angle of the propeller shaft.

b) $\sum_1^2 F_y = 0$; sum of wings' carrying capacity = weight of ship

$$Y_1 + Y_2 + T\sin(\tau+\varepsilon) = g\cdot\Delta\,, \tag{6}$$

$$c_{y1}\cdot S_1\cdot\frac{\rho\cdot v^2}{2} + c_{y2.}\cdot S_2\cdot\frac{\rho\cdot v^2}{2} + T\sin(\tau+\varepsilon) = g\cdot\Delta\,, \tag{7}$$

where:

Y_1, Y_2 - fore wing respectively aft carrying capacity;

$g\cdot\Delta$ - weight of hydrofoil boats;

S_1, S_2 - surface area of the aft respectively fore wing;

c_{y1}, c_{y2} - carrying capacity of coefficient of the fore respectively aft wing;

v - ship speed;

ρ - water density.

c) $\sum M_0 = 0$; the moments are taken around the point 0 in Figures 2, 3 and 4.

$$\begin{aligned} &c_{y1}\cdot S_1\cdot\frac{\rho\cdot v^2}{2}\cdot(x_1 - y_1\sin\tau) + c_{y2}\cdot S_2\cdot\frac{\rho\cdot v^2}{2}\cdot(x_2 - y_2\sin\tau)\pm \\ &c_{x1}\cdot S_1\cdot\frac{\rho\cdot v^2}{2}\cdot(x_1\sin\tau + y_1)\pm c_{x2}\cdot S_2\cdot\frac{\rho\cdot v^2}{2}\cdot(x_2\sin\tau + y_2) - \\ &g\cdot\Delta(x_g - y_g\sin\tau) + T\cdot l_p = 0 \end{aligned} \tag{8}$$

where:

x_1, x_2 - the x abscissa of buoyancy or drag resistance of the aft respectively fore wing;

ISSN (Print): 1844-6116
ISSN (Online): 2501-8795 http://www.cmu-edu.eu/jmte

y_1 y_2 - the ordered of buoyancy or drag resistance of the aft respectively fore wing;

x_g - abscissa of the ship's centre of gravity;

y_g - ordered of the ship's centre of gravity;

l_p - distance from the centre point propeller 0;

c_{x1}, c_{x2} - drag resistance coefficient of the aft respectively fore wing.

c_{y1}, c_{y2} - the carrying capacity of the aft respectively fore wing coefficient; the ± sign in equation (8) represents the possible situation, encountered when the stern and trim immersion locates the centre of the moments under the place of the carrying capacity of the hydrofoil fore, thus resulting in a change of sign moments.

In order to settle these balanced relations, we shall make the following two assumptions:

I - The drag resistance of the wings and uprights is constant. This means that the ship has a longitudinal trim.

II - We introduce into the scheme for computing the longitudinal trim of the ship and hydrofoil immersion.

This requires an iterative solution or computer graphics.

For the carrying capacity and the drag resistance of a wing, we can write:

$$Y = F_{y-wing} = \frac{1}{2} \cdot \rho \cdot v^2 \cdot S \cdot c_y(\alpha, \frac{h}{c}), \quad (9)$$

$$X = F_{x-wing} = \frac{1}{2} \cdot \rho \cdot v^2 \cdot S \cdot c_x(\alpha, \frac{h}{c}). \quad (10)$$

- resistance to drag of the hull R_c ;

- ship weight $g \cdot \Delta$;

- coordinates the gravity centre of the ship x_g , y_g ;

- h position fore and aft of the wings measured from the keel h_1, h_2;

- wings' fore and aft dimensions and of their uprights (string c_i, scale l_i);

- fore and aft wing angle of attack α;

- longitudinal trim angle τ ;

- inclination angle of the propeller shaft ε ;

- E.H.P power of propulsion machinery;

- speed propeller n ;

- the maximum speed of the ship in displacement mode v_p ;

- maximum speed of ship v on hydrofoil;

- carrying capacity system.

In the specialized literature, there are theoretical and analytical results on experimental hydrofoil ships. These results are often synthesized in the form of graphics so they can be used to design.

From the equation (13), it is clear that, in order to compute the hydrofoil drag of the ship in the quasi-stationary regime, it is necessary to estimate the behaviour of a group of hydroglider to a range of displacements $0 < \Delta^* < \Delta$. The experimental results obtained in the study concerning a hydroglider ship were summarized in three graphs shown in Figure 5, namely:

$c_R = f(Fr); \tau = f(Fr)$ and $\bar{y} = f(Fr)$,

where:

Fr - Froude number of width;

c_R - drag coefficient of the body;

τ - longitudinal trim angle of the ship;

$\bar{y}$ - stern relative immersion.

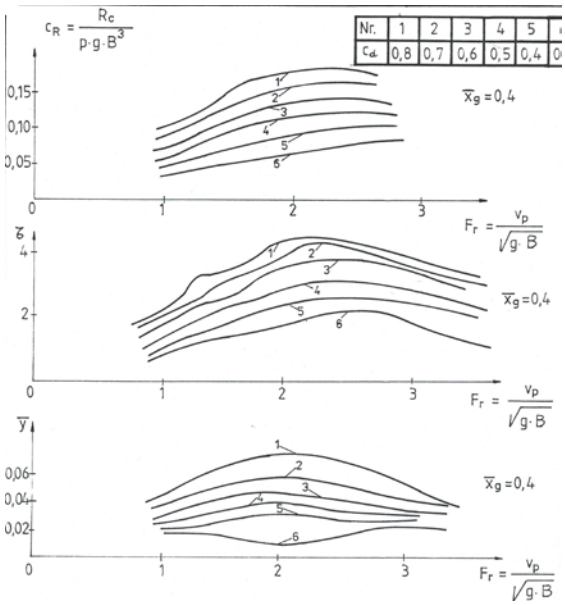

Figure 5 The experimental results

The three graphs were raised to the same abscissa value relative to the centre of gravity $\bar{x}_g$ and for several values of the load factor c_d .

In conclusion, we can write the following relations:

$$c_R = \frac{R_c}{\frac{1}{2} \cdot \rho \cdot g \cdot B^3} = f(Fr, c_d, \bar{x}_g); \quad (14)$$

$$\tau = f(Fr, c_d, \bar{x}_g), \quad (15)$$

$$\bar{y} = \frac{y_k}{L} = f(Fr, c_d, \bar{x}_g), \quad (16)$$

where:

ISSN (Print): 1844-6116
ISSN (Online): 2501-8795
http://www.cmu-edu.eu/jmte

$$Fr = \frac{v_p}{\sqrt{g \cdot B}} \quad (17)$$

$$c_d = \frac{g \cdot \Delta}{\rho \cdot g \cdot B^3}, \quad (18)$$

$$\overline{x_g} = \frac{X_g}{L}; \quad (19)$$

y_k – stern immersion.

Furthermore, for this study we shall also use the variation curves of the bearing capacity coefficient c_y and the drag resistance coefficient c_x of the wing depending on the angle of incidence α for a range of values of the relative immersion wings h, comprised between 0,1 şi 1,5.

Thus:

$$c_y = f(\alpha, \bar{h}) \Rightarrow \text{fig. 6.a.} \quad (20)$$

$$c_x = f(\alpha, \bar{h}) \Rightarrow \text{fig. 6.b,} \quad (21)$$

where: $\bar{h} = \frac{h}{c}$ - immersion of the relative wing; h - immersion wing; c - wing chord.

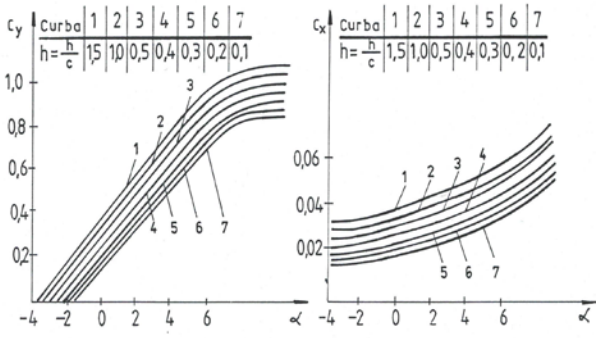

Figure 6a Figure 6b

The dependence $c_y = f(\alpha, \bar{h})$ The dependence $c_x = f(\alpha, \bar{h})$

For the settlement of the equilibrium equations (5), (7) and (8), a graphical procedure could be used too. To this end, it is necessary to settle the equation (7). In this equation, the thrust T is replaced with the one produced from the relationship (5) and then with the one obtained from the relationship (8), resulting in the following two equations denoted as $\sum_1$ and $\sum_2$.

$$\sum\nolimits_1 = c_{y1} \cdot S_1 \cdot \frac{\rho \cdot v^2}{2} + c_{y2} \cdot S_2 \cdot \frac{\rho \cdot v^2}{2} + \sum_i^6 \frac{1}{2} \cdot \rho \cdot v^2 \cdot c_{xi} \cdot S_i \cdot tg(\tau + \varepsilon) = g \cdot \Delta \quad (22)$$

$$\sum\nolimits_2 = c_{y1} \cdot S_1 \cdot \frac{\rho \cdot v^2}{2} \cdot (x_1 - y_1 \sin\tau) \cdot \frac{\cos(\tau + \varepsilon)}{l_p} + c_{y2} \cdot S_2 \cdot \frac{\rho \cdot v^2}{2} (x_2 - y_2 \sin\tau) \frac{\cos(\tau + \varepsilon)}{l_p} \pm \pm c_{x2} \cdot S_2 \cdot (x_2 \sin\tau + y_2) + \frac{l_p}{\cos(\tau + \varepsilon)} \cdot \sum_i^6 c_{xi} \cdot S_i = = \frac{2g \cdot \Delta \cdot (x_g - y_g \cdot \sin\tau)}{\rho \cdot v^2} \quad (23)$$

Through this method it can be provided the simultaneous settlement of the equations (22) and (23) obtaining thus y and τ for a value of v. The settlement by the graphic form has allowed the development of a computer program.

5. CONCLUSIONS

The input data are read in a network that has access throughout the development of the program. Using the entry data of the computation program for the quasi-stationary regime it determines the fore and aft hydrofoil immersion and it assists the c_x and c_y coefficients c_M and the hydrofoil interpolated based on immersion of wings and the trim angle τ. The values $\sum_{1a}$ and $\sum_{1b}$, $\sum_{2a}$ and $\sum_{2b}$ are computed to determine the adjustment points corresponding to the y and for each value of v.

This calculation is continued until the body is marching on the wings (Δ^* = 0 in the equation.13).

The computation program of the hydrofoil buoyancy system starts with the reading of the input data.

The buoyancy coefficients c_y and of the drag resistance c_x are read into a network, and the trim angle is obtained from the equations of balance.

By means of the trim angle τ the buoyancy and drag resistance of the wings and uprights can be computed.

In the end, the program outlines for the two march regimes of the ship which the study has been carried on, the drag resistance curve depending on the speed, $R = f(v)$, like in Figure 1. In addition, with this program the stall speed of the ship, that is the speed at which the ship hull completely comes out of the water, can be determined.

We can estimate that in this way we have developed a design methodology of hydrofoil ships on the existing data.

The synthesis of data on the ship's hull and hydrofoil enables the design of computations for ship operations on quasi-stationary regime and on the hydrofoil march regime. The computation program has been carried out in AUTOCAD.

6. REFERANCES

[1] LATORE R.–*Development of Hydrofoil Resistance Calculation Program* UNO-HYFI, Proceeding International Symposium on Ship Resistance and Powering Performance , Shanghai, 1989.
[2] LATORE R.– *Small Craft Design*, NAME 4151; Informal Notes, School of Naval Architecture and Marine Engineering, University of New Orleans, 1984.
[3] ZAITSEV N. A., MASKALIC A.I. – *Soviet Hydrofoil Craft*, Sudostroyenyie Publishing House, Leningrad, 1967.
[4] YEGOROV J.I., SOKOLOV V.T. – *The Hydrodynamics of High Speed Craft*, Sudostroyenyie Publishing House, Leningrad, 1971.
[5] ALI B. – *Performance Calculation of hydrofoil craft*, A XV- a Scientific Communication sessions of Teachers, "Mircea cel Bătrân" Naval Academy Constanta, 1997.

ISSN (Print): 1844-6116
ISSN (Online): 2501-8795 http://www.cmu-edu.eu/jmte

ISSN (Print): 1844-6116
ISSN (Online): 2501-8795 http://www.cmu-edu.eu/jmte

Journal of Marine technology and Environment Year 2017, Vol.1

HIGH PERFORMANCE CONTROLLABLE PITCH PROPELLERS

Beazit Ali[1], Adrian Popa[1], Gheorghe Iachimoaei[1] & Levent Ali[2]

[1]Marine Engineering and Naval Weapons Department, "Mircea cel Batan" Naval Academy, Constanta, Romania, e-mail: ali.beazit@yahoo.com, [2]Bureau Veritas Romania Controle International, Romania

Abstract: In order to maximize the design of the Controllable Pitch Propellers for low acoustic signature is necessary to analyse more aspects the general features of propeller and the effect of air emission, the effect of cavitation by using different computer programme which can stimulate a lot of parameters developed on the model on scale and on the full scale model. The result made possible a new way for improvement of design techniques to obtain more and more less noisly Controllable Pitch Propellers.

Keywords**:** air emission, blade geometry, cavitation, propeller, pitch, ship propulsion.

1. INTRODUCTION. GENERAL FEATURES OF THE CONTROLLABLE PITCH PROPELLERS SYSTEM

VA TECH Escher Wyss has delivered or has on order complete propeller systems for five different MEKO® Class Frigates for four different end users. All of these systems are equipped with shaft line mounted actuating units. Four of these sets have an air emission system with the air inlet box being located at the forward end of the gearbox.

Figure 1 Escher Wyss Controllable Pitch Propellers with calculated streamlines

2. BLADE BEARING SYSTEM

Escher Wyss Controllable Pitch Propellers are commonly known for their unique type of blade fastening. The Escher Wyss hubs of the trunnion bearing type with blades and trunnions cast in one piece are especially applicable for naval vessels, see Figure 2 (below). This design delivers the following beneficial features:

• By eliminating blade bolts, the flow in the blade palm area is smooth which reduces the vortex formation and delays cavitation inception. With bolted-on blades, the bolt heads and the pockets in the blade root constitute flow obstacles which can contribute to early inception of cavitation.

• The number of propeller blades can be increased up to seven with an acceptable low hub ratio (approx. 32%).

3. HUB SHAPE

The hub shape has been developed in order to achieve a minimum hub resistance and a high inception speed of the hub vortex cavitation. Cavitation predictions in the model scale as well as full scale viewings

ISSN (Print): 1844-6116
ISSN (Online): 2501-8795 http://www.cmu-edu.eu/jmte

confirmed that, for this type of hub shape, hub vortex cavitation is not present during a straight ahead course. During the full scale viewings, such vortex cavitation could only be observed at extreme propeller loadings in the manoeuvring mode.

4. AIR EMISSION

Emitting air (see Figure 2), can reduce or eliminate the increase of the noise levels associated with cavitation inception at the higher frequency range. The emission of air is also effective at ship speeds with developed cavitation. The large number of delivered propellers with air emission systems for naval vessels is proof that the benefits of this system are highly appreciated. Up to date, any detrimental impact of the air emission on the propeller efficiency could not be verified during the sea trials (and is impossible to detect in model scale). No erosion damages around the blade air emission holes have ever been discovered.

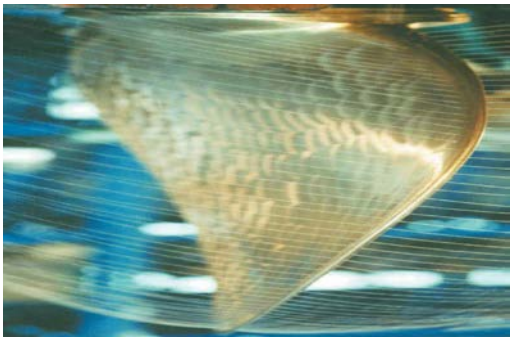

Figure 2 Air emission test with water

5. DEVELOPMENT OF THE BLADE DESIGN

By making immediate use of the rapid progress in computer technology of the past 25 years, VA TECH Escher Wyss was able to optimize the blade designs on computer screens. At present VA TECH Escher Wyss is able to adapt a blade design completely to the given design conditions by calculation, prior to verifying the design by model tests. The major progress consists of the ability to control the blade design's cavitation behaviour and thus increase the cavitation free ship's speed without sacrificing propeller efficiency. However, although the present design tools, as well as the analytical procedures enable the propeller designer to optimize the blade geometry, the hull and appendages ahead of the propeller regulate the limits for a successful blade design. Therefore, if a quiet propeller is required, the ship's hull and appendages must be appropriately designed and fabricated.

6. WAKE DATA PROCESSING. 3D-WAKE SURVEY

For the adaptation of the blade design to the given wake field, an experimental 3D-Wake Survey is necessary. The blade designer is able to optimize the blade geometry locally after access to all three velocity components in the propeller plane.

Usually, navy vessels are twin screw vessels whose wake field typically looks like the one illustrated in Figure 3. The wake survey report of the model basin comprises, as a standard, the plot of the transversal components (top plate) as well as the axial velocity isolines (bottom plate). The wake peak due to the propeller shaft is clearly visible as well as the spikes created by the struts. An illustrative presentation of the "wake peak" shows the mountain in the middle of the plot where the region of reduced axial velocities are readily visible as a groove.

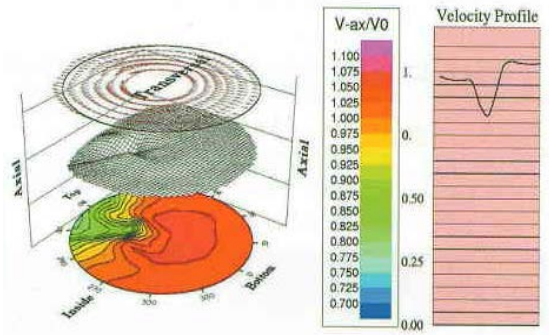

Figure 3 Typical 3D wake of a twin screw navy vessel

7. WAKE ADAPTION OF THE BLADE DESIGN. BLADE TIP AND BLADE SURFACE

The wake adaptation of a blade design consists of step by step modifications to the blade geometry and to the subsequent cavitation calculations. Though VA TECH Escher Wyss has developed strategies for the wake adaptation of ship propellers, a sizable number of

ISSN (Print): 1844-6116
ISSN (Online): 2501-8795 http://www.cmu-edu.eu/jmte

calculation loops remain necessary to reach a satisfactory status.

When considering blade geometry, the cavity volumes and cavitation extension are calculated with the program system PUF-3A, which was originally developed by the M.I.T., Cambridge, Massachusetts and has been continuously updated by the University of Texas in Austin, USA. PUF-3A calculates - for a given wake field and blade geometry - the surface pressure on a large number of panels on the blade surface, and, based on sophisticated criteria (not only the vapour pressure), determines whether cavitation will take place at this panel. From the surface pressures on the suction side and pressure side, mean values as well as the fluctuations of the forces and moments for the cavitating and non-cavitating case are computed. The pressure pulses on a given hull can be calculated by means of the utility program HULLFPP (another M.I.T. product).

The present design-tool PUF-3A is based on a potential theory technique, which does not allow the prediction of the tip vortex structure and the complex processes in the vortex.

8. DEVELOPED CAVITATION

The large differences between the calculated developed cavitation and the calculated incipient cavitation in the chordwise extension, as well as in the cavity volumes, require different post-processing techniques. In order to visualize the developed cavitation, VA TECH Escher Wyss has implemented a rendering program which superimposes the calculated cavitation as well as the surface pressures on the three-dimensional blade surface, as illustrated in Figure 4. With decreasing pressure the colour changes from blue to red. The suction side sheet cavitation is depicted in pink in order to distinguish between the regions of low pressure from those regions in which the program predicts cavitation. On the back, where a low pressure area has been calculated, the cavitation inception criterion of the program is not satisfied. Nevertheless, by experience, mid-chord bubble cavitation has to be expected.

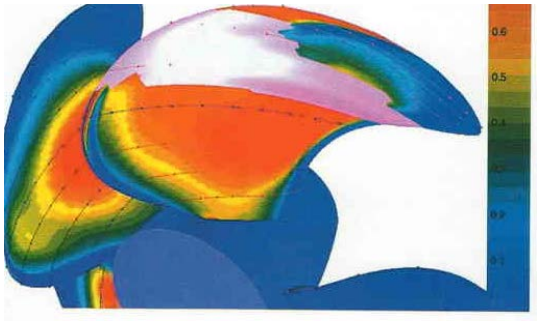

Figure 4 Calculated developed cavitation (PUF-3A)

9. INCIPIENT CAVITATION

Cavitation inception is crucial for the noise signature of a vessel's propeller, and for this necessitates a precise determination of the first indication of cavitation. In order to depict the few cavitating panels which have only a small chord wise extension of cavitation, a specific kind of presentation is needed. Figure 5 shows a typical plot of incipient cavitation that is characterized by a small angular sector in the vicinity of the top position of the blade where the cavitation occurs, and by the restricted radial extension.

The colour scale facilitates the identification of the chord wise extension of the cavitation sheet. In comparing the cavitation extension as calculated in this manner with full scale viewings, it has been found that calculated sheet lengths up to 1% chord length seem to vanish in an uncertainty range, and that cavitation sheet lengths only greater than 1% chord length are significant. PUF-3A is not able to calculate tip vortices. This appears to be an important disadvantage. However, previous studies showed, that the presence of a tip vortex agreed with the program's indication of a sheet cavitation which might be sufficient for a practical approach.

ISSN (Print): 1844-6116
ISSN (Online): 2501-8795 http://www.cmu-edu.eu/jmte

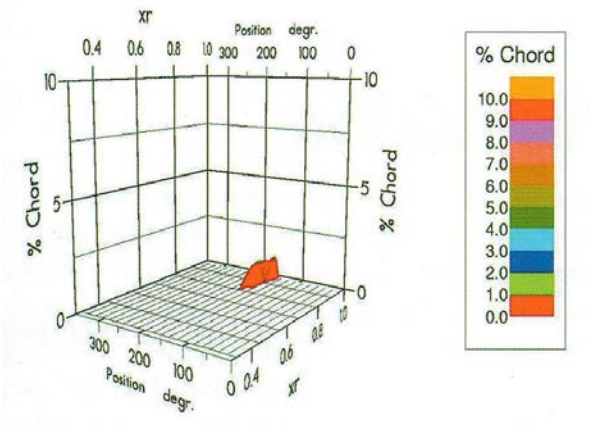

Figure 5 Calculated incipient cavitation (PUF-3A)

10. BLADE ROOT

In the past, interest has been focused on the flow around the blade tip since the cavitation inception used to first occur here. Meanwhile, the analysis tools and countermeasures have been developed in such a way that the blade tip does not necessarily constitute the inception point of cavitation on the propeller. In some cases, cavitation inception has been observed earlier on the root (or even on the appendages). Therefore, the knowledge of flow phenomena in the root region is of interest, in particular if the blades are fastened with blade bolts.

11. SIMULATION OF CAVITATING TIP VORTEX

The simulation of three dimensional tip vortex structures at Controllable Pitch Propellers becomes significantly more stringent when dealing with noise target requirements. The induced vortex from the blade tip is strongly dependent on friction and turbulence structures. VA TECH Escher Wyss simulates such tip vortices with a RANSE-solver. The RANSE-solver FENFLOSS (Finite Element based Numerical Flow Simulation System) has been developed by the University of Stuttgart's Institute of Fluid Mechanics and Hydraulic Machinery. FENFLOSS is able to calculate the three dimensional, turbulent flow under consideration of the friction around the propeller. Both blades have been calculated with FENFLOSS for three different operation points each simulating the wake peak, the mean wake and the minimum wake. The propellers investigated by VA TECH Escher Wyss are highly loaded. Furthermore, they are characterized by a small rake and a reduced pitch near to the blade tip. The skew is adapted to the wake.

One blade is meshed with roughly one million calculation elements for simulations. The wall shear stresses are calculated with a logarithmic wall function. The wake ahead of the propeller is simplified as a homogeneous boundary condition. The influence of different operation points is realized through various axial velocities at the inlet of the calculation model. A radial constant axial velocity is thus defined as an inflow boundary condition. Additionally a degree of turbulence of 5% is applied at the inlet. A natural boundary condition dp/dx=0 is defined at the outlet. A symmetrical boundary condition is applied for the surface of the calculation model.

Three different wake fractions are compared for the studied blade geometry. Figure 6 shows a comparison of streamlines around the tip of each propeller blade. It seems that the variant two can hamper the tip vortex rolling up.

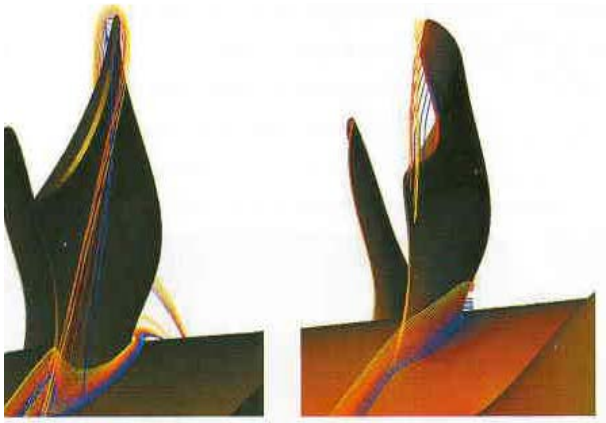

Figure 6 Comparison of two geometrical variations of blade tip with calculated streamlines (FENFLOSS)

ISSN (Print): 1844-6116
ISSN (Online): 2501-8795 http://www.cmu-edu.eu/jmte

However, the evaluation of the pressure distribution behind the propellers illustrates that the low pressure peak for both geometries is quite similar, as to be seen in Figure 7.

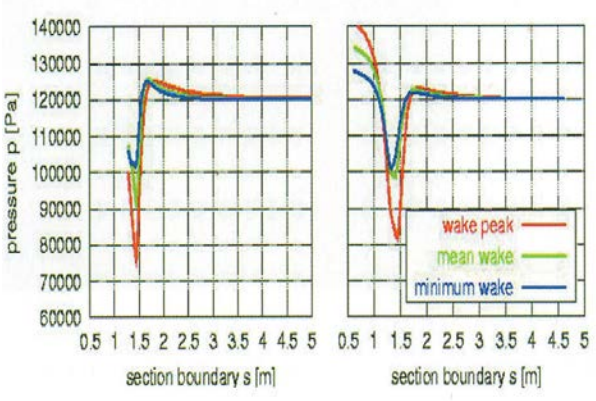

Figure 7 Comparison of the calculated pressure distribution behind the propellers for both geometries (FENFLOSS)

12. CONCLUSIONS

Due to the strong impact of the hull and appendages on the propeller performance, the given wake field constitutes the limits for a successful blade design. Therefore, the ship's hull and appendages must be designed and fabricated appropriately if a quiet propeller is required. By means of a M.I.T. program system, the cavity volumes and the surface pressures of a given blade geometry can be calculated and optimized in several design loops.

However, the analysis shows clearly that the variation and calculation of a propeller with modern RANS-solver is possible and leads to a new way of propeller design.

13. REFERENCES

[1] CRISTIAN BAUER, *High Performance CP Propellers for acoustic signatures* , VA TECH Escher Wyss.

[2] M. ABDEL-MAKSOUD, H-J.HEINKE, *Investigation of the Viscous Flow around Modern Propultion System*, 95-th general meeting of the German Society for Maritime Technology, Hamburg, 2000.

[3] M. ABDEL- MAKSOUD, RIECK K., *Calculation of the pressure reduction in the tip vortex core of a skew propeller in model and full scale* , 4-th Numerical Towning Tank Symposiym (Nu TTS 01) Hamburg, Germany, 2001.

ISSN (Print): 1844-6116
ISSN (Online): 2501-8795 http://www.cmu-edu.eu/jmte

ISSN (Print): 1844-6116
ISSN (Online): 2501-8795 http://www.cmu-edu.eu/jmte

Journal of Marine technology and Environment Year 2017, Vol.1

A RISK OF CIBERNTICS IN THE BLACK SEA SYSTEMS

Nikolay Petrov[1], Fanel-Viorel Panaitescu [2] & Mariana Panaitescu [2]

[1]Technical University Sofia, Bulgaria, e-mail address:nikipetrov_1953@abv.bg
[2]Constanta Maritime University, Faculty of Naval Electro-Mechanics, 104 Mircea cel Batran Street, 900663, Constanta, Romania, e-mail address:marianapan@yahoo.com, viopanaitescu@yahoo.ro

Abstract: Cybernetics consider the machines, living organisms and sea society as a organizing comprehensive form (system) – sea risky system that naturally historical or artificially reaches a certain level of organization according to relevant quality fixed structure or level of complexity. Basic laws and principles of cybernetics are inextricably linked to the reliability of functioning cybernetic systems. Cybernetics (cyber society) consider the objects as a system, not as a control system of a general nature, but as a system of defined set of general and specific structural and functional properties (presence in the world of living systems and social structures).

Key words: sea , risk, system, reliability, cybernetics, management.

1. INTRODUCTION

Cybernetic system is a complex dynamical system on the base of operation, in which stands the information interaction between the functional elements (FE) of its subsystems and the entire system with the external environment. In this interaction a key role plays the feedback and its management.

Under a complex dynamical system it should be understood, evolving in time and space system of objects that consist of multiple FE (with links between them), and possessing various properties of its constituent elements [1].

The complex dynamical system may be seen in terms of processes and operations management. For its part should consider the following definition of a system of control: „Processes and operations causing systematic transformation of the system from one state to another and ensuring its reliability and stability of functioning" [2].

For the purpose of introducing a definition for cybernetic system (CS) it is important to establish what means by the external environment, because it is wrongly the systems to be differed and classified by type of attitude towards it [3].

Cybernetics study sea systems, which have reached defenetely and sufficiently high level of organization, and which have appropriate structure allowing their designation as information systems that are managed in a certain algorithm (program) [4].

The methods of cybernetics can not be distributed as a whole on the phenomena of inorganic nature. Therefore, these phenomena as part of inorganic nature can not be regarded as cyber systems. In more general terms, however, it is still possible examination of information processes in inorganic nature. In cybernetics as science the object of study are the principles of operation and reliability of systems that are "open to energy, but are closed to information" [5].

The Cyber machine (the ship and seamen) and biological system (living nature and sea) are not identical. The process of constant renewal of the chemical constituents of biological systems is making its mark on all manifestations of vital activity. Not with standing the qualitative distinction between animate and in-animate nature, we should not think that there is eternal limit, i.e. between the two types of nature are many join things in common.

The paper presents the method and research regarding sea risk systems.

2. METHOD AND RESEARCH

Let denote the function of uncertainty of a specific system with $f_{UN}(y)$ where y is the number of its outlets. Then by a system with one possible outcome $y = 1$ the uncertainty will not exist, i.e. there will be met following equality [6]:

$$f_{UN}(1) = 0. \qquad (1)$$

From (1) and from literature [7], follow three properties of the function of uncertainty:

$$f_{UN}(1) = 0;$$

$$f_{UN}(m) \leq f_{UN}(n); m \leq n;$$

ISSN (Print): 1844-6116
ISSN (Online): 2501-8795 http://www.cmu-edu.eu/jmte

$$f_{UN}(m.n) = f_{UN}(m) + f_{UN}(n), \quad (2)$$

where:
m and n are respectively the number of outputs of examined system at different moments of time.
Single function that satisfies the condition (2) is the logarithmic function. From it follows that the uncertainty is not any function of number outputs of system and it is proportional to the logarithmic function. If there is carried out indication of function of uncertainty $f_{UN}(y) = N$, and the number of outputs of the test system is n, it will follow the

$$N = k.logn, \quad (3)$$

where: k is defined by the selected base of logarithm. After the occurrence of respectively event with the system in question, the uncertainty N becomes information for the reliability of the event, as the probability of non-failure work (NFW) realization of the event is $P_{NFW}(\Delta t) = 1$ in considered time interval Δt [8, 9, 10]. The function of the amount of information is represented by I from what follows

$$I = N = k.logn\,. \quad (4)$$

There is conversion of (4) by the following manner:

$$I = k.logn = -klog\,1/n = -k\sum_{i=1}^{n} 1/i\,.\,log\,1/n\,. \quad (5)$$

From (5) follows the equality

$$I = -k\sum_{i=1}^{n} 1/i\,.\,log\,1/n\,. \quad (6)$$

The equation (6) is formed at an unspecified base of logarithm as the cost of coefficient k depends on the selected base. Let's consider carefully (6). By n is denoted a number of possible cases or the number of possible outputs of the system.

2.1 Sea risk System

Let a Sea Risk System (SRS) for management to have a number of outputs n and each output has probability for realization (by the condition of setting in) p_i as there is executed the condition $0 \le p_i \le 1$. In this case it will be executed

$$\sum_{i=0}^{n} p_i = 1. \quad (7)$$

because of at least one of possible cases p_i must become true.

From (7) will follow the conversion of (6) in the form:

$$I = -k\sum_{i=1}^{n} p_i \log p_i. \quad (8)$$

It remains to solve the issue of measurement information by formula (8), i.e. the unit of measure. Naturally for the unit we must to accept the least amount of information. Given the properties of the function of the uncertainty of SRS management $f_{UN}(y)$, represented by (2), it will follow that at least the non-zero amount of data will be received by $n = 2$. This is characteristic for management system with two outputs, i.e. the information communication system with two levels of 0 and 1; TES in two states "working - non-working (defective)"; diag-nostic system with two states ,,has – has'nt"; situations monetary ,,coin heads or tails " and others.

As noted above, two symbols are sufficient to transmit each discrete message. Therefore, the amount of information to transmit two characters will be

$$I_2 = -k\sum_{i=1}^{n} 1/i\,log 0{,}5 = 1. \quad (9)$$

As an unspecified factor k, we can accept it as an equal unit of which follows:

$$I_2 = -\sum_{i=1}^{2} 1/i\,log 0{,}5 = 1,$$

where it is determined the base of the logarithm in equation (8).

It is easily seen that the base of the logarithm will be equal to two. Hence, the amount of information I_2 will be the unit of measure. It is called "*Bit*". Everyone system with two possible states of output (,,yes-no") contains in itself one bit of information.

Formula (8) is written in final form:

$$I = -\sum_{i=1}^{n} p_i \log_2 p_i\,;$$

$$\sum_{i=0}^{n} p_i = 1. \quad (10)$$

The Formula (10) is called *the Shannon formula* for the amount of data passing through any technical and economic governance system, in particular the SRS, which is increasingly expanding its applications in scientific, technical, social and educational systems and networks, management of information and culture of the most developed societies.

From (10) follows the important conclusion:as a tested system (in particular SRS) has more possible output states (greater uncertainty), so its reliability in the present state space is smaller.

ISSN (Print): 1844-6116
ISSN (Online): 2501-8795 http://www.cmu-edu.eu/jmte

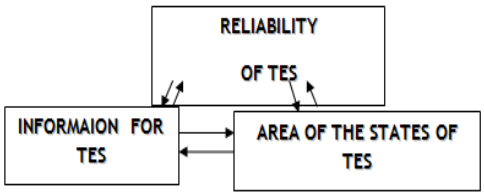

Figure 1 Reliability and information structural design of SR

The above statement gives oppoertunity to build a following reliable information structural scheme of functioning of SRS on the basis of techno-economic system and its cybernetic management (Figure 1).

2.2 Determination on quantity of reliable informations

From this diagram of operation of SRS comes a new formula for the amount of information flowing through the system and the reliability of operation of SRS, i.e. formula for the amount of reliable information (RI) [12]:

$$I_{RI} = -\sum_{i=1}^{n} p_i . log_2 p_i . P_{NFW}(\Delta t). \qquad (11)$$

In (11) the probability of non-failure work of system $P_{NFW}(\Delta t)$ in the inter-val of observation $\Delta t = t_2 - t_1$ is determined of the basic ,,Law for Reliability of SRS" in stationary right stream of failures and lack of consequences, according to the equation:

$$P_{NFW}(\Delta t) = exp\left[-\int_{t_1}^{t_2} \omega(t) . dt\right], \qquad (12)$$

where:
$\omega(t)$ is the intensity of flow from refusals (violations) in the SRS for the observed time interval $\Delta t = t_2 - t_1$.

By (11) and (12) goes the next final formula for the amount of reliable in-formation I_{RI} passing through an Sea Risk System (SRS)

$$I_{RI} = -\sum_{i=1}^{n} p_i . log_2 p_i . exp\left[-\int_{t_1}^{t_2} \omega(t) . dt\right]. \qquad (13)$$

The unit for so introduced new reliability feature regarding the amount of information is *Bit-Fita*.

Here, it should be recalled that the unit of measurement the Intensity of a stream of refusals is called Fit, as 1
Fit = 1 diversion/h occurred with the ship floating in the sea.

3. CONCLUSIONS

The Cyber machine (the ship and seamen) and biological systems (Living nature an Sea) are not identical. The process of constant renewal of chemical constituents of biological systems is making its mark on all manifestations of vital activity and behavior. Not withstanding the qualitative distinction between animate and in-animate nature, should not think that there is eternal limit, i.e. between the two types od nature there are many things in common and that is the reliability of cybernetic system - Sea, ship and people, as well as the related assessment of risks and risk management.

4. REFERENCES

[1] Bârsan E., Carp D., 2003, *Economic impact study of Constanta port versus Constanta county*, Journal of Coastal Research, Vol.19, no.4, The Coastal Education and Research Foundation, Palm Beach, Fl. US.
[2] Vladut, I., Tanase, C., *Operative commandment for marine depollution in context of national system, Brochure* „History of accidents in the Black Sea Basin", project „IUCRISKMAN", 2014.
[3] http://en.wikipedia.org/wiki/File:Black_Sea_map.
[2] Government Decision no. 893/2006, amending Government Decision nr.1593/2002, approving the National Plan of preparedness, response and cooperation in marine pollution by hydrocarbons;
[1] Berg, A. Kibernetika i nadejdnost. Nauka, Moskaw, 1964.
[2] Berg, A., N. Bernstain, i dr. Kibernetika. Filosofskaя ensiclopedia, Moskow, 1962.
[3] Muller, K. The New Science of Cybernetics. The Evolution of Living Research Designs. Vol. 1. Methodology. ,,Remaprint", Vienna, 2008.
[4] Petrov, N. Probability, Independence, Information Society. Monograph.Poland, 2012, Publ. ,,Wydawnictwo Astra", Lodz, First public-cation, ISBN 978-83-63158-20-0, pp 1-168.
[5] Petrov, N.I. Relativity Index of the Reliability of Space Systems. International Journal of Computing, v. 10, Is. 2, 2011, pp 179-182.
[6] Petrov, N. Reliability's Investigation of Risk Technical Systems. Monograph. Trakia University – Turkey – Bulgaria - Greece, First additionally publication, 2006.
[7] Shannon, C. A. Mathematical Theory of Communication. The Bell Sy-stem Technical Journal, Vol. 27, pp 379-423, 1948.

[8] Petrov, N., N. Atanasov. A Theorem for the Price of Reliability. International Journal of Innovative Science, Engineering & Technology, ISSN 2348–7968, V. 1, Is. 8, 2014, pp 117-122.
[9] Petrov, N., N. Atanasov. Probability and Orderliness in the Nature. IJMSEA, vol. 7, № III, 2013, pp 287-293, ISSN 0973-9424.
[10] Petrov, N. Izsledvane na operatsiite по osiguryavane na nadejdnostta na riskovi technoko-ikonomicheski sistemi. AI „Prof. Marin Drinov", BAS, Sofia, 2014.
[11] Petrov, N. Reliability as a basical tecno-economical problem by cybernising of society. Thesis for the award of degree „ Doctor of Economic Sciences". Varna Free University „Chernorizets Hrabar", Varna, May, 2015.
[12] Petrov, N.I., Reliability of information as a problem of cybernetics in sea risk systems, Final Book-Risk management and assessment for prevention on ecological and technological risks in the Black sea basin, 2015,pp. 33-38, Burgas, Bulgaria.

ISSN (Print): 1844-6116
ISSN (Online): 2501-8795 http://www.cmu-edu.eu/jmte

Journal of Marine technology and Environment Year 2017, Vol.1

USE OF PRISMATIC CELL PANEL IN SHIPCONSTRUCTION

Popa Adrian[1], Scurtu Ionut Cristian[1], Ali Beazit[1], Jenaru Andreea [2]

[1]Naval Academy Mircea cel Bătrân Constanța România, e-mail address: adrian.popa@anmb.ro
[2]Constanta Maritime University, Faculty of Naval Electro-Mechanics, 104 Mircea cel Batran Street, Romania

Abstract : This study was carried out starting from a real need: the possibility to create a fast rescue ship, able to operate in shallow waters in environments with explosive potential. That why, the idea of the designers was to use aluminium alloys in order to obtain a light boat. The hosed material is AL5083H116.

Key words: prismatic cell panel, Ansys, results for impact.

1. INTRODUCTION

Naval designers use aluminum alloys in order to obtain a light boats for a long time. Using a strong new light weight material can improve small boat construction.

The hoosed material is AL5083H116. According with

http://asm.matweb.com/search/SpecificMaterial.asp ?bassnum =MA5083H116, it's composition and properties are:

Table 1. Composition of the AL5083H116

(http://asm.matweb.com/search/SpecificMaterial.asp?bassnum=MA5083H116)

Component	Wt. %	Component	Wt. %	Component	Wt. %
Al	92.4 - 95.6	Mg	4 - 4.9	Si	Max 0.4
Cr	0.05 - 0.25	Mn	0.4 - 1	Ti	Max 0.15
Cu	Max 0.1	Other, each	Max 0.05	Zn	Max 0.25
Fe	Max 0.4	Other, total	Max 0.15		

Table 2. Mechanical properties of the AL5083H116 – just for information

(http://asm.matweb.com/search/SpecificMaterial.asp?bassnum=MA5083H116)

Hardness, Brinell	**85**	**85**	**500 kg load with 10 mm ball. Calculated value.**
Hardness, Knoop	109	109	Converted from Brinell Hardness Value
Hardness, Rockwell A	36.5	36.5	Converted from Brinell Hardness Value
Hardness, Rockwell B	53	53	Converted from Brinell Hardness Value
Hardness, Vickers	96	96	Converted from Brinell Hardness Value
Ultimate Tensile Strength	317 MPa	46000 psi	AA; Typical
Tensile Yield Strength	228 MPa	33000 psi	AA; Typical
Elongation at Break	16 %	16 %	AA; Typical; 1/2 in. (12.7 mm) Diameter

ISSN (Print): 1844-6116
ISSN (Online): 2501-8795
http://www.cmu-edu.eu/jmte

Modulus of Elasticity	70.3 GPa	10200 ksi	In Tension
Modulus of Elasticity	71 GPa	10300 ksi	AA; Typical; Average of tension and compression. Compression modulus is about 2% greater than tensile modulus.
Compressive Modulus	71.7 GPa	10400 ksi	
Poisson's Ratio	0.33	0.33	Estimated from trends in similar Al alloys.
Fatigue Strength	159 MPa	23000 psi	AA; 500,000,000 cycles completely reversed stress; RR Moore machine/specimen
Fracture Toughness	43 MPa-m½	39.1 ksi-in½	K_{IC}; TL orientation.
Machinability	30 %	30 %	0-100 Scale of Aluminum Alloys
Shear Modulus	26.4 GPa	3830 ksi	
Shear Strength	190 MPa	27600 psi	Calculated value.

Note: The data marked with AA are provided by the Aluminum Association, and usually are not recommended for design purposes.
During design checks, there were considered the data from the ANSYS Library.

2. THE CONCEPT OF THE RESEARCH

For this study, we used ANSYS 12.1 software available at the Naval Academy "Mircea cel Batran". We considered a prismatic cell panel, like in above figure:

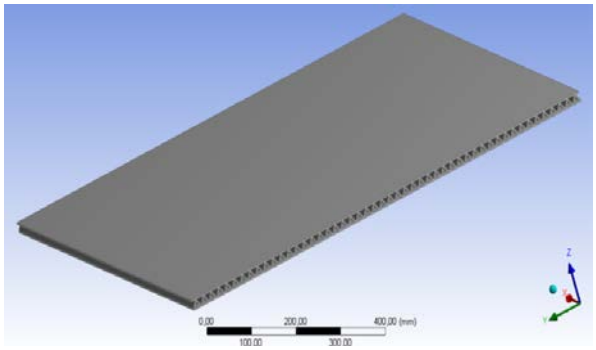

Figure 1 Isometric view of the AL5083H116 prismatic cell panel

The panel is composed by 1m long prismatic cell, with 3 mm thickness. Above the prismatic cells there is a 3mm sheet of the AL5083H116.

The panel is hit by a 0,2mx0,2mx0,004m steel plate like in figure:

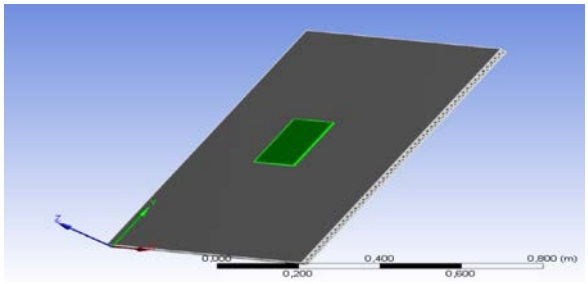

Figure 2 Steel plate hitting the AL5083H116 prismatic cell panel

3. SYSTEM OF COORDINATES AND LOAD CASES

The origin of the coordinates system is situated on upper face of the AL5083H116 prismatic cell panel.

The axes and their directions are presented in Figure 2.

Initial speed was considered to be -50m/s, alongside Oz axes. The analysis was carried out considering following load cases:

Table 3. Load Cases

Load Case	Incident angle	Steel plate edge orientation relative with the longitudinal direction of the prismatic cells	Image

ISSN (Print): 1844-6116
ISSN (Online): 2501-8795
http://www.cmu-edu.eu/jmte

Load Case	Incident angle	Steel plate edge orientation relative with the longitudinal direction of the prismatic cells	Image
1	0	Perpendicular	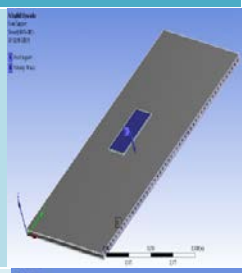
2	15	Perpendicular	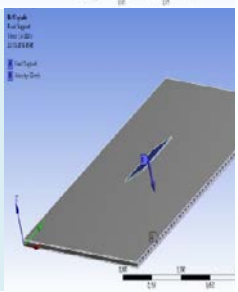
3	30	Perpendicular	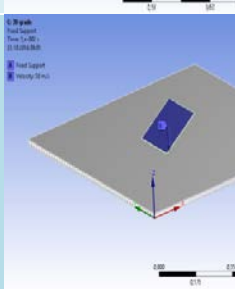
4	45	Perpendicular	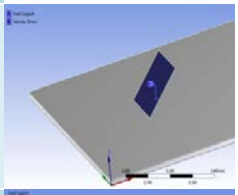
5	60	Perpendicular	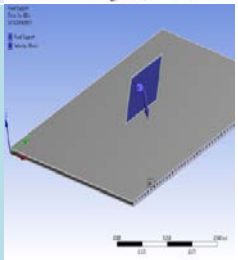

Load Case	Incident angle	Steel plate edge orientation relative with the longitudinal direction of the prismatic cells	Image
6	75	Perpendicular	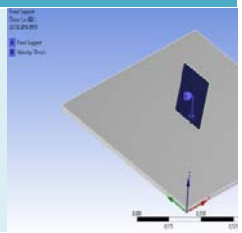
7	90	Perpendicular	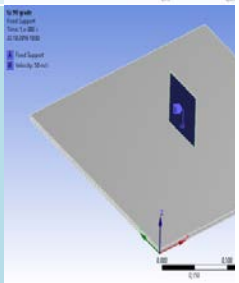
8	15	Parallel	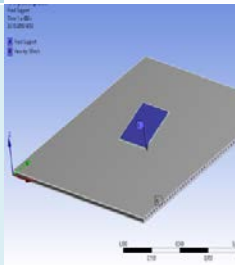
9	30	Parallel	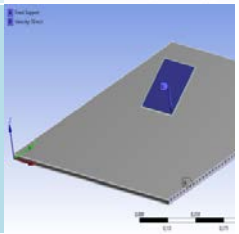
10	45	Parallel	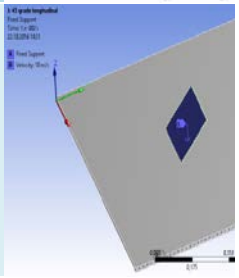

ISSN (Print): 1844-6116
ISSN (Online): 2501-8795
http://www.cmu-edu.eu/jmte

Load Case	Incident angle	Steel plate edge orientation relative with the longitudinal direction of the prismatic cells	Image
11	60	Parallel	
12	75	Parallel	
13	90	Parallel	

3. MESHING, INITIAL CONDITIONS AND ANALYSIS SETTINGS

The mesh is a structured one. It was created using a sweep method, both for the panel and for the steel plate. The mesh consists in 44182 nodes and 30775 elements. As exemplification, in the bellow picture is presented the mesh for Load Case 4

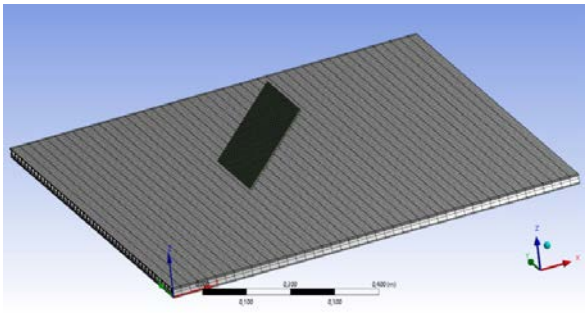

Figure 3 Grafical representation for Load Case 4 mesh

Initial conditions are:

- The AL5083H116 prismatic cell panel contour is considered to be in fixed support
- The speed of the steel plate is vertical, alongside Oz axe, with the value of -50m/s.

Initial conditions for Load Case 4 are presented in Figure 4.

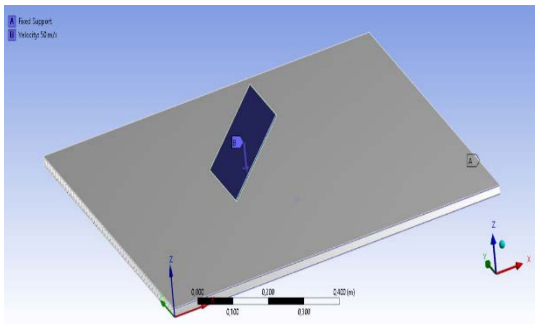

Figure 4 Initial conditions for Load Case 4

About the analysis setting, those are:

Table 4 Analysis settings

Object Name	*Analysis Settings*
State	Fully Defined
Analysis Settings Preference	
Type	High Velocity
Step Controls	
Resume From Cycle	0
Maximum Number of Cycles	1e+07
End Time	1,e-002 s
Maximum Energy Error	0,1
Reference Energy Cycle	0
Initial Time Step	Program Controlled
Minimum Time Step	Program Controlled
Maximum Time Step	Program Controlled
Time Step Safety Factor	0,9
Characteristic Dimension	Diagonals
Automatic Mass Scaling	No
Solver Controls	
Solve Units	mm, mg, ms
Beam Solution Type	Bending
Beam Time Step Safety Factor	0,1
Hex Integration Type	Exact
Shell Sublayers	3
Shell Shear Correction Factor	0,8333

ISSN (Print): 1844-6116
ISSN (Online): 2501-8795 http://www.cmu-edu.eu/jmte

Shell BWC Warp Correction	Yes
Shell Thickness Update	Nodal
Tet Integration	Average Nodal Pressure
Shell Inertia Update	Recompute
Density Update	Program Controlled
Minimum Velocity	1,e-006 m s^-1
Maximum Velocity	1,e+010 m s^-1
Radius Cutoff	1,e-003
Minimum Strain Rate Cutoff	1,e-010
Euler Domain Controls	
Domain Size Definition	Program Controlled
Display Euler Domain	Yes
Scope	All Bodies
X Scale factor	1,2
Y Scale factor	1,2
Z Scale factor	1,2
Domain Resolution Definition	Total Cells
Total Cells	2,5e+05
Lower X Face	Flow Out
Lower Y Face	Flow Out
Lower Z Face	Flow Out
Upper X Face	Flow Out
Upper Y Face	Flow Out
Upper Z Face	Flow Out
Euler Tracking	By Body
Damping Controls	
Linear Artificial Viscosity	0,2
Quadratic Artificial Viscosity	1,
Linear Viscosity in Expansion	No
Artificial Viscosity For Shells	Yes
Hourglass Damping	AUTODYN Standard
Viscous Coefficient	0,1
Static Damping	0,
Erosion Controls	
On Geometric Strain Limit	Yes
Geometric Strain Limit	1,5
On Material Failure	No
On Minimum Element Time Step	No
Retain Inertia of Eroded Material	Yes
Output Controls	
Save Results on	Equally Spaced Points
Result Number Of Points	50
Save Restart Files on	Equally Spaced Points
Restart Number Of Points	5
Save Result Tracker Data on	Cycles
Tracker Cycles	1
Output Contact Forces	Off

5. RESULTS

As results, we considered Equivalent Stress (von Mises) and total deformations for AL5083H116 prismatic cell panel. We present the distribution diagram at the moment when maximum values is reached. For the von Mises distribution diagram, we present the combined diagram for both bodies (the panel and the steel plate) in order to see how it was affected the steel plate.

There is some situation in which the position of the maximum value for the von Mises tensions are in the steel plate. In such situation, we marked some spots on the panel to emphasis the von Mises values in the panel. In all the graphics, the red line represents the minimum values and the green line represents the maximum values

5.1 Results for Load Case 1

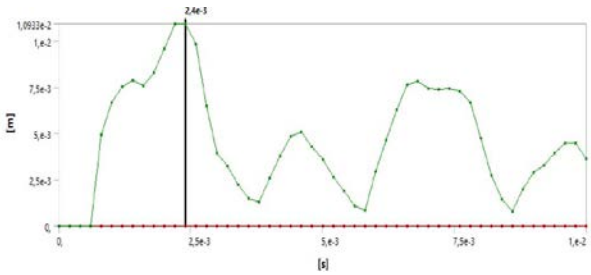

Figure 5 Total deformation values in panel for load case *1*

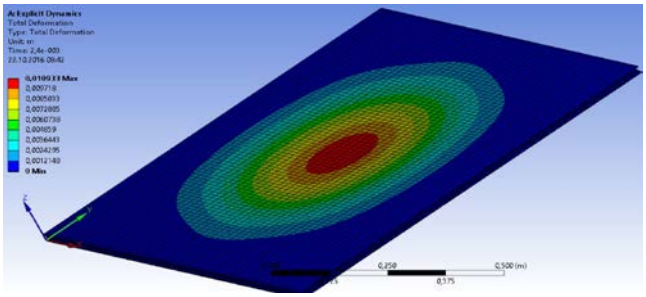

Figure 6
Total deformation distribution when maximum values occurs, for load case 1

ISSN (Print): 1844-6116
ISSN (Online): 2501-8795
http://www.cmu-edu.eu/jmte

Journal of Marine technology and Environment Year 2017, Vol.1

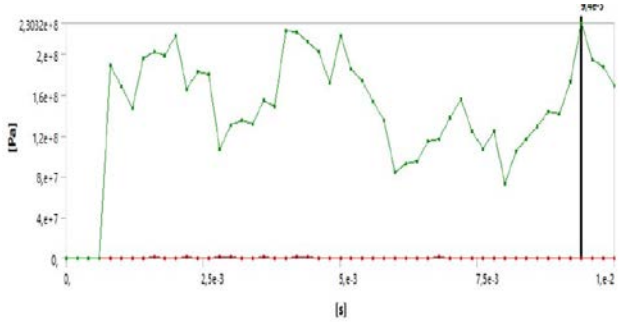

Figure 7 Von Mises stress values in the panel for load case 1

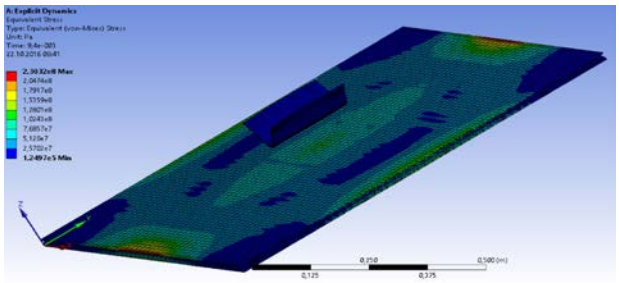

Figure 8 Von Mises stress distribution when maximum values occurs, for load case 1

5.2 Results for Load Case 2

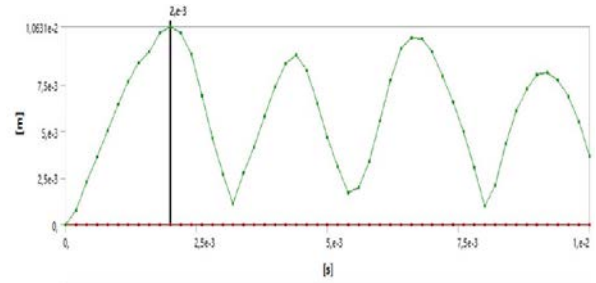

Figure 9 Total deformation values in panel for load case 2

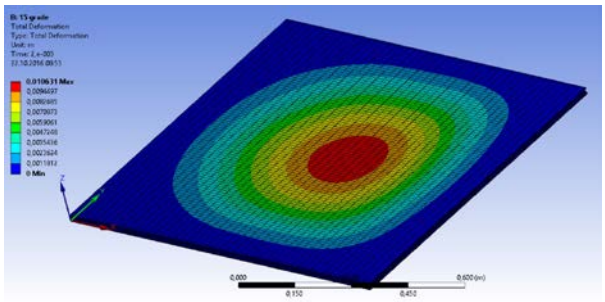

Figure 10 Total deformation distribution when maximum values occurs, for load case 2

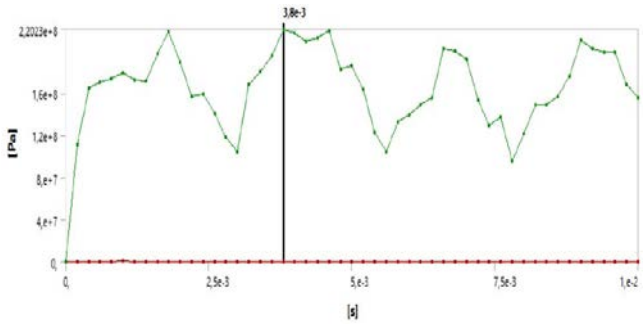

Figure 11 Von Mises stress values in the panel for load case 2

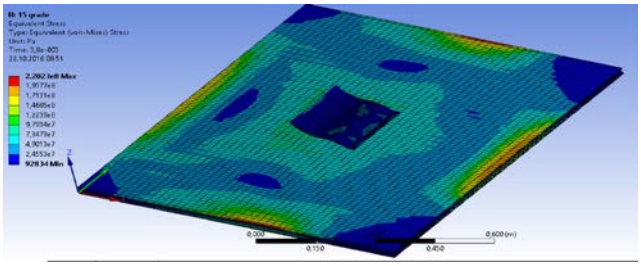

Figure 12 Von Mises stress distribution when maximum values occurs, for load case 2

5.3 Results for Load Case 6

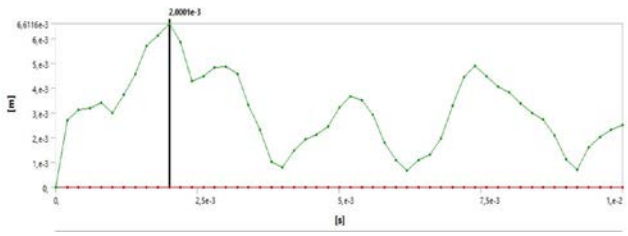

Figure 13 Total deformation values in panel for load case 6

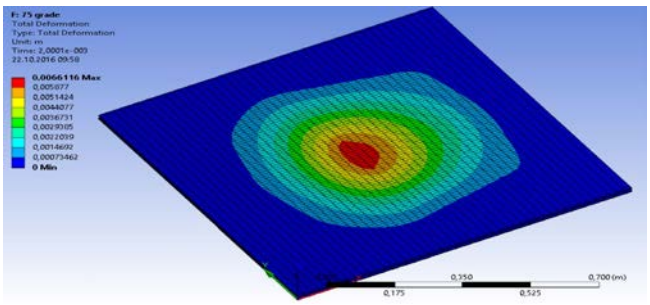

Figure 14 Total deformation distribution when maximum values occurs, for load case 6

ISSN (Print): 1844-6116
ISSN (Online): 2501-8795
http://www.cmu-edu.eu/jmte

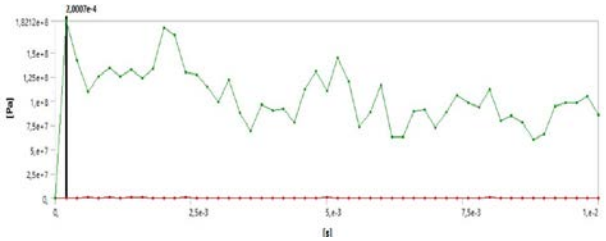

Figure 15 Von Mises stress values in the panel for load case 6

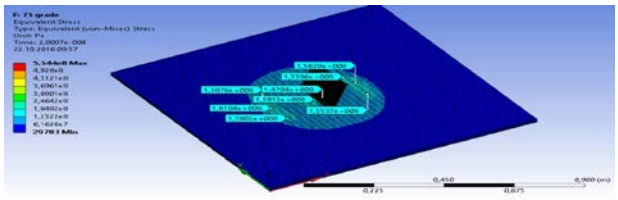

Figure 16 Von Mises stress distribution when maximum values occurs, for load case 6

5.4 Results for Load Case 7

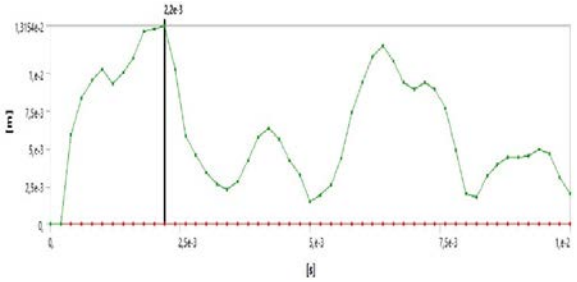

Figure 17 Total deformation values in panel for load case 7

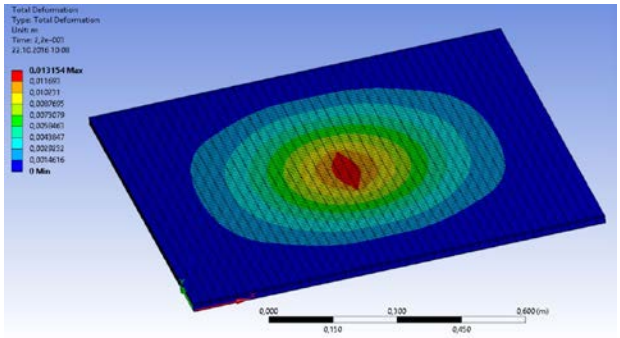

Figure 18 Total deformation distribution when maximum values occurs, for load case 7

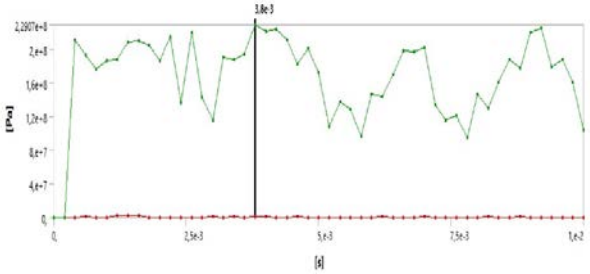

Figure 19 Von Mises stress values in the panel for load case 7

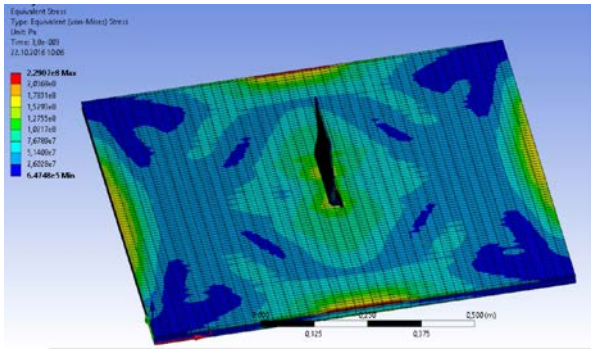

Figure 20 Von Mises stress distribution when maximum values occurs, for load case 7

5.5. Results for Load Case 8

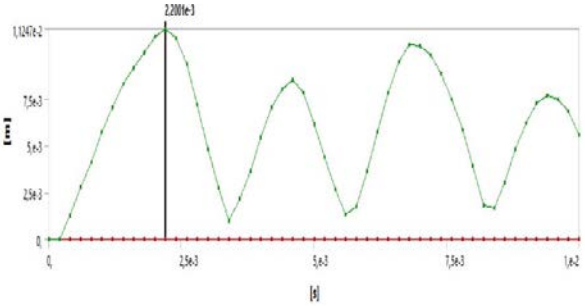

Figure 21 Total deformation values in panel for load case 8

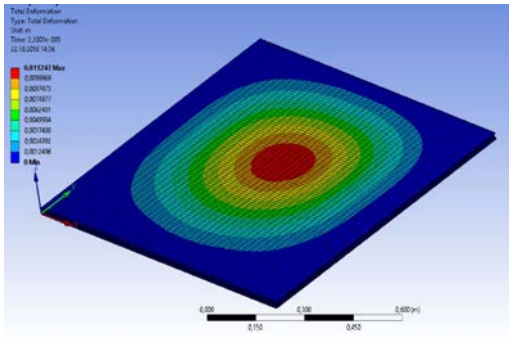

Figure 22 Total deformation distribution when maximum values occurs, for load case 8

ISSN (Print): 1844-6116
ISSN (Online): 2501-8795
http://www.cmu-edu.eu/jmte

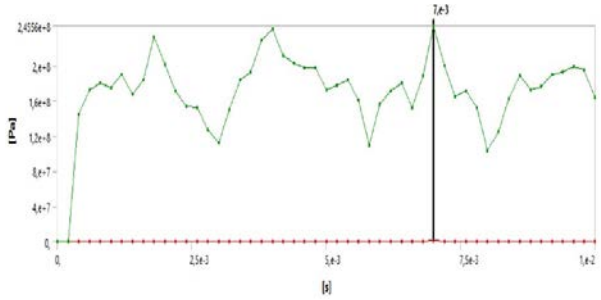

Figure 23 Von Mises stress values in the panel for load case 8

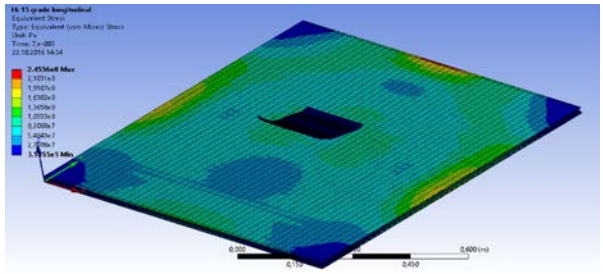

Figure 24 Von Mises stress distribution when maximum values occurs, for load case 8

5.6. Results for Load Case 9

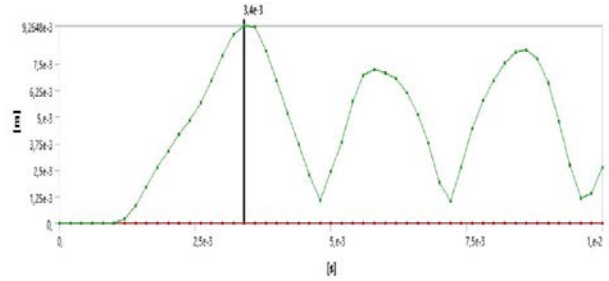

Figure 25 Total deformation values in panel for load case 9

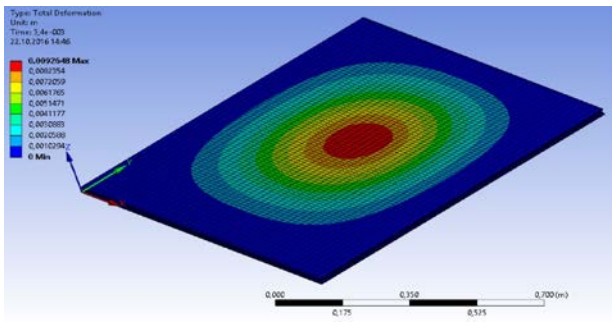

Figure 26 Total deformation distribution when maximum values occurs, for load case 9

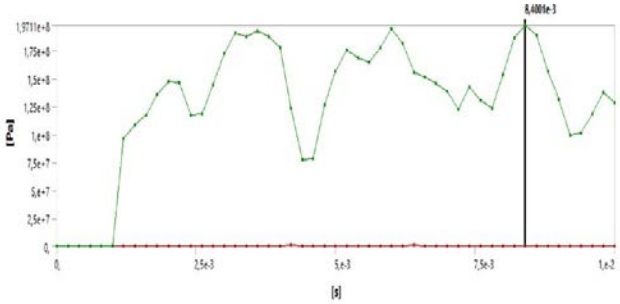

Figure 27 Von Mises stress values in the panel for load case 9

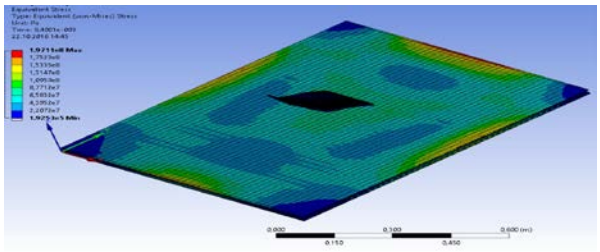

Figure 28 Von Mises stress distribution when maximum values occurs, for load case 9

5.7 Results for Load Case 13

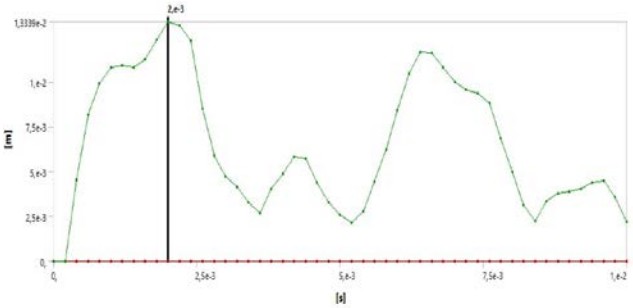

Figure 29 Total deformation values in panel for load case 13

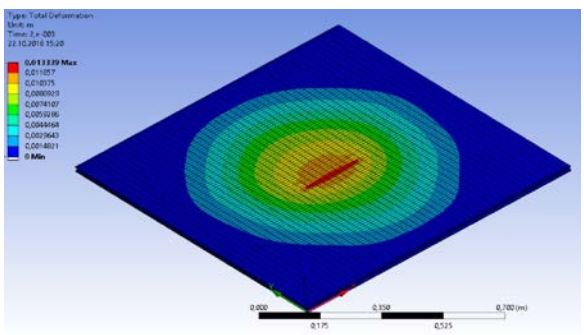

Figure 30 Total deformation distribution when maximum values occurs, for load case 13

ISSN (Print): 1844-6116
ISSN (Online): 2501-8795
http://www.cmu-edu.eu/jmte

Journal of Marine technology and Environment Year 2017, Vol.1

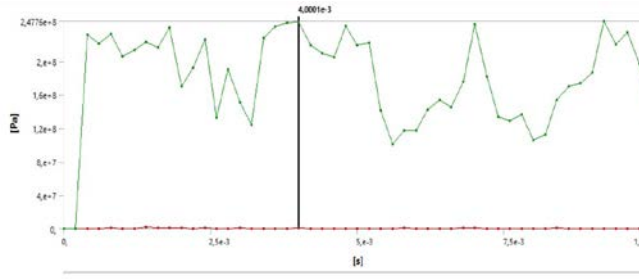

Figure 31 Von Mises stress values in the panel for load case 13

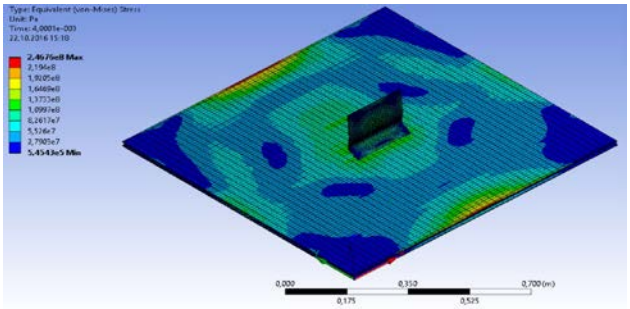

Figure 32 Von Mises stress distribution when maximum values occurs, for load case 13

6. CONCLUSIONS

On this study, we presented the results of an analysis regarding the effects on an AL5083H116 prismatic cell panel during the impact with a 0,2mx0,2mx0,004m steel plate.

From the structural perspective, we have to check if the maximum values of the von Mises stress are bellow ultimate strength.

According with Table 2, the ultimate tensile strength is 317MPa. This is the point when the panel brakes.

In the bellow chart are presented all the determined values of the von Mises stress in all load cases, compared with the ultimate strength.

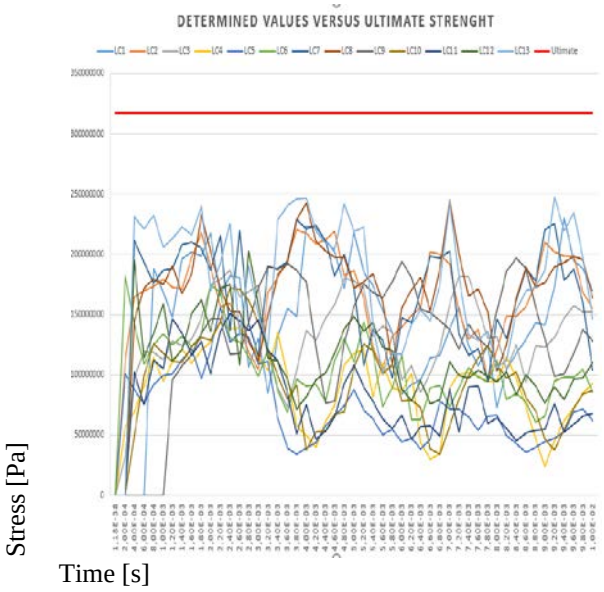

Figure 33 Von Mises values compared with the value of ultimate strength, for all load cases

As it can be seen in Figure 33, maximum values of the von Mises stress is 247760000 [Pa], and occurs in Load Case 13 at 0,0092seconds from the beginning of the simulation.

This value represents 78,2% from the AL5083H116 ultimate strength. As a final conclusion, we strongly recommend the naval engineers to consider the use of the AL5083H116 prismatic cell panels when designing fast rescue ship, able to operate in shallow waters in environments with explosive potential.

7. REFERENCES

[1] www.ansys.com
[2] Domnisoru L, Găvan E, POPOVICI O – Analiza structurilor navale prin metoda elementului finit, Editura Didactica si Pedagogica, Bucuresti 2005, ISBN 973 – 30 – 1075 – 8
[4] Călimănescu I., Stan L. C., Computer fluid dynamics (CFD)study of a micro annular gear pump, Atom 2016, Conference Paper.
[5] Stan L. Călimănescu I.,. C.A New innovative turbocharger concept numerically tested and optimised with cfd, 2016, Conference Paper.

ISSN (Print): 1844-6116
ISSN (Online): 2501-8795 http://www.cmu-edu.eu/jmte

ISSN (Print): 1844-6116
ISSN (Online): 2501-8795 http://www.cmu-edu.eu/jmte

Journal of Marine technology and Environment Year 2017, Vol.1

CONSIDERATIONS REGARDING DESIGNING 50 X 6 METERS SUSPENDED CROSSING

Popa Adrian[1], Scurtu Ionut Cristian[1], Ali Beazit[1], Duse Anastasia[2]

[1] Naval Academy Mircea cel Bătrân Constanța România, e-mail address: adrian.popa@anmb.ro
[2]Constanta Maritime University, Faculty of Naval Electro-Mechanics, 104 Mircea cel Batran Street, Constanta, Romania

Abstract : This paperwork is designing a suspended 50mx6m suspended crossing over a channel or a small river considering not only the design load but the response spectrum too.

***Keywords*:** Mechanical engineering, Structural engineering, Response spectrum.

1. INTRODUCTION

The present paperwork presents a complex analysis for a simple civil engineering situation: designing a small bridge for crossing a small river or a channel.

As a solution, we considered a 50x6 meters concrete runaway supported by 5 AH36 beams, with a parallelepipedal 50x400mm cross sections.

For designing this we considered three types of analysis:

- A static structural analysis, to design the bridge to operate in normal conditions
- A modal analysis to find the natural frequencies of the bridge,
- A response spectrum analysis in order to check the harmonic response of the bridge,

All the analysis was carried out using ANSYS 12.1 software.

2. GEOMETRY

As it was written in chapter 1 of this paperwork, the geometry consists in an 50x6 meters concrete runaway supported by 5 AH36 beams, with a parallelepipedal 50x400mm cross sections.

The 3D model is a 1:1 scale model.

The geometry looks like in above figure:

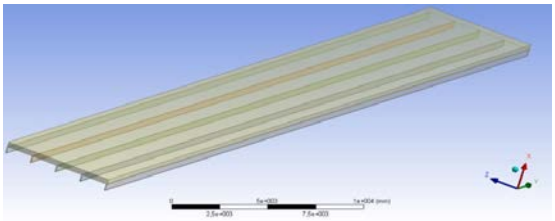

Figure 1 Geometry of the 3D model

3. STRUCTURAL ANALYSIS

3.1. Design requirements

The bridge is design to be able to support a pressure of 10 [KN/m^2].

3.2 Mesh

The discretisation network was automatically generated by software, and its main characteristics are:

Table 1. Mesh characteristics

Object Name	*Mesh*
State	Solved
Display	
Display Style	Body Color
Defaults	
Physics Preference	Mechanical
Relevance	100
Shape Checking	Standard Mechanical
Element Midside Nodes	Program Controlled
Sizing	
Statistics	
Nodes	197149
Elements	32398
Mesh Metric	None

ISSN (Print): 1844-6116
ISSN (Online): 2501-8795 http://www.cmu-edu.eu/jmte

The discretization network is presented in below figure:

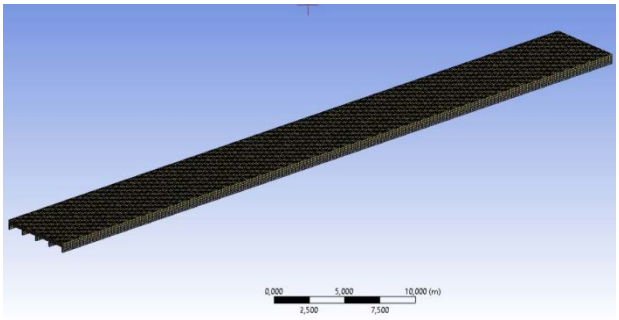

Figure 2 Mesh structure

3.3. Supports and loads

Supports and loads for the analysis are:
- Fixed supports on sides,
- Gravitational acceleration
- 10KPa pressure

Supports and loads are graphically presented below:

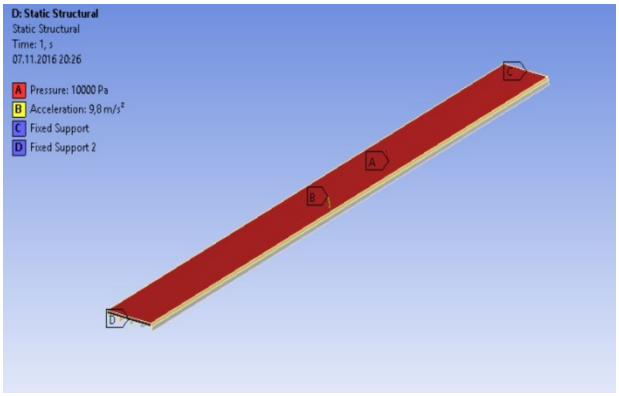

Figure 3 Supports and loads

3.4. Static structural analysis and preliminary conclusions

As results, we considered to be eloquent the total deformation and von Mises stress (equivalent stress).

In the bellow figures, we present the graphical distribution diagrams:

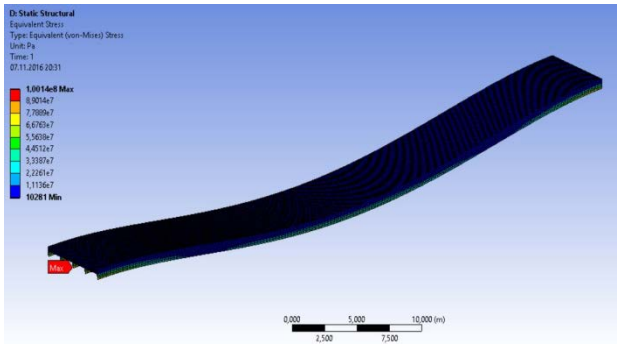

Figure 4 Von Mises distribution diagram

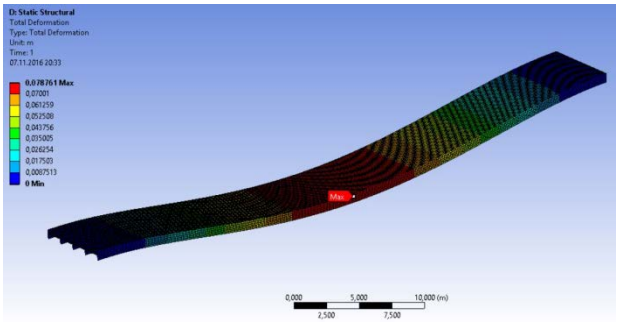

Figure 5 Total deformation distribution diagram

The position where is placed the maximum values are indicated with the red tag on the figures.

As it can be seen, maximum value for the von Mises stress is 1,0014e8 [Pa] (100,14 [N/mm^2]).

This value is acceptable, considering the AH36 ultimate tensile yield strength, which is 355 [N/mm^2].

Maximum total deformation value is 0,078761m.

As an intermediate conclusion, on the designed bridge, considering the design requirements, occurs equivalent stress up to 28,20% of the ultimate tensile yield strength and deformations up to about 8cm.

This values are acceptable, giving us a safety coefficient of 3,5.

4. MODAL ANALYSIS

A modal analysis is usually carried out in order to find the natural frequencies of a body.

Having dynamic loads with these frequencies, the energy transfer to the body is maximum.

In this situation, for our bridge, we found the first 15 frequencies.

The modes, and how the bridge behave, are graphically presented in below:

ISSN (Print): 1844-6116
ISSN (Online): 2501-8795 http://www.cmu-edu.eu/jmte

Table 2 Natural frequencies of the bridge

Mode	Frequency [Hz]
1,	1,0036
2,	2,4489
3,	2,7574
4,	5,2326
5,	5,3811
6,	8,5827
7,	8,8399
8,	9,1745
9,	12,619
10,	13,101
11,	17,384
12,	18,124
13,	22,507
14,	22,88
15,	23,867

In the following figures, there are presented the behavior pattern of the body, also known as mode shape results:

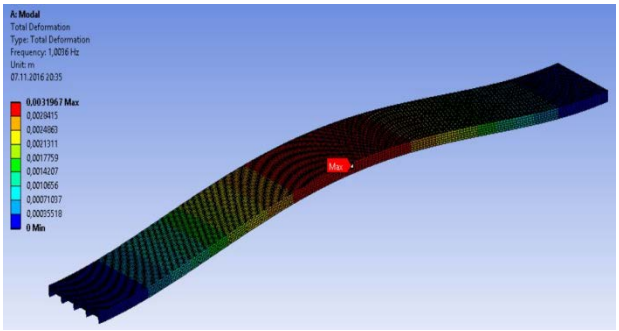

Figure 6 Total deformation for mode 1

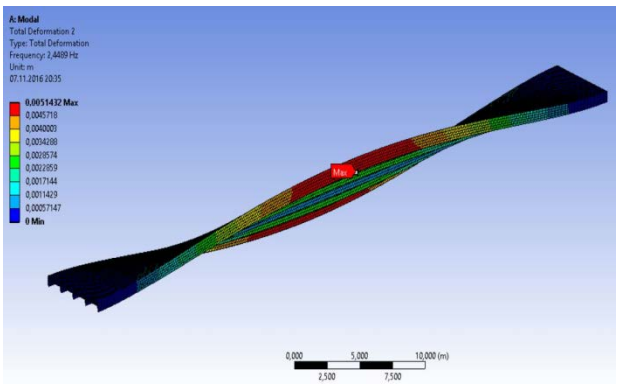

Figure 7 Total deformation for mode 2

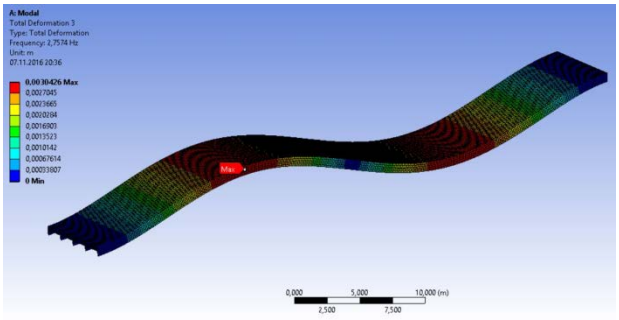

Figure 8 Total deformation for mode 3

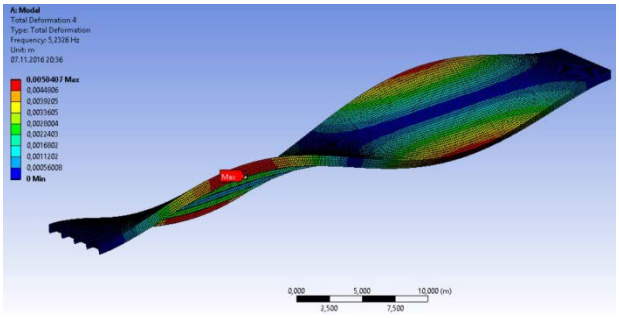

Figure 9 Total deformation for mode 4

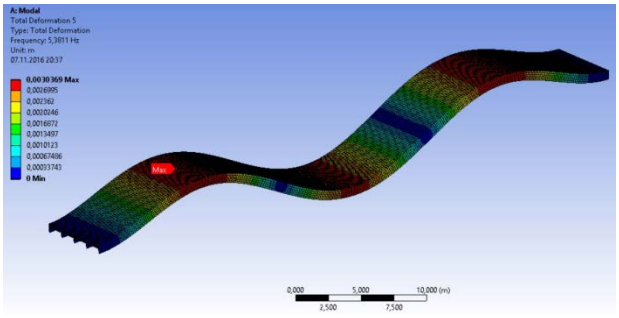

Figure 10 Total deformation for mode 5

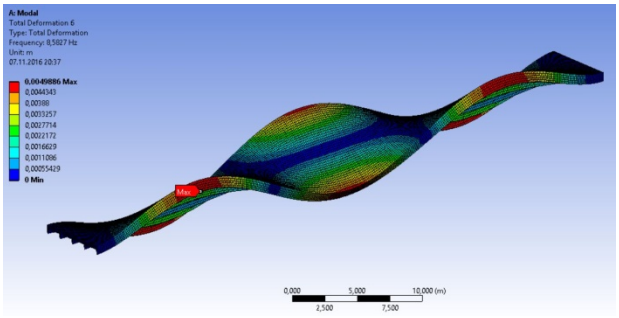

Figure 11 Total deformation for mode 6

ISSN (Print): 1844-6116
ISSN (Online): 2501-8795 http://www.cmu-edu.eu/jmte

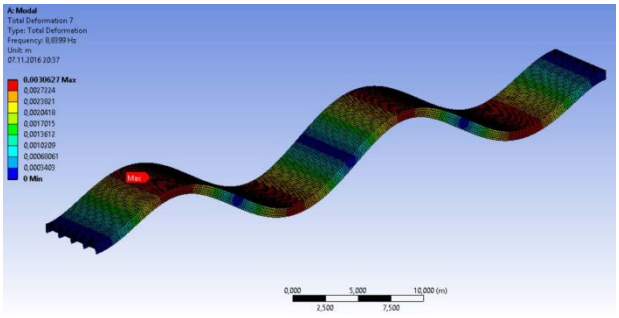

Figure 12 Total deformation for mode 7

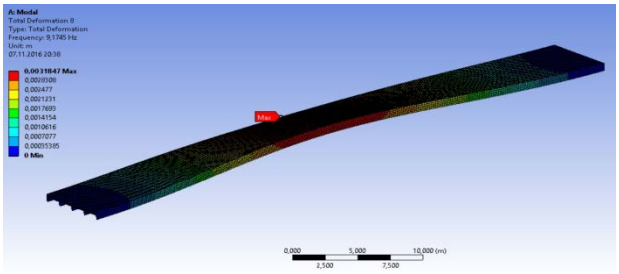

Figure 13 Total deformation for mode 8

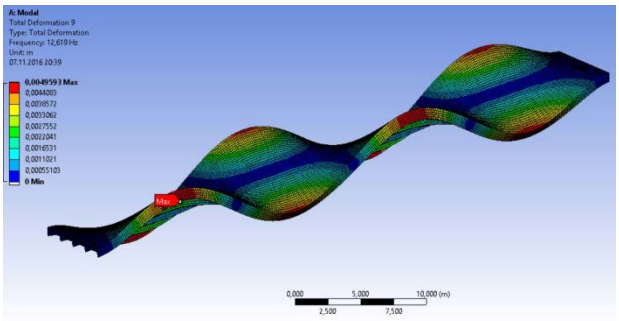

Figure 14 Total deformation for mode 9

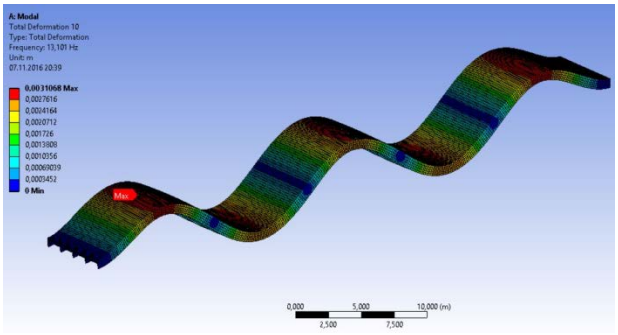

Figure 15 Total deformation for mode 10

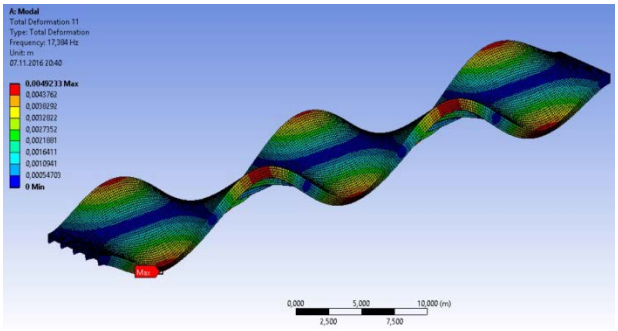

Figure 16 Total deformation for mode 11

In all the figures, the maximum value of the total deformation is marked with the red tag "Max".

5. RESPONSE SPECTRUM ANALYSIS

This analysis was carried out in order to find how the bridge respond having specific vibrations as loads. Because we intend to check our structure, we will consider the bridge on the effect of the first five natural frequencies.

We also consider these frequencies to induce each one a 1m/s^2 acceleration in the fixed support. This loads actually are the loads induced in the dilatation gaps at the beginning and at the end of the bridge.

The loads are presented in the below table:

Table 3 Bridge excitation frequencies

Frequency [Hz]	Acceleration [(m/s²)]
1,006	
2,4489	
2,7574	1,
5,2326	
5,3811	

The response of the bridge only due to the excitations on the first five natural frequencies are:

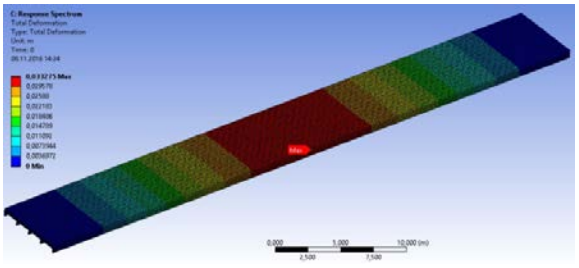

Figure 17 Total deformation response as vibration excitation

ISSN (Print): 1844-6116
ISSN (Online): 2501-8795 http://www.cmu-edu.eu/jmte

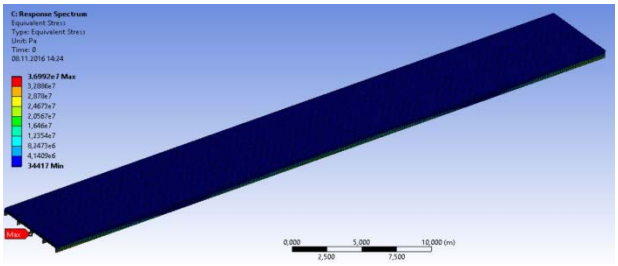

Figure 18 Von Mises stress response as vibration excitation

As it can be seen, the vibrations are inducing a 3,6992e7 [Pa] (36,992 [N/mm^2]) von Mises stress and a total deformation of 0,033275 [m].

6. CONCLUSIONS

If we consider the worst-case scenario, we should combine the both effect, the one from static analysis with the ones from response spectrum analysis.

Doing that we get a maximum value for the von Mises stress to be 1,37132e8 [Pa] (137,132 [N/mm^2]) and a total deformation of 0,11203 [m].

The values are acceptable, considering the AH36 ultimate tensile yield strength, which is 355 [N/mm^2]. This means we have a 38,681% load, and a safety factor of 2,58.

The structural response of the combined loads, on design pressure and due to vibrations on the first 5 natural frequencies is to be acceptable.

Considering all the analysis we must emphasize the following aspect: **the von Mises stress induced by vibrations in this situation represent about 35% of the von Mises stress induced by the design load**.

Neglecting this loads should not be an option for the civil engineers, as it was seen in this paperwork, the effect should be considered.

7. REFERENCES

[1] **www.ansys.com**
[2] DOMNISORU L, GĂVAN E, POPOVICI O, *Analiza structurilor navale prin metoda elementului finit*, Editura Didactica si Pedagogica, Bucuresti 2005, ISBN 973 – 30 – 1075 – 8
[3] Stan L. Călimănescu I.,. C.A New innovative turbocharger concept numerically tested and optimised with cfd, 2016, Conference Paper.

ISSN (Print): 1844-6116
ISSN (Online): 2501-8795 http://www.cmu-edu.eu/jmte

ISSN (Print): 1844-6116
ISSN (Online): 2501-8795 http://www.cmu-edu.eu/jmte

Journal of Marine technology and Environment Year 2017, Vol.1

MAGNUS EFFECT STUDIED WITH ANALYTICAL AND NUMERICAL METHODS

Andrei Alexandru Scupi[1]

[1]Constanta Maritime University, Faculty of Naval Electro-Mechanics, 104 'Mircea cel Batran Street, 900663, Constanta, Romania, e-mail andrei.scupi@cmu-edu.eu

Abstract: Different physical phenomena can be studied with the help of numerical programs. These programs are highly used in academic institutions for a better understanding of the phenomenon itself. A good correspondence between analytical representation and numerical representation is presented for different potential flows. The paper also presents a practical usage of potential flow when investigating the performance of an unconventional system that uses Flettner rotor for helping ship propulsion. The simulation, performed with CFD (Computational Fluid Dynamics) was made for different working conditions by varying the incidence angle. .

Key words : academic teaching, CFD, Flettner rotor, Magnus effect, numerical programs, potential flow.

1. INTRODUCTION

Various flows can be treated as frictionless and irrotational. This is because the viscous effects are limited to a thin layer next to the body called the boundary layer. Although this hypothesis has a narrow range of applications, different phenomena can still be correctly studied, such as: the outer flow field for airfoils, Magnus effect, water waves, groundwater flow and electro osmotic flow.

Magnus effect has a wide range of applications, one of which can be used as an unconventional propulsion system for ships and with the help of Flettner rotors it creates a force normal on the direction of the flow that in certain circumstances can help reduce the fuel consumption.

Research nowadays can be done not only by analytical and experimental way, since the first method is inapplicable when studying complicated phenomena and the latter is very expensive; but with the help of computers and numerical programs we can have a tool to study different phenomena. Computational Fluid Dynamics (CFD) is a branch of fluid mechanics that uses numerical methods to solve problems that involve fluid flow. CFD is used in academic institutions for better explanations of the phenomena, since numerical programs present various advantages: the simulation can be stopped at any time to observe how parameters evolve; the program offers the possibility of visualizing the distribution of different parameters.

2. ANALYTICAL SOLUTIONS AND NUMERICAL SIMULATION

Different potential flows are to be explained both by analytical and numerical methods. For instance the source has a complex potential of [1]:

$$W(z)=\frac{Q}{2\pi}\ln z\,. \tag{1}$$

This leads us to an analytical representation like in Figure 1.

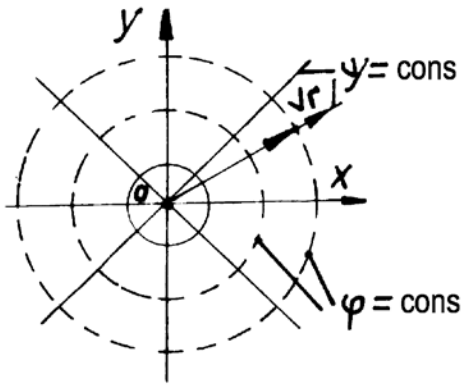

Figure 1 Analytical representation of the source streamlines and equipotential lines

ISSN (Print): 1844-6116
ISSN (Online): 2501-8795
http://www.cmu-edu.eu/jmte

We can also represent the velocity distribution and the streamlines and equipotential lines using numerical programs [2]:

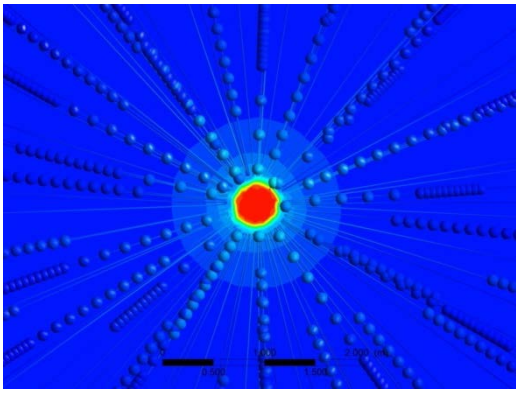

Figure 2 Local velocity and equipotential lines distribution of the source

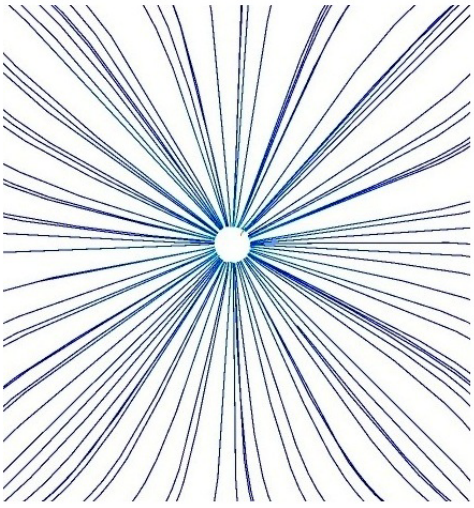

Figure 3 Streamlines distribution of the source

Similar we have the sink, with the difference that streamlines are converging towards the centre of the circle. The source has a complex potential of [2]

$$W(z) = -\frac{Q}{2\pi}\ln z\,. \qquad (2)$$

Figure 4 shows the analytical representation of the source streamlines and equipotential lines, while Figures 5 and 6 show the numerical equivalent solution.

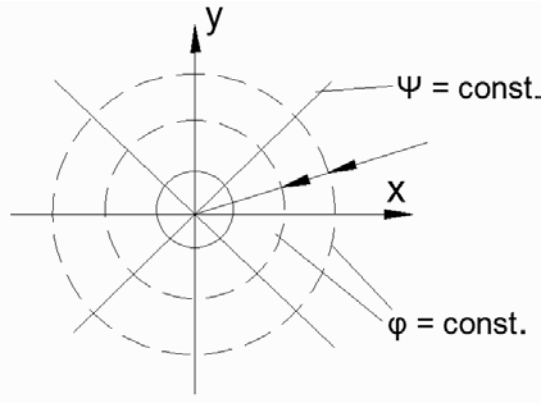

Figure 4 Analytical representation of the sink streamlines and equipotential lines

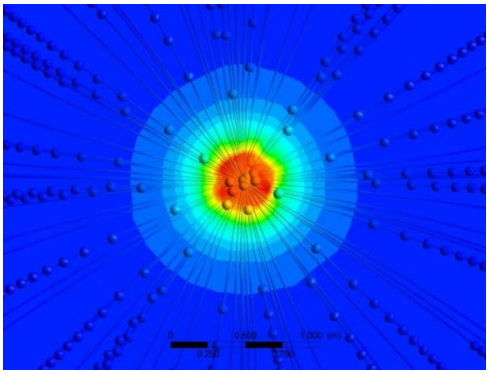

Figure5 Local velocity and equipotential lines distribution of the sink

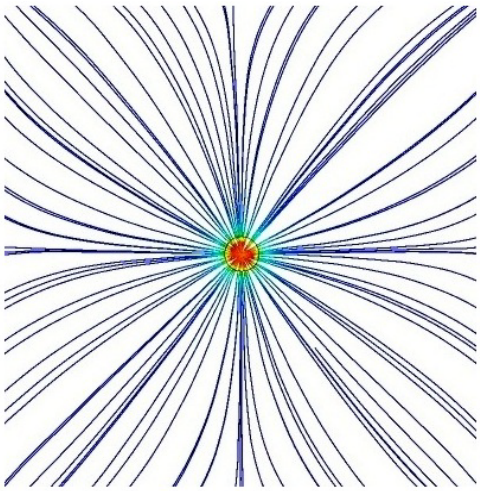

Figure 6 Streamlines distribution of the sink

ISSN (Print): 1844-6116
ISSN (Online): 2501-8795 http://www.cmu-edu.eu/jmte

The flow around a cylinder with circulation is a plane potential motion that consists of an axial stream (directed along axis Ox), a dipole of moment (with a source at the left of suction) and a whirl (in direct trigonometric sense). It produces the Magnus effect. The complex potential of motion will have the form:

$$W(z)=v_0\left(z+\frac{r_0^2}{z}\right)-\frac{i\,\Gamma}{2\pi}\ln z\,. \qquad (3)$$

If we plot the other streamlines we shall get some asymmetric curves with respect to axis Ox. On the inferior side of the circle, the velocity due to the axial stream is summed up with the velocity due to the whirl (Figure 7) [1]. A graphical representation of the velocity distribution will also emphasize the non-symmetric distribution of velocities around the profile (Fig. 8). This non-symmetric distribution of velocities will make the pressure distribution to be also non-symmetric (Fig. 9) [2].

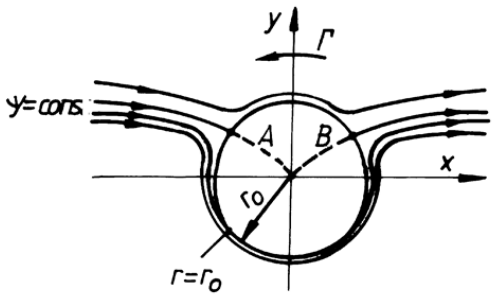

Figure 7 Analytical representation of the streamline distribution around a cylinder with circulation

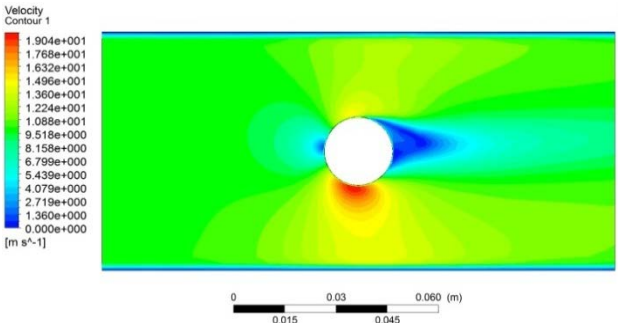

Figure 8 Velocity distribution around a cylinder with circulation, using numerical programs

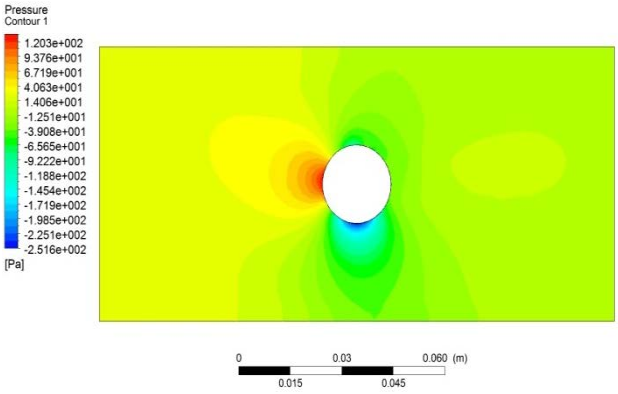

Figure 9 Pressure distribution around a cylinder with circulation, using numerical programs

3. PRACTICAL APPLICATIONS OF POTENTIAL FLOWS

A topic, which is under study nowadays, consists in finding clean solutions to air pollution by promoting different propulsion systems.

Emissions reduction is not simply achieved by reducing maritime transport but can be attained by improving the old technologies and/or by adapting and exploiting new operating systems that have the lowest impact on the environment.

The new systems are generally called unconventional for their exploit has nothing in common with traditional propulsion systems. They represent a step in designing and developing new systems that must be effective (in terms of their applicability) and environmental friendly (to reduce harmful emissions by as large a percentage number). As there no fully developed methods to propel a maritime ship by simply using these unconventional systems, they will mostly operate as support systems, auxiliary to traditional propulsion systems.

The development of this systems aims to minimize harmful emissions by reducing fuel consumption at the main engine [3].

We will focus on this paper on the flow around four Flettner rotors used as auxiliary propulsion systems. A Flettner rotor is a cylinder mounted on the main deck of a ship (Fig. 10) and rotated with a certain velocity can produce thrust using Magnus effect [5], [6].

ISSN (Print): 1844-6116
ISSN (Online): 2501-8795
http://www.cmu-edu.eu/jmte

Figure 10 General representation of the system [7]

Because the wind's direction is different from ship's direction we had chosen 5 different positions of the incidence angle between rotating rotors and air direction.

The system is composed of four cylinders mounted on the main deck (Fig. 11) that have the following characteristics: a length of 25 m and a diameter of 4m.

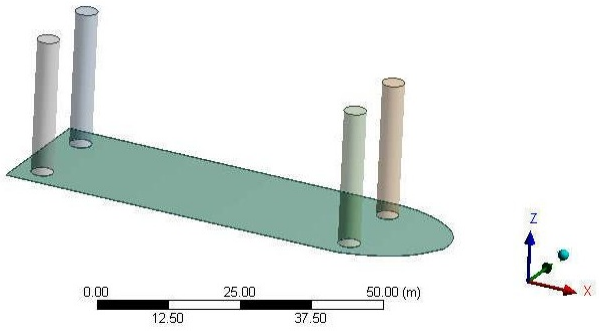

Figure 11 Flettner rotating rotors system design

We have chosen to represent only the main deck and the rotating cylinders due to the fact that the hull of the ship does not influence the values of the drag and lift forces that appear upon rotating cylinders. The system in enclosed into a flow volume domain large enough not to influence the flow of air around the rotating rotors. The domain is 350 m long and 250 m wide.

Analytically, the drag force and the lift can easily be calculated using the following formulas: [1]

$$L = \frac{\rho}{2} C_y A v^2, \quad (4)$$

$$D = \frac{\rho}{2} C_x A v^2; \quad (5)$$

where:
L = lift force, perpendicular to the direction of airflow;
D = drag force, acting in the direction of airflow;
A = body surface;
v = velocity of airflow;
C_y, C_x = coefficient depending on the shape profile and the angle of inclination;
ρ = air density (at 1 atmospheric pressure and temperature 15^0C);

Due to the complexity of the phenomenon analytical solutions cannot be applied. That is ways we used a numerical program ANSYS-Fluent to determine the aerodynamic forces that act upon the rotors.

3.1 Flettner rotating rotors system discretization

After the geometric representation of the rotors, we went to its discretization. In mathematics, discretization concerns the process of transferring continuous models and equations into discrete counterparts. This process is usually carried out as a first step toward making them suitable for numerical evaluation and implementation on digital computers. In order to be processed on a digital computer another process named quantization is essential. Quantization is the process of mapping a large set of input values to a smaller set – such as rounding values to some unit of precision. A device or algorithmic function that performs quantization is called a quantifier. The error introduced by quantization is referred to as quantization error or round-off error [3].

An unstructured grid was created using the automatic method. In total it was made of 2.6 x 10^6 cells 5.9 x 10^6 nodes. The volume was divided into 2 parts: a contact region near the rotor and the rest of it. The contact region near the rotor is consisting of 1.7 x 10^6 of small prisms with an edge length of 0.2 m. This was discretized into 3 layers using inflation method. The rest of the flow volume is made up of 0.8 x 10^6 growing tetrahedrons (Fig. 12 and Fig. 13).

ISSN (Print): 1844-6116
ISSN (Online): 2501-8795
http://www.cmu-edu.eu/jmte

Journal of Marine technology and Environment Year 2017, Vol.1

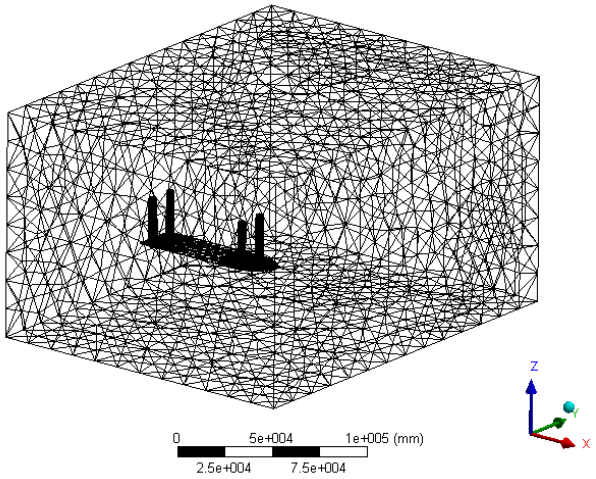

Figure 12 Domain discretization

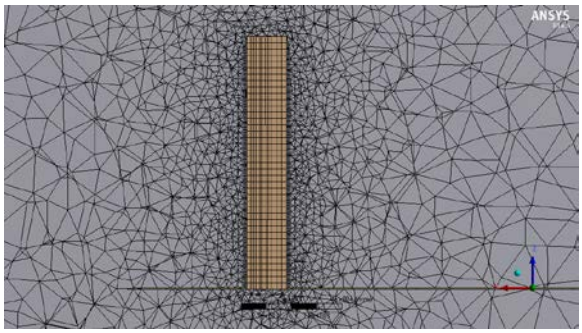

Fig. 13 Rotor discretization

3.2 Calculation of the aerodynamic forces

Using Fluent version 13.0, we have put the following boundary conditions:

– the rotors are attacked with a velocity of 10 m/s, under different angles: 0^0, 30^0, 45^0. 60^0, 90^0.

– the cylinders are rotating with 60 rpm;

– the atmospheric pressure at the end of the domain is 101325 Pa.

– the air density is considered constant and it is equal to 1.225 $\frac{kg}{m^3}$;

– the air dynamic and cinematic viscosity are also considered constant and are equal to 1.7894 10^{-5} $\frac{kg}{ms}$, 0.0001460735 $\frac{m^2}{s}$, respectively;

The flow was numerically computed using Fluent. We have chosen realisable k-epsilon model. Each case apart was run for about 20000 iterations, Fluent allowing us to visualize and export the coefficients of drag and lift forces (C_d and C_l). After the solution being stabilized, we have averaged the values of the coefficients mentioned

above and therefore obtain the two sought forces: drag and lift. The results are presented in table 1.

Table 1. Drag and lift forces

Incidence Angle [^{0}]	**Drag force D** [N]	**Lift force L** [N]
0^0	26555.631	11546.159
30^0	25722.94	12133.45
45^0	21713.12	18654.93
60^0	14970.22	26878.55
90^0	12693.37	29269.347

4. CONCLUSIONS

Potential flows are still studied and used today for investigating different phenomena. Numerical programs are widely used in academic and research institutions due to their numerous advantages (inexpensive, reliable, offer plenty of details).

A similar correspondence has been obtained when comparing analytical variation of parameters and numerical variation of parameters.

Comparing variation of parameters using an analytical and numerical method or comparing results obtained by experiment and numerical simulation has been performed in various papers with good correspondence between them [7], [8].

5. REFERENCES

[1] DINU, D., “Mecanica fluidelor pentru navigatori”, Ed. Nautica, Constanţa, 2010.

[2] Scupi A A, Dinu D 2015 Fluid Mechanics – Numerical Approach Nautica Publishing House Constanţa ISBN 978-606-681-064-7

[3] SCUPI A., DINU D., Unsteady Flow Over A Bluff Body With Application In Unconventional Propulsion System, 6th WSEAS International Conference on Manufacturing Engineering, Quality And Production Systems (MEQAPS '13), pp. 173 - 177, 4 pg., BDI, ISSN: 2227-4588, ISBN: 978-1-61804-193-7, Braşov, România, 2013

[4] Scupi A., E. J. Avital, D. Dinu, J. J. R. Williams, A. Munjiza Large Eddy Simulation Of Flows Around A Kite Used As An Auxiliary Propulsion System Journal of Fluids Engineering- Transactions of the ASME 137 10 pp. 101301-1 ÷ 101301-8, 2015

[5] Michael Traut a, Paul Gilbert, Conor Walsh, Alice Bows, Antonio Filippone, Peter Stansby, Ruth Wood, Propulsive power contribution of a kite and a Flettner rotor on selected shipping routes, Applied Energy 113 (2014) 362–372

[6] T. J. Craft, H. Iacovides and B. E. Launder, Dynamic Performance Of Flettner Rotors with and without Thom Discs, Proceedings TSFP7: 7th International; Symposium on Turbulence & Shear Flow Phenomena; 28 Jan 2012-31 Jan 2012; Ottawa, Canada 2011. pp. 6C13-6C18.

[7] Ikram Z, Avital EJ and Williams JJR (2012), Large Eddy Simulation of Free-Surface Flow past a Submerged Submarine Fairwater at Moderate Reynolds Number, Trans. ASME, J. Fluids Eng. 134 (6) 061103-1 to 061103-12

[8] Yu G, Avital EJ and Williams JJR (2008) Large Eddy Simulation of Flow Past Free Surface Piercing Circular Cylinders, Trans. ASME, J. Fluids Eng. 130 (10) 101304-1 to 101304-9

ISSN (Print): 1844-6116
ISSN (Online): 2501-8795 http://www.cmu-edu.eu/jmte

Journal of Marine technology and Environment Year 2017, Vol.1

VALIDATION OF THERMAL BALANCE EQUATION OF DIVER IN HYPERBARIC ENVIRONMENT AT SATURATION WITH HELIOX

PhD student eng. Stanciu Tamara

"Diving Center", 19, 1 May bvd., Constanta, Romania,tamara.stanciu@navy.ro

***Abstract*:** I presented the validation of diver thermal balance equation in subsea hyperbaric environment at diving with air, in a previous paper. The same equation was validated, at saturation diving using Heliox breathing mixture, in the simulator of Laboratory Hyperbaric Diving Center. The subjects were separated into two groups of four: the first group dived in saturation with Heliox at 60msw "stage depth" and the second one at 30msw. I calculated, with equation (1.1), theoretically temperatures divers, after sinking into warm water (20 ^{0}C) and into cold water (17 ^{0}C). At the end diving temperatures were measured each subject, for each scenario diving (depth, water temperature, stationary time, thickness suit, etc.). Theoretically temperatures were compared with those obtained experimentally and the differences between theoretical and real values were $\approx 1^0$C. The mathematical proposed model is valid for Heliox saturation diving in wet hyperbaric environment, up to 60 msw.

Key words: saturation diving, validation, "stage depth", "work depth", correction factor.

1. INTRODUCTION

The theoretical equation of thermal balance of the diver, who was obtained in wet hyperbaric environment, has provided an easy solution used to estimate the body temperature during the diving. This solution can be validated by unit air diving and by saturation diving with Heliox, in wet hyperbaric environment. This paper refers to the saturation diving with Heliox [Constantin A.., 2013].

$$T_{(t)} = \left(T_0 - T_a - \frac{\dot{Q}_m - l_{(p)}\rho_{(p)}x_{(p)}\dot{V}_{(p)}}{\frac{A}{R_{(p)}} + \rho_{(p)}c\dot{V}_{(p)}} \right) e^{-\frac{\frac{A}{R_{(p)}}+\rho_{(p)}c\dot{V}_{(p)}}{mc_c}t} + \frac{\dot{Q}_m - l_{(p)}\rho_{(p)}x_{(p)}\dot{V}_{(p)}}{\frac{A}{R_{(p)}} + \rho_{(p)}c\dot{V}_{(p)}} + T_a \ . \tag{1.1}$$

The saturation diving in the hyperbaric ensemble (dry hyperbaric chamber and wet hyperbaric chamber), consists in the saturation of the human tissue with inert gas at constant pressure, such that the stay at "stage depth"; from the dry chamber can be prolonged more. Only one decompression is performed after completion of works underwater, decompression that depends only on the depth of immersion was made. In this way the activity of the divers can be prolonged, because they can work, eat, sleep and rest inside the dry chamber, without needing any decompression. "Stage depth"; from the dry chamber represents a level of pressurization which is a little inferior to the "work depth" of the wet simulator, such that the partial pressure of the oxygen is maintained at the limit of 400 [mbar], unlike the one of the water which is maintained at the limit of 600 [mbar]. The stages of saturation diving are:

- pressurization of the divers up to the "stage depth" into the dry chamber and the pressurization of the wet chamber (simulator);
- transfer of the divers in the simulator;
- pressurization of the wet chamber up to the "work depth";
- descent of the divers into the water until they reach the "work depth";

ISSN (Print): 1844-6116
ISSN (Online): 2501-8795 http://www.cmu-edu.eu/jmte

- water divers return after a period of maximum 3 hours;
- depressurizing the simulator to the "stage depth"; and the transfer of the divers in the caisson for rest and physiological needs;
- repetition of this cycle until the work is finished;
- controlled decompression into the dry chamber.

[9].

The work depth over 50 m imposes the use of helium as a diluting gas for oxygen, instead of nitrogen from the atmospheric air. Utilizing the binary mixture of Heliox and enlarging the scope of the dives in saturation, determines different thermal phenomena, due to the physical properties of helium, different from the ones of nitrogen. The hyperbaric conditions and the scope of saturation diving, influence the heat changes between the organism of the diver and the surrounding medium. The phenomena are complex and they have been studied through a series of tests performed at Hyperbaric Laboratory.

2. THEORETICAL CONSIDERENTIONS

Most studies derived from the thermal equilibrium equation of a diver in hyperbaric environment, as did Dr. Anna Majchrzycka, but in a dry hyperbaric environment. [5]

The differential equation who governs heat transfer through the body, in wet hyperbaric environment was deducted considering two ways of transfer by skin (conduction and convection) and respiratory heat loss (heating and humidification of air).

$$\dot{Q}_p = mc_c \frac{dT}{dt} = Q_m - Q_c - Q_r \,. \quad (2.1)$$

[7].

Assumption: Diver's body is considered a cylinder with radius r_0, with parallel walls. [1].

The conductive and convective thermal flux loss at skin level is (2.2) [2].

$$\dot{Q}_c = K_{(p)}\left(T - T_a\right) = \frac{1}{R_{(p)}}\left(T - T_a\right). \quad (2.2)$$

Global coefficient thermal transfer at skin level $K_{(p)}$ depends on the convection of the layers and the free convection of suit and water. Thermal flux at respiratory system has two major components [8]:

$$\dot{Q}_r = \dot{Q}_x + \dot{Q}_s \,; \quad (2.3)$$

$$\dot{Q}_x = l_{(p)}\rho_{(p)}x_{(p)}\dot{V}_{(p)} \,, \quad (2.4)$$

$$\dot{Q}_s = \rho_{(p)}c\dot{V}_{(p)}\left(T - T_a\right), \quad (2.5)$$

The total thermal flux density lost by every subject is:

$$\dot{q}_{(p)} = \dot{Q}_p \Big/ A \; [W/m^2]\,. \quad (2.6)$$

Assumption: As the diver goes in depth, the pressure regulator delivers breathing gas at a higher pressure. Although the respiratory gas is saturated, pressure increases, water vapor remains at a constant pressure, density is constant. The temperature of inspired wet gas remains at 37^0C (body internal temperature), so not reach saturation. While pressure increases, specific vaporization latent heat $l_{(p)}$ decreases. Absolute humidity $x_{(p)}$ decreases.

Specific heat at constant pressure helium cp and cv specific heat at constant volume are much higher than those of nitrogen from the air. This leads to a dangerous cooling of the diver, Helium causes problems [4].

Table 1. Characteristics of gazes utilized at breathing mixtures [3]

Gas	R	Molar mass	c_p	c_v	Adiabatic k
	[J/kg K]	[kg/kmol]	[J/kg K]	[J/kg K]	[-]
Air	287	28,97	1006	718	1,4
Helium	207,7	4,003	5192,6	3115,6	1,667
Oxgen	259,8	31,99	918	658	1,395
Nitrogen	296,8	2,.013	1039	763	1,4
Water vapor	461,5	18,015	1872,3	1410,8	1,327

This phenomenon has been studied by many researchers who have observed that at depths between 24 to 30 msw, for the same flow rates, the rate of heat loss increases by 3-4 compared to the surface value. The researchers found that a diver equipped with a heated suit, loses [0.25 ^{0}C/h] at the saturation diving [6].

3. EXPERIMENTAL PROCEDURES

Experimental diving took place in the hyperbaric complex of the "Diving Center" in two stages: saturation at 60 msw (warm water) and saturation at 30 msw (cold water) at "stage depth". Two teams with 4 divers participated for each dive. The divers where both subjects and team buddy. "Work depth" was of 70 m, respectively 40 m. The utilized breathing mixture was Heliox 95/5.

At surface, before pressurization, the following amounts were measured: the temperature on the skin (on the arm), the internal temperature (at the ear of the diver), the volume flow rate at forced exhale and the

ISSN (Print): 1844-6116
ISSN (Online): 2501-8795
http://www.cmu-edu.eu/jmte

vital pulmonary capacity. After compression, the respiratory measurements were done again in a dry environment, at "stage depth", as well as in a wet environment, at "work depth". Temperature was measured underwater. Two immersed professional thermometers were used: Cole – Parmer industrial Probe RTD GEN PURP 10 and a digital mobile thermometer – hygrometer with a response time of 1 [s]. Both skin temperature and internal temperature have been recorded once every 2 minutes until the moment t = 16 [min].

The main experimental values collected during saturation diving, refers to the variation of breathing flow and the variation of body temperature.

The rate of breathing flow was measured in the dry chamber, at the "stage depth". For testing the thermal loss, the divers were transferred into the wet chamber. These values were processed to obtain a quantification of the flux density loss when breathing Heliox mixture.

The total thermal flux density lost by every subject, during the saturation diving, was assessed for a period of 16 [min] since entering the water.

Figure 1 The hyperbaric complex with the wet chamber and the dry chamber

Shiller Spirovit SP-10 spirometer was used with the accuracy of +-2%, which was plugged on the exterior of the caisson, at the discharge respiratory circuit, for collecting the forced exhale of the diver from the mask. Three measurements were done for each diver. The average value of the three measurements was taken into account.

Figure 2 Divers rest in dry chamber

4. RESULTS

The initial water temperature and the human body characteristics dictates the loss of heat flux density in the beginning of the dive, but after 10 minutes spent underwater, the loss of heat flux density gets steady at 1000 $[W/m^2]$, when it breaths Heliox .

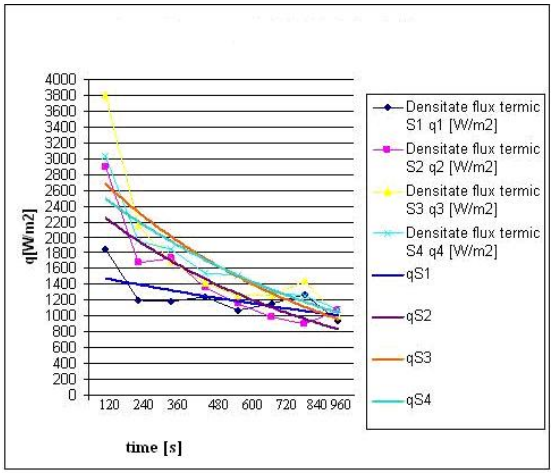

Figure 3 The total thermal loss of the divers at the saturation (60 msw) with 20^0C water temperature

See the Figures 3 and 4 when are showed the variation of total thermal flux density lost in time for the saturation at 60 msw (warm water 20^0C) and 30 msw (cold water 17^0C). It observes that thermal loss is greater in cold water (30 msw) than in warm water, even if the gas density is increased for the warm water (60 msw). The conductive heat loss by the skin was decisive.

ISSN (Print): 1844-6116
ISSN (Online): 2501-8795
http://www.cmu-edu.eu/jmte

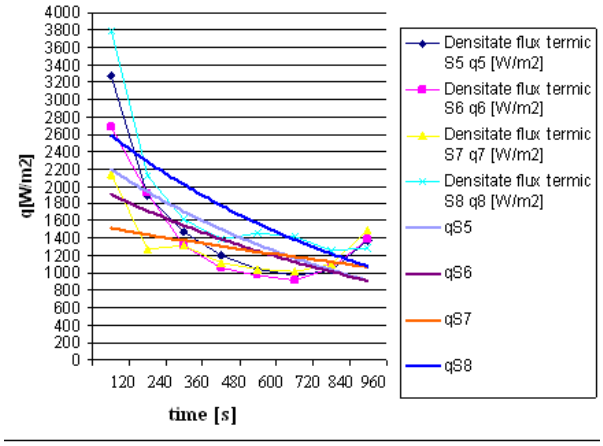

Figure 4 The total thermal loss of the divers at the saturation (30 msw) with 17^0C water temperature

In Figure 5 is an example of total heat flux loss for the same subject at the same depth and temperature, but with different breathing mixtures: air and Heliox.

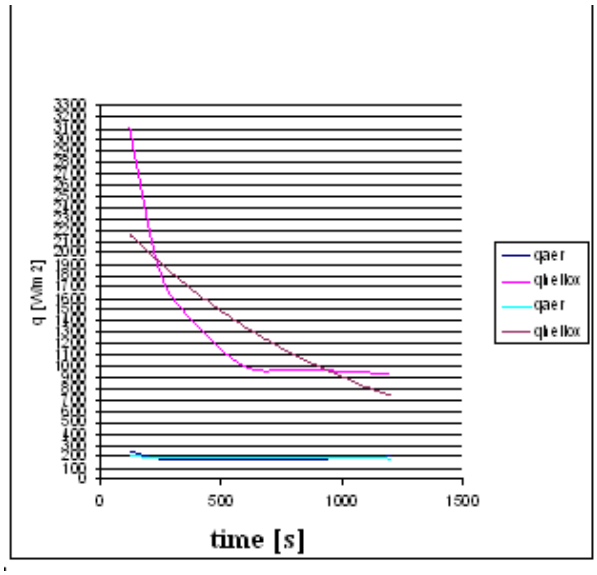

Figure 5 The total thermal loss of a diver at 30 msw, with air and Heliox breathing mixtures

Figure 5 highlights as for the same subject diving at 30 msw, the total heat loss is 250 [W/m^2] for air and 750 [W/m^2] for Heliox saturation. It can be concluded that the total heat loss of a diver are about 3 times higher when using Heliox as breathing gas than the air, at similar water temperature and depth.

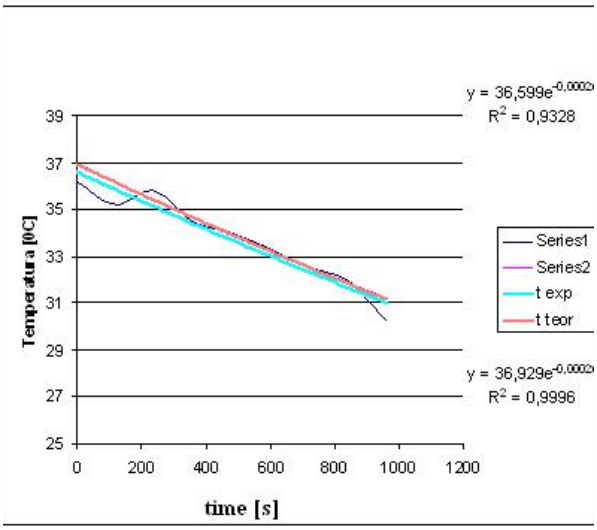

Figure 6 Variation of theoretical and experimental temperature of a diver at saturation (30 **msw) with 17^0C** water temperature

To validate the solution for thermal balance equation in hyperbaric conditions, at use of Heliox, we compared the measured temperature values with the theoretical values calculated. The difference between the calculated and measured values is at most 1^0C after 20 minutes of immersion.

Analyzing the initial hypotheses, we propose a correction factor due to radiation heat loss, given the fact that tests were done under conditions of simulation, by pressurizing the hyperbaric chambers at a rate that influence the body's reaction.

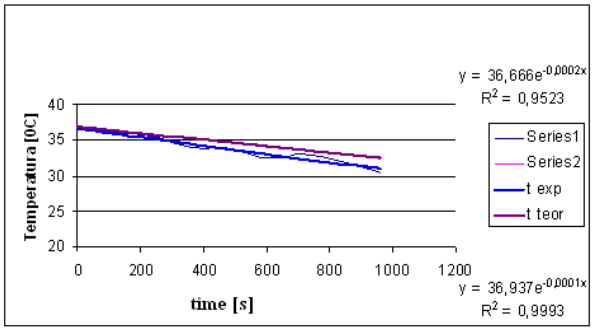

Figure 7 Variation of theoretical and experimental temperature of a diver at saturation (60 msw) with 20^0C water temperature

ISSN (Print): 1844-6116
ISSN (Online): 2501-8795 http://www.cmu-edu.eu/jmte

Journal of Marine technology and Environment Year 2017, Vol.1

5. CONCLUSIONS

Comparing the theoretical and experimental results, during the tests, it is observed that is a difference about 1[^{0}C] between the calculated and measured values at saturation diving with Heliox.

If we have Heliox, just as we found in the case of air, the solution of equation is close to the measured values. The experimental results were in good accordance with the temperature predicted by the mathematical model. Consequently, the solution of thermal balance of the diver can be utilized to predict the body temperatures of the subjects, after a given time, depending on the parameters specified: diving depth, protection suit, respiratory flow rate, characteristics of gaseous utilized at breathing mixtures

Correction factor due to loss by radiation, for Heliox is: $c_H = 1$[^{0}C].

The solution equation T(t) becomes:

$$T_{(t)} = \left(T_0 - T_a - \frac{\dot{Q}_m - l_{(p)}\rho_{(p)}x_{(p)}\dot{V}_{(p)}}{\frac{A}{R_{(p)}} + \rho_{(p)}c\dot{V}_{(p)}} \right) e^{-\frac{\frac{A}{R_{(p)}}+\rho_{(p)}c\dot{V}_{(p)}}{mc_c}t} + \frac{\dot{Q}_m - l_{(p)}\rho_{(p)}x_{(p)}\dot{V}_{(p)}}{\frac{A}{R_{(p)}} + \rho_{(p)}c\dot{V}_{(p)}} + T_a - c_H \quad (5.1)$$

While it uses Heliox, diver's body cools much more than with respiratory air.

In Figure 8 it can be seen that after 3 hours of dive, diver's C temperature drops to 17.5^{0}C. This phenomenon should be avoided..

In Figure 9 it shows the temperature fall to a slim diver and one corpulent. After 3 hours of saturation diving and same conditions, the adipose tissue of the corpulent diver led to a temperature higher with 1^{0}C than the temperature of the slim diver.

The charts show the most unfavorable circumstances, with the steepest decreases of body temperatures. In reality, the divers are moving, metabolic heat increases and thermal comfort provided is longer. Depending on the dive plan (residence time, water temperature, depth), we can estimate the temperature body that will have divers and can apply appropriate strategies for achieving thermal protection to prevent hypothermia temperature (28^{o}C).

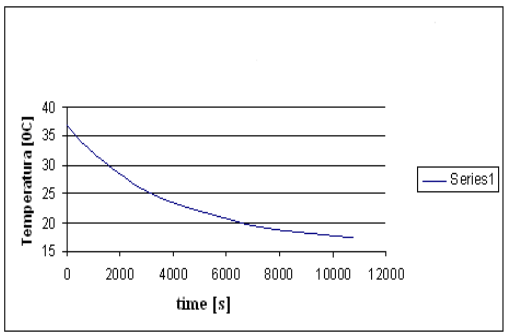

Figure 8 Variation of theoretical temperature of diver C at saturation (30 msw) with 17^{0}C water temperature

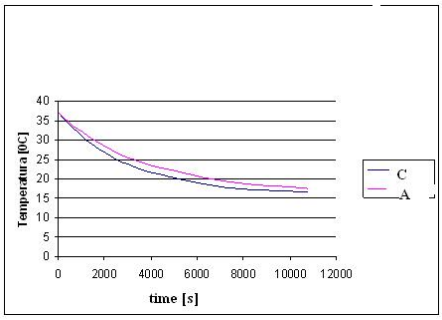

Figure 9 Temperature variations over time (3 hours) in the same conditions, at the saturation with Heliox for a slim / corpulent diver

Another aspect that should be stressed is faster cooling of the diver's body, using synthetic mixture Heliox 95/5, because the specific heat at constant pressure of the mixture synthetic is almost 5 times greater than at air. In Figure 10 it is observed that after 3 hours of immersion at saturation Heliox, the speed of the heat loss of the subject, has a rapid rise to a temperature with about 3-4 [° C] less than at the air diving.

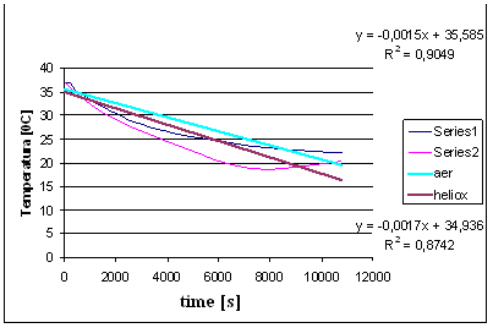

Figure 10 Temperature's evolution of a diver, immersed in warm water, who breathes air and Heliox

ISSN (Print): 1844-6116
ISSN (Online): 2501-8795 http://www.cmu-edu.eu/jmte

Journal of Marine technology and Environment Year 2017, Vol.1

The graph into Figure 11: after 3 hours of saturation with Heliox, speed faster of heat loss causes a temperature internal of the subject to about 8-10 [° C] less than at the diving with air.

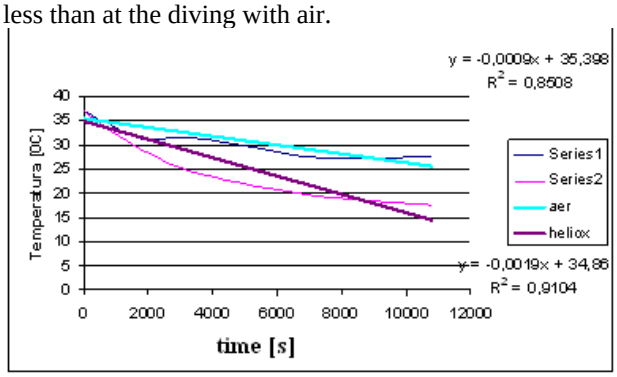

Figure 11 Temperature's evolution of a diver, immersed in cold water, who breathes air and Heliox

Assumptions adopted:

- For tissue was used a minimal model, where the resistance's values of the skin's layers of the diver depend on constitution and on effort.
- Heat lost through evaporation has been neglected, considering the diver's body in direct contact with water in wet suit.
- For radiation was adopted the correction factor c_H.
- The mathematical model proposed is valid for the saturated diving with Heliox, in wet hyperbaric environment, until 60 msw.

The mathematical model proposed is valid, for diving in hyperbaric environment simulated wet, up to 60 msw, for saturation diving with Heliox 95/5.

6. REFERENCES

[1] Constantin A., *Termotehnica, Ovidius Universiy Press*, Constanţa 2002
[2] Constantin A., Stanciu T., *Transient heat transfer in subsea hyperbaric environment,* 13thInternational Multidisciplinary Scientific GeoConference SGEM, Marine and Ocean Ecosystems, Albena Bulgaria, iunie 2013
[3] Degeratu M., Petru A., Georgescu Şt., Ioniţă S., *Tehnologii hiperbare pentru scufundări unitare şi în saturaţie,* pag. 78, 82,83,84,85, MATRIX ROM, Bucureşti, 2008
[4] Goodman et al., *Hyperbaric respiratory heat loss study*, Westinghouse Research Report, Office of Naval Research Report, 1971
[5] Majchrzycka A., *Model of Thermal Comfort in the Hyperbaric Facility*, Polish Maritime Research 1(68),vol 18; pp. 37-44, 2011.
[6] Piantadosi C.A., *Respiratory heat loss limits in helium-oxygen saturation diving*, Navy Experimental Diving Unit, USA, iunie 1980
[7] Stanciu T., Anca Constantin, *Experimental determination of the thermal flux density variation lost in time by a diver*, Annals of the Oradea University, Fascicle of Management and Technological Engineering, Volume IX (XIX), pp3.59-3.67, 2010.
[8] Stanciu T., *Experimental determinations of the respiratory thermal losses during the diving*, Annals of the Oradea University, Fascicle of Management and technological engineering, 2012
[9] Statul Major al Marinei Militare. *Norme privind pregătirea, organizarea şi protecţia muncii în activitatea de scufundare*". Constanta., 1996.

ANNEX NOTATIONS

$\dot{Q}_p\ [W]$ - total heat lost by the diver

m [kg] - mass diver

$c_c [J/kgK]$ - specific heat body

$t\ [s]$ - time

$\dot{Q}_m\ [W]$ - metabolic heat flux

T [K] – internal body temperature

T_0 [K] – initial body temperature

T_a [K] – water temperature

$\dot{Q}_c\ [W]$ - heat flux lost at skin level

$R_{(p)}\left[\frac{K}{m^2W}\right]$ - thermal resistance of the outer layers of human body

$\dot{Q}_r\ [W]$ - heat flux lost at respiratory level $K_{(p)}$ global coefficient thermal transfer at skin level

$\dot{Q}_x$ - latent heat flux that brings the inhaled dry gas to 100% humidity exhaled gas;

$\dot{Q}_s$ - sensible heat flux that increases the inhaled gas temperature to the body temperature

$l_{(p)[J/kg]}$ - specific vaporization latent heat

$\rho_{(p)}[kg/m^3]$ - gas density

$x_{(p)[kg/kg]}$ - absolute humidity of respiratory gas

$\dot{V}_{(p)}[m^3/s]$ - respiratory volume flow rate

c_p [J/kgK] - gas specific heat at constant pressure

c_H – Heliox correction factor

ISSN (Print): 1844-6116
ISSN (Online): 2501-8795 http://www.cmu-edu.eu/jmte

Journal of Marine technology and Environment Year 2017, Vol.1

THE USE OF SIMULATION IN REMEDIAL INTERVENTIONS TO MARINE AREAS POLLUTED BY OIL

Sundri Mirela-Iuliana[1], Panaitescu Mariana [2] & Panaitescu Fanel-Viorel [3]

[1]Constanta Maritime University, Faculty of Naval Electro-Mechanics, Department of Engineering Sciences and Environment, 104 Mircea cel Batran Street, 900663, Constanta, Romania, iuliana_sundri@yahoo.com
[2]Constanta Maritime University, Faculty of Naval Electro-Mechanics, Department of Engineering Sciences and Environment, 104 Mircea cel Batran Street, 900663, Constanta, Romania, marianapan@yahoo.com
3Constanta Maritime University, Faculty of Naval Electro-Mechanics, Department of Engineering Sciences and Environment, 104 Mircea cel Batran Street, 900663, Constanta, Romania, viopanaitescu@yahoo.ro

Abstract: Unloading of hydrocarbons into the marine environment has a signifiant economic impact for both the activities performed on the shores and exploiting the resources of the sea. In this context it is necessary to adopt a strategy and a national system of intervention to respond quickly and effectively in the event of a disaster caused by an accidental oil pollution in the area of the continental shelf or in the Romanian coastal belt. Quick resolution of such problems, as a result of work techniques developed as a result of simulations, reduces major negative consequences.

In the present work was chosen using two simulation programs, HYSPLIT and ADIOS,both developed by NOAA, for forecasting events due to oil spills of the Black sea romanian coast and the choice of methods of remediation For simulations were used two types of oils: Abu-Dhabi and Horcon. The results of simulatios were: visualizing graphs oil removal, the charts of evaporated oil, the oil dispersing proces, the content of water in oil, the concentration of benzene in air. HYSPLIT and ADIOS programs for simulation the processes of removal oil discharged into the sea permit: making a prognosis; evaluation methods of remediation; the possibility of taking measures in advance to protect areas located at shore.

Key words: simulation, pollution, sea, impact, oil, dispersion, prognosis, evaluation, shore, remediation.

1. INTRODUCTION

Marine pollution with hydrocarbons was recognized for the first time during the first World War (1914-1918). Starting from 1920 the different countries have adopted measures to prevent the discharge of oil into territorial waters, trying to hear to penalize illegal downloads by means of fines. The adoption of international measures were not realized until after second world war.

From 1950, the transport of hydrocarbons has known a large expansion, the danger of contamiation by becoming increasingly older.

Unloading of hydrocarbons into the marie enviroment has a signifiant economic impact for both the activities pwerformed on the shores and exploiting the resources of the sea. The presence of hydrocarbons on the surface of marine water causes consequences of physical, biological and social. Spread on the marine surface the petroleum pollutant is undergo specific chemical and physical evolution, depending on its mature and wheater conditions. By dispersion, emulsification and dissolution, the hydrocarbons alter the quality of the marine environment by impurification of water, by their concentration and accumulation of sediments in water and in organisms.

In this context it is necessary to adopt a startegy and a national system of intervention to respond quickly and effectively in the event of a disaster caused by an accidental oil pollution in the area of the continental shelf or in the romanian coastal belt.

Simulations represent a model of issues or events that can be used to learn what needs to be done in the case. There are many programs that can be simulated for various events that can occur in the environment, with different effects on the status of the natural ecosystems.

ISSN (Print): 1844-6116
ISSN (Online): 2501-8795 http://www.cmu-edu.eu/jmte

Quick resolution of such problems, as a result of work techniques developed as a result of simulation, reduces major negative consequences.

The present paper contains the results of simulations with two programs for two types of oils in the same conditions of simulation.

2. RESEARCH AND METHODOLOGY

It was chosen using two simulation programs, HYSPLIT and ADIOS, both developed by NOAA [1],[2], [3], [4], for forecasting events due to oil spills of the Romanian coast of Black Sea and the choise of methods of remediation [5], [6].

HYSPLIT program can be used in many applications for monitoring and impact studies on pollutio of the atmosphere generally and specifically with particles. His meteorological data base contains weather maps of the entire globe.

ADIOS, being designed program as a tool used in the process of responding to an oil pollution, allows a quick access to information about the properties of crude oil or refined, or about how a particular petroleum product may be scattered in the water.

For it was chosen from data base of ADIOS program two types of oil with different viscosity grades:

- HORCON (Mexico) with viscosity 996 cSt at 4^0C, 531 cSt at 14^0C and 351 cSt at 20^0C (Figure 1);
- ABU-DHABI (United Arab Emirates) wth viscosity 25.5 cSt la 4^0C, 13.6 cSt at 14^0C şi 9 la 21^0C (Figure 2).

2.1 Study assumptions:

Pollution simulation date: 8.02.2008.

Near 10 km from coast of the Black Sea, in point of city Constanta, instantaneous spill of (Figure 3):

ABU-DHABI oil : 1000 tons

HORCON: 1000 tons.

Oance at the surface oil participate in various chemical and physical processes, and, naturally, it evaporate or be dispersed with different speeds, depending on environmental conditions. Oil removal can be achieved through processes of dispersion, burning it on the spotor by “harvesting” with the help of skimmers. Oil removal process must take place in a short time, so that it will not reach the shore. For the choice of the methods of remediation it necessary to be known not only water, but also the atmospheric conditions at the time (Figure 1, Figure 2). For removal in a very short time has an important parts of oil discharged, if the incident occurred on the high seas and are weather conditions that lead to the movement of the smoke cloud, then burning is the first choice, especially since the efficiency is much higher in the early hours when volatile substances have not evaporated. In weather conditions from that time which require a wind speed of 10 m/s, the combustion process is difficult to start, but may have very high efficiency.

Oil Type
HORCON
Location = MEXICO
Synonyms = none listed
Product Type = crude
API = 20.8
Pour Point = -9 deg C
Flash Point = unknown
Density = 0.945 g/cc at 4 deg C
Viscosity = 996.1 cSt at 4 deg C
Adhesion = unknown
Aromatics = unknown

Emulsification
Mousse begins to form when 5% of the oil has evaporated.

Wind and Wave Conditions
Wind Speed = 10 m/s from 225 degrees
Wave Height = computed from wind speed, unlimited fetch (default)

Water Properties
Temperature = 4 deg C
Salinity = 15 ppt
Sediment Load = 50 g/m3 (avg. river/estuary)
Current = 1.0 m/s towards 18 degrees

Release Information
Instantaneous Release
Time of Release = February 08, 1700 hours
Amount Spilled = 1000 tons

Dispersant Operations
Dispersant Operation = 1
Time of Application = February 09, 1100 hours
Duration of Spray = 3 hours
Percent of Slick Sprayed = 70 %
Dispersant Effectiveness = 80 %

In-Situ Burn Operations
In-Situ Burn Operation = 1
Time of Burn = February 09, 0800 hours
Area of Burn = 10000 sq. meters
Oil Thickness = 55 mm

Figure 1 HORCON characteristics and details of incident.

ISSN (Print): 1844-6116
ISSN (Online): 2501-8795
http://www.cmu-edu.eu/jmte

Oil Type
ABU DHABI
Location = UNITED ARAB EMIRATES
Synonyms = none listed
Product Type = crude
API = --
Pour Point = -6 deg C
Flash Point = unknown
Density = 0.840 g/cc at 4 deg C
Viscosity = 25.5 cSt at 4 deg C
Adhesion = unknown
Aromatics = unknown

Emulsification
Mousse begins to form when 32% of the oil has evaporated.

Wind and Wave Conditions
Wind Speed = 10 m/s from 225 degrees
Wave Height = computed from wind speed, unlimited fetch (default)

Water Properties
Temperature = 4 deg C
Salinity = 15 ppt
Sediment Load = 50 g/m3 (avg. river/estuary)
Current = 1.0 m/s towards 18 degrees

Release Information
Instantaneous Release
Time of Release = February 08, 1700 hours
Amount Spilled = 1000 tons

Dispersant Operations
Dispersant Operation = 1
Time of Application = February 09, 0900 hours
Duration of Spray = 1 hours
Percent of Slick Sprayed = 50 %
Dispersant Effectiveness = 70 %

Figure 2 ABU-DHABI characteristics and details of incident

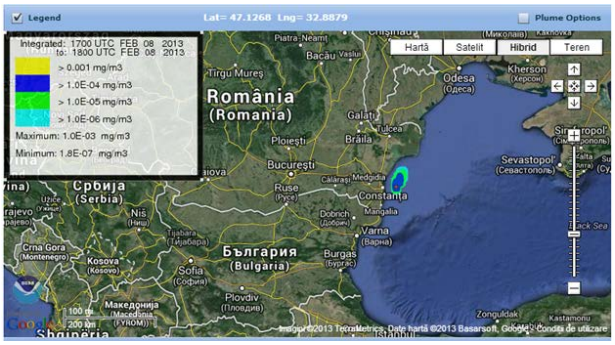

Figure 3 The incident location in the Black Sea [1]

3. RESULTS

3.1 HYSPLIT simulation

In 4 hours after ignition of oil smoke cloud would arrive over the Sulina city and would be retained in that area for 7 hours ago (Figure 4, Figure 5).

Considering the low particle concentration 1 μg/m^3, it is acceptable to use the method of combustion, where efficiency in the conditions of environmental data. It is proposed to use it in case of oil viscozity HORCON showing far greater and so is likely to be spreaded harder than oil ABU-DHABI.

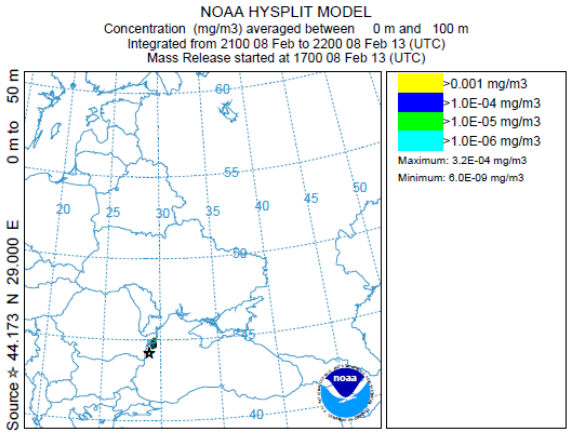

Figure 4 The cloud of smoke after 4 hours of travel from the place of incident [4]

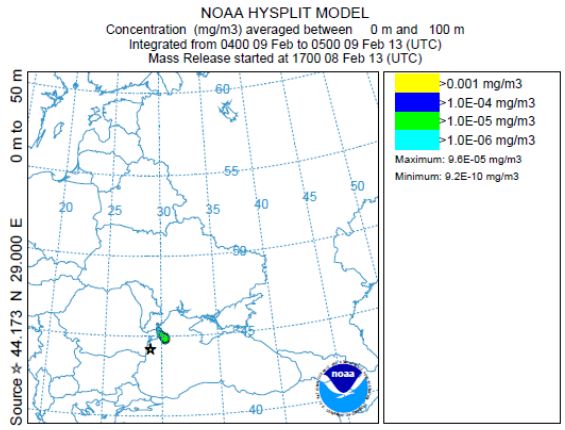

Figure 5 The cloud of smoke after 11 hours of travel from the place of incident [4]

ABU-DHABI's oil, according to the specific environment (Figure 2), presents naturally within the first 6 hours of the spill, the evaporation rate of ~ 33% and 10% spread (Figure 6)[7].

Very strong wind scattering the oil slick determines. Therefore, only a day after the incident would be effective.

The harvesting of oil with skimmers are very difficult during the storm, they propose an additional dispersion with chemicals, on the 9th February at 9 am, over 1 hour, on 50% of the surface of a puddle of oil, with an efficiency of 70%.

ISSN (Print): 1844-6116
ISSN (Online): 2501-8795
http://www.cmu-edu.eu/jmte

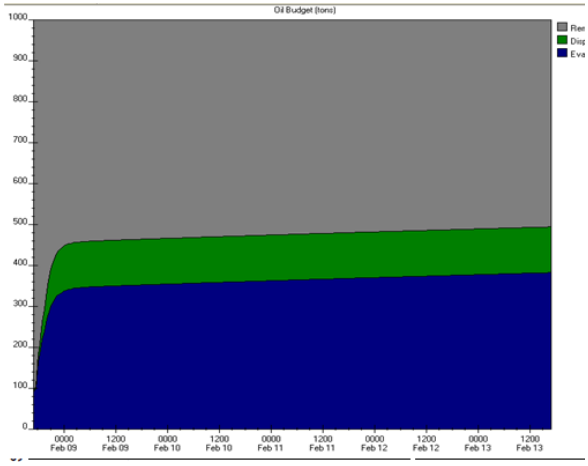

Figure 6 The evaporation and dispersion of oil ABU-DHABI

With a view t removing 80% of the amount of oil (33% through evaporation and the rest through dispersion) (Figure 7).

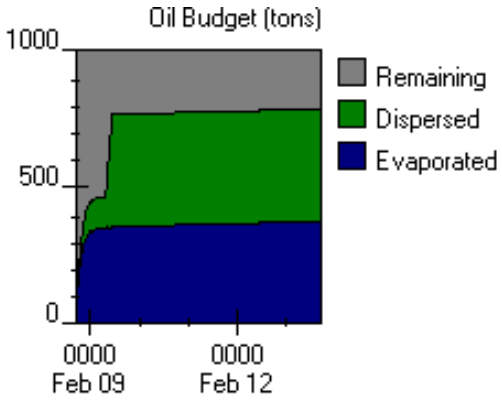

Figure 7 Oil budget

Due to strong winds from the S-SE direction and marine currents in the area, with the direction of the S-SV, supposedly the stain of oil was fragmented and blended with water, which causes the interruption of the oil removal methods until the storm [8].

3.2 ADIOS simulation

The ADIOS program allows you to view graphs of removal oil (Figure 8), evaporated oil (Figure 9), dispersed oil (Figure 10), the content of water in oil (Figure 11), the concentration of benzene in the air born (Figure 12).

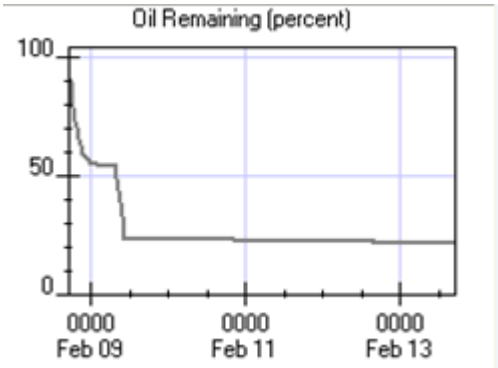

Figure 8 The removal of oil

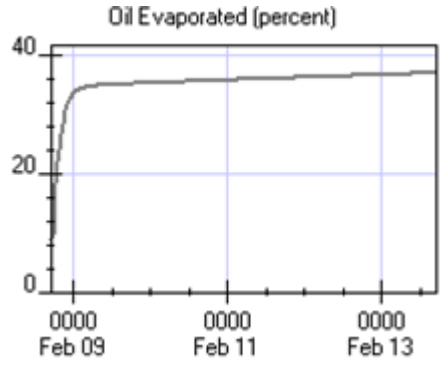

Figure 9 The evaporation of oil

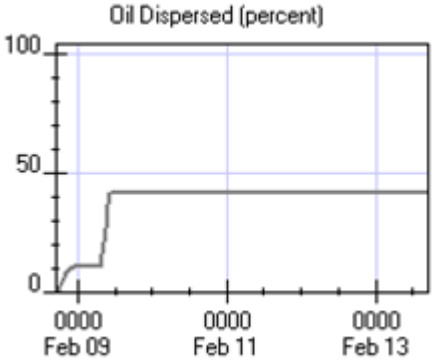

Figure 10 The dispersion of oil

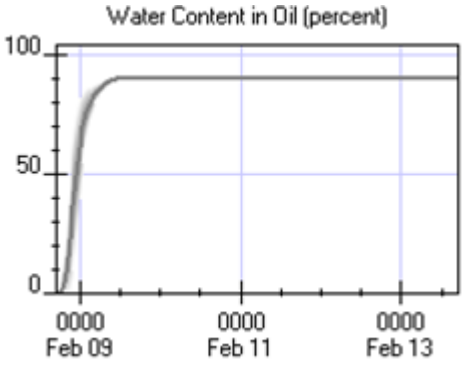

Figure 11 The content of water in oil

ISSN (Print): 1844-6116
ISSN (Online): 2501-8795
http://www.cmu-edu.eu/jmte

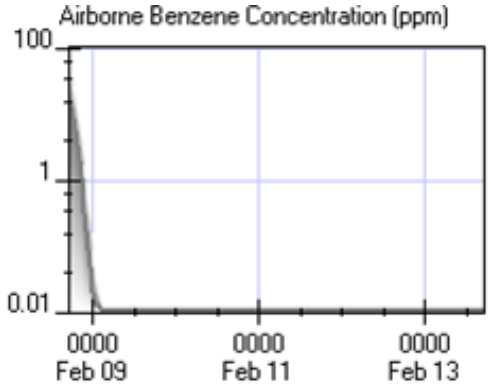

Figure 12 The airborne Benzene concentration

For HORCON oil under the same conditions of simulation (Figure 1), assume the use of the method of in situ combustion, the day after incident, at 8.00.

The burning took place in an area of 10 000 m^2 , for 22 minutes, the concentration of particles in the cloud of smoke being 150 μg in area up to 2000 m distance (Figure 13). At 11.00 apply dispersants for 3 hours on 70% of the surface, with an efficiency of 80%.

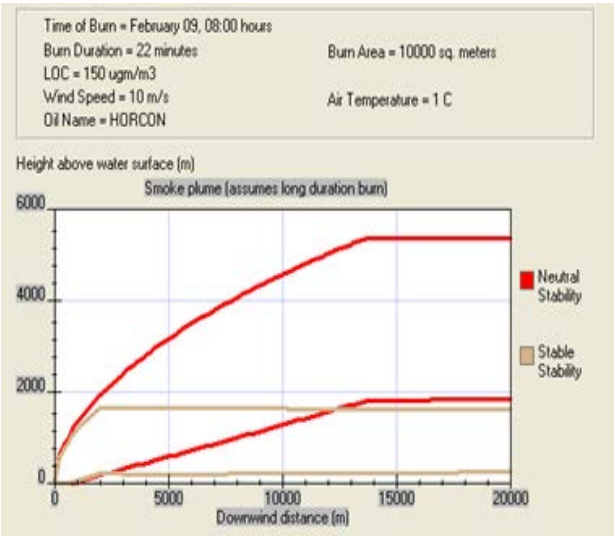

Figure 13 The smoke plume

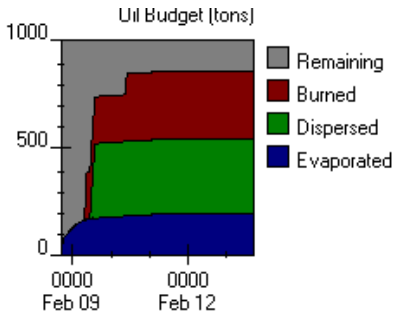

Figure 14
Oil budget

Finally, the process implemented in leading to the removal of approximatelly 90% of oil discharged (Figure 14).

5. CONCLUSIONS

The use of HYSPLIT and ADIOS programs in simulation for removal of oil discharged into the sea allows:

- the user's familiarity with the methods used for removing oil;
- making a prognosis regarding the fate of oil discharged into the environment, depending on the type of oil and weather conditions;
- evaluation methods of remediation, facilitating the decision in choosing the most suitable, according to quality of oil and weather conditions;
- the possibility to apply the measures in advance to protect areas located at shoreline, in the case of the movement of the volatile evaporated compounds or cloud of smoke resulting from the combustio of oil.

6. REFERENCES

[1] Draxler, R.R., G.D. Hess, 2004, *Description of the HYSPLIT_4 Modeling System*, NOAA Technical Memorandum ERL ARL-224, Revised January 2004.
[2] Leung Siu Ki, F., 2006, B*ackward Trajectory Analysis using NOAA HYSPLIT Model*, Summer Internship at the Hong Kong Observatory.
[3] *** HYSPLIT, 2009, *User's guide*, Version 4.9, January, 2009.
[4] http://www.arl.noaa.gov/ready/hysplit4.html
[5] http//response restoration.noaa.gov//adios
[6] Samuels, W., Amstutz, D., Bahadur, R., 2013, *Development of a Global Oil Spill Modeling System*, Earth Science Research, vol. 2, (2).
[7] Dumitrescu, L.G., Voicu, I., Panaitescu, F.V., Panaitescu, M., 2015, *The evolution of an accidental release of oil, near Burgas*, Journal of Marine Technology and Environment, vol. 2, pp. 31-35, Nautica Publish House.
[8] Dumitrescu, L.G., Voicu, I., Panaitescu, F.V., Panaitescu, M., 2015, *Oil leakage simulation and spill prediction near Odessa harbour*, Journal of Marine Technology and Environment, vol. 2, pp.27-31, Nautica Publish House.

ISSN (Print): 1844-6116
ISSN (Online): 2501-8795 http://www.cmu-edu.eu/jmte

ISSN (Print): 1844-6116
ISSN (Online): 2501-8795 http://www.cmu-edu.eu/jmte

Journal of Marine technology and Environment Year 2017, Vol.1

V-BELT TRANSMISSION DESIGN EFFICIENCY, USING MATHCAD PROGRAM

Turof Mihaela

Constanta Maritime University, Faculty of Naval Electro-Mechanics, 104 Mircea cel Batran Street, 900663, Constanta, Romania, e-mail address:mihaela_turof@yahoo.com

Abstract : The Mathcad interface allows users to combine a variety of different elements (mathematics, descriptive text, and supporting imagery) into the form of a worksheet, which is naturally readable. Because the mathematics are core to the program, the math is inherently live, dynamically recalculating as upstream values are altered. This allows for simple manipulation of input variables, assumptions, and expressions, which in turn update in real-time.
The paper proposes the design by using Mathcad program of V-belt drives for speed reducer with a spur wheel stage.

Key words : mathcad program, speed reducer, V-belt drives.

1. INTRODUCTION

Mathcad, Parametric Technology Corporation's engineering calculation solution, is used by engineers and scientists in various disciplines – most often those of mechanical, chemical, electrical, and civil engineering. Originally conceived and written by Allen Razdow (of MIT, co-founder of Mathsoft), Mathcad is now owned by PTC and is generally accepted as the first computer application to automatically compute and check consistency of engineering units such as the International System of Units (SI), throughout the entire set of calculations. Mathcad today includes some of the capabilities of a computer algebra system, but remains oriented towards ease of use and simultaneous documentation of numerical engineering applications.

Mathcad is oriented around a worksheet, in which equations and expressions are created and manipulated in the same graphical format in which they are presented - as opposed to authoring in plain text, an approach later adopted by other systems such as Mathematica and Maple.

Mathcad is part of a broader product development system developed by PTC, and often utilized for the many analytical touch points within the systems engineering processes. It integrates with PTC's other solutions that aid product development, including Creo Elements/Pro, Windchill, and Creo Elements/View. Its live feature-level integration with Creo Elements/Pro enables Mathcad analytical models to be directly used in driving CAD geometry, and its structural awareness within Windchill allows live calculations to be re-used and re-applied toward multiple design models.

The paper proposes the design by using Mathcad program of V-belt drives for speed reducer with a spur wheel stage.

2. REDUCER DESIGN SPECIFICATION

Consider a speed reducer with a cylindrical stage spur gear with the following specifications:

- → The speed of the shaft II has to be $n_{II} = 1000 RPM$
- → The power for the second shaft is $P_{II} = 24 kW$
- → The transmission ratio of the reducer is $i_R = 2$
- → The mean time in service between two successive repairs Lh= 9000 hours.

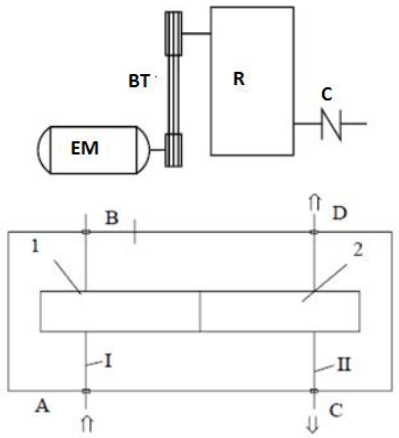

Figure 1 Cinematic scheme of speed reducer with a step

ISSN (Print): 1844-6116
ISSN (Online): 2501-8795 http://www.cmu-edu.eu/jmte

In the Figure 1:
EM – electrical motor;
BT – belt transmission;
R – reducer;
C – coupling.

In the diagram above the reducer shafts are denoted with I and II as they are transmitting the motion, the gears are 1 and 2 and the bearings are A and B for the shaft I and C and D for shaft II.

As a function of the designed machine particularities and the service environment , the designer is free to select an overloading coefficient, in our case this will be $C_S = 1$

This coefficient is usually given in the machine design specification and since the costumer is not specifying it the designer is free to suppose that the reducer is for general usage and so the chosen $C_S = 1$.

But usually it is bigger than one.

3. CALCULATION OF THE TRANSMISSION RATIOS IN ORDER TO SELECT THE ELECTRICAL MOTOR

The overall transmission ratio is :

$$i_{tot} = \frac{n_M}{n_{II}}, \quad (1)$$

where n_M is the speed of the electric motor and n_{II} is the speed of the second reducer shaft.

One may write:

$$i_{tot} = i_{BT} \cdot i_R, \quad (2)$$

where i_R is the ratio of the reducer and i_{BT} the belt transmission ratio.

The reducer's electrical motors usually are working for long periods of time with constant loading and for this situation the electrical motor power will be:

$$P_{EM} = \frac{P_{II}}{\eta_{tot}} = \frac{P_{II}}{\eta_{BT} \cdot \eta_b^2 \cdot \eta_{12}}, \quad (3)$$

where:

η_{tot} – is the total efficiency of the transmission assembly;

η_{BT} – is the efficiency of the belt transmission;

η_b – is the bearing efficiency;

η_{12} – is the efficiency of the gears.

In the following table are shown some efficiencies to be use in calculation:

Table 1. Efficiency value

Friction joints	***Efficiency***
Gearing	0,97...0,99
Belt Transmission	0,94...0,97
Bearing pair	0,99...0,995

$$P_{EM} = \frac{24}{0{,}94 \cdot 0{,}99^2 \cdot 0{,}97} = 26{,}85kW \cdot \quad (4)$$

We choose the Electrical Motor type *200La* with the nominal power $P_{EMN} = 30kW > 26{,}85kW$ and the speed $n_1 = 2870rot/\min > n_{I-II} = 1000 \cdot 2 = 2000rot/\min$ imposed by the design specification.

The moments developed for the two shafts of the reducer are:

$$M_{tI,II} = \frac{955 \cdot 10^4 \cdot P_{EMN}}{n_{I-II}}; \quad (5)$$

$$M_{tI} = \frac{955 \cdot 10^4 \cdot 30}{2000} = 143250Nmm, \quad (6)$$

$$M_{tII} = \frac{955 \cdot 10^4 \cdot 30}{1000} = 286500Nmm \cdot \quad (7)$$

We'll have:

$$i_{tot} = \frac{n_1}{n_{II}} = \frac{2870}{1000} = 2{,}87 \cdot \cdot \quad (8)$$

For a cylindrical gear the recommended ratio is inside the range 2.5 ... 6.3 with a maximum of 10.

For the transmission belt:

$$i_{BT} = \frac{i_{tot}}{i_R} = \frac{2{,}87}{2} = 1{,}435 \cdot \quad (9)$$

For the first transmission belt pulley the moment is:

$$M_{tTBI} = \frac{955 \cdot 10^4 \cdot 30}{2870} = 100526Nmm \cdot \quad (10)$$

4. TRANSMISION BELT DESIGN

This transmission allows the transmission of power and motion rotation between parallel shafts. Construction has two gear wheels that intermediate element is wound elastic and flexible strap, fitted with pretension (initial tensile force) is recommended distances between the axes of rotation of the drive shaft and the drive.

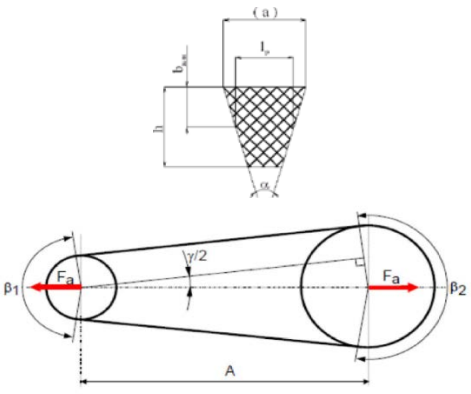

Figure 2 The V-Belt section and geometry

ISSN (Print): 1844-6116
ISSN (Online): 2501-8795 http://www.cmu-edu.eu/jmte

The calculation stages are:

• Selecting the V-belt is based on the chart shown in the Figure 3 for narrow V-Belts as a function of the EM power $P_{EMN} = 30kW$ and the speed of the first pulley $n_1 = 2870rot/\min$

The selected type is *SPA* with $Dp_1 = 90...250mm$.

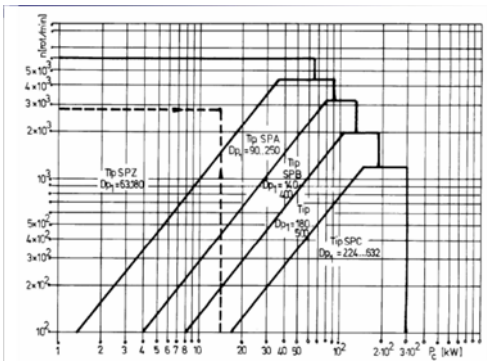

Figure 3 Chart for V-belt selection

Table 2. V-belt dimensions

Type	Dimension $l_P x h$	a mm	h ± δ h mm	$D_{\max}$ mm	α grade	Primitive lenght L_p mm		$D_{p\min}$ mm	Section area cm²
						Minim	Maxim		
SPZ	8,5x8,0	-	8±0,4	2,0	40±0,1	630	3550	71	0,54
SPA	11,0x10	-	10±0,5	2,8		800	4500	100	0,90
SPB	14,0x13	-	13±0,5	3,5		1250	8000	160	1,50
16x15	16,0x15	-	15±0,5	4,0		1600	10000	200	1,98
SPC	19,0x18	-	18±0,6	4,8		2000	12500	224	2,78

Primitive Lenght L_p mm	Preffered	400	500	630	800	1000	1250	1600	2000
		2500	3150	4000	5000	6200	8000	10000	12500
	To be avoided	450	560	710	900	1120	1400	1800	2240
		2800	3550	4500	5600	7100	9000	11200	-

Primitive Lenght L_p	450	500	560	630	710	800	900	1120	1250	1400	1600	1800	2000	2500
Primitive Diameter D_{p1}	63	71	80	90	112	125	140	160	180	200	224	250	280	315

The narrow V-Belts have the advantage of a smaller size. The zone where the perpendicular lines falls is within the SPZ region, but being close to the oblique line border we are allowed to go for a SPA type.

• In order to choose the primitive diameter of the driving pulley *Dp*1 we'll use table 2 from standard

We choose $D_{p1} = 125mm$

• Calculation of the diameter of the driven pulley:

$$D_{p2} = i_{BT} \cdot D_{p1} = 1{,}435 \cdot 125 = 179{,}37 \approx 180mm. \quad (11)$$

If no restrictions are in place to dictate the maximum diameter of the pulley (and we haven't) the closest diameter from table 2 is chosen.

• In order to calculate the center distance of the pulleys:

$$0{,}7 \cdot (D_{p1} + D_{p2}) = 0{,}7 \cdot (125 + 180) = 213{,}5mm \le A_{prel};$$

$$A_{prel} \le 2 \cdot (D_{p1} + D_{p2}) = 2 \cdot (125 + 180) = 610mm \quad (12)$$

$$\Rightarrow \quad 213{,}5mm \le A_{prel} \le 610mm. \quad (13)$$

ISSN (Print): 1844-6116
ISSN (Online): 2501-8795
http://www.cmu-edu.eu/jmte

We'll choose a preliminary distance $A_{prel} = 400mm$.

• The angle between branches is:

$$\gamma_{prel} = 2 \cdot \arcsin\left(\frac{D_{p2} - D_{p1}}{2A_{prel}}\right) = \quad (14)$$

$$= 2 \cdot \arcsin\left(\frac{180-125}{2 \cdot 400}\right) = 7{,}88°$$

• The contact angle for the driving and driven pulleys:

$$\beta_{1prel} = 180° - \gamma_{prel} = 180° - 7{,}88° = 172{,}22°; \quad (15)$$

$$\beta_{2prel} = 180° + \gamma_{prel} = 180° + 7{,}88° = 187{,}88°. \quad (16)$$

• Primitive length of the V-belt

$$L_{pinitial} = 2 \cdot A + \frac{\pi(D_{p1} + D_{p2})}{2} + \frac{(D_{p2} - D_{p1})^2}{4 \cdot A} \quad (17)$$

$$L_{pinitial} = 2 \cdot 400 + \frac{\pi(180+125)}{2} + \frac{(180-125)^2}{4 \cdot 400} =$$

$$= 800 + 479{,}09 + 1{,}89 = 1281mm \quad (18)$$

The primitive length will be chosen from the Table 2 (the closest value).

We'll take $L_p = 1250mm$

• Now we'll recalculate the real distance between pulley axis:

$$A \approx \frac{L_p - \frac{\pi(D_{p1} + D_{p2})}{2}}{2} = \frac{1250 - 479{,}09}{2} = 385{,}45mm. \quad (19)$$

• Belt peripheral speed (for driving pulley):

$$v = \frac{\pi \cdot D_{p1} \cdot n_1}{60000} = \frac{\pi \cdot 125 \cdot 2870}{60000} = 18{,}78m/s. \quad (20)$$

It is recommended that the peripheral speed to be less than *30 m/s* for the normal V-Belts and less than *40 m/s* for narrow *V Belts.*

• The preliminary number of V Belts in transmission:

$$z_0 = \frac{c_f \cdot P_c}{c_L \cdot c_\beta \cdot P_0}, \quad (21)$$

where:

$P_c = 30kW$

$c_L = 0{,}89$ – length coefficient as a function of the primitive length L_p from Table 3

c_f – is the service coefficient chosen in function of the driving engine (electrical motor) and the machine driven by the reducer. We'll take $c_f = 1$ since the reducer is for general usage.

c_β – the contact angle coefficient is:

$c_\beta = 1 - 0{,}003(180 - \beta_1) = 0{,}9766$;

$P_0 = 6{,}12kW$ - is the nominal power one belt can transmit and the value is taken from the standard. For intermediate values one may use the linear interpolation.

Table 3. Length coefficient

Primitive Lenght L_p **mm**	**Belt type**			
	SPZ	**SPA**	**SPB**	**SPC**
400				
450				
500				
560				
630	0,82			
710	0,84			
800	0,86	0,81		
900	0,88	0,83		
1000	0,9	0,85		
1120	0,93	0,87		
1250	0,94	0,89	0,82	
1400	0,96	0,91	0,84	
1600	1,00	0,93	0,86	
1700	1,01	0,94	0,87	
1800	1,01	0,95	0,88	
2000	1,02	0,96	0,90	
2240	1,05	0,98	0,92	0,82
2500	1,07	1,00	0,94	0,86
2800	1,09	1,02	0,96	0,88
3150	1,11	1,04	0,98	0,90
3550	1,13	1,06	1,00	0,92
3750	-	1,07	1,01	0,93
4000	-	1,08	1,02	0,94

$$z_0 = \frac{1 \cdot 30}{0{,}89 \cdot 0{,}9766 \cdot 6{,}12} = 5{,}6, \quad (22)$$

z_0 – the preliminary number as seen above is not integer.

The final number is:

$$z = \frac{z_0}{c_z} = \frac{0{,}56}{0{,}85} = 6{,}63 \approx 7, \quad (23)$$

where c_z is the belts number coefficient taken from Table 4. The final number is rounded to integer. It is recommended that $z \leq 8$.

Table 4. Belt number coefficient

Preliminary belt number z_0	c_z
2...3	0,95
4...6	0,90
over 6	0,85

ISSN (Print): 1844-6116
ISSN (Online): 2501-8795
http://www.cmu-edu.eu/jmte

• The bending frequency of the belt is:

$$f = 10^3 \cdot x \cdot \frac{v}{L_p} = \frac{1000 \cdot 2 \cdot 18{,}78}{1250} = 30{,}048\,, \quad (24)$$

where
x - is the number of the pulleys,
v - is the peripheral speed of the belt,
L_p - is the primitive length.

It is recommended that the bending frequency to be below 40 Hz…80 Hz.

The force transmitted is:

$$F = 1000 \cdot \frac{P_c}{v} = 1000 \cdot \frac{30}{18{,}78} = 1597N \quad (25)$$

The tensioning force F_0 and the pushing force against the shafts F_a is:

$$F_0 = F_a = (1{,}5...2) \cdot F = 1{,}7 \cdot 1597 = 2715N \quad (26)$$

The belts and the pulleys are standardized so that the shape and dimensions are shown in Figure 4.

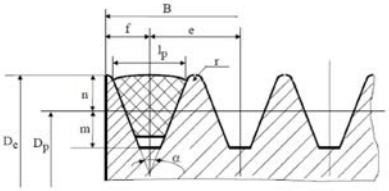

Figure 4 Pulley shape

The width of the pulley is:

$$B = (z-1) \cdot e + 2f = (7-1) \cdot 15 + 2 \cdot 10 = 110mm \quad (27)$$

From the standard we have:

$e = 15$

$f = 10$

5. MATHCAD SOFTWARE APPLICATION FOR DESIGNING BELT DRIVES

The calculation program MATHCAD initial design data is entered. Enter formulas and standards chosen dates thereafter. The program calculates and generates results.

MATHCAD application program looks like this:

Introduce your data in the yellow fields

VARIABLE

nII := **1000**

PII := **24**

iRT := **2**

Lh := **9000**

ηTCT := **0.94**

ηr := **0.99**

ηa12 := **0.97**

Dp1 := **125**

cL := **0.89**

cf := **1**

P0 := **6.12**

e := **15**

f := **10**

FORMULAS

$$PMinitial := \frac{PII}{\eta TCT \cdot (\eta r)^2 \cdot \eta a12}$$

PMinitial = **26.856**

PM := **30**

n1 := **2870**

cz := **0.85**

$$itot := \frac{n1}{nII}$$

$$iTCT := \frac{itot}{iRT}$$

Dp2initial := iTCT·Dp1

Dp2initial = **179.375**

Dp2 := **180**

LimitaStanga_Aprel := **0.7**·(Dp1 + Dp2)

LimitaDreapta_Aprel := **2**·(Dp1 + Dp2)

LimitaStanga_Aprel = **213.5**

LimitaDreapta_Aprel = **610**

Aprel := **400**

$$\gamma prel := 2 \cdot a\sin\left(\frac{Dp2 - Dp1}{2 \cdot Aprel}\right)$$

$$\beta 1 prel := \pi - \gamma prel$$

$$\beta 2 prel := \pi + \gamma prel$$

$$Lpinitial := \left[2 \cdot Aprel + \frac{\pi \cdot (Dp1 + Dp2)}{2}\right] + \frac{(Dp2 - Dp1)^2}{4 \cdot Aprel}$$

Lpinitial=1.281 x 10³

ISSN (Print): 1844-6116
ISSN (Online): 2501-8795 http://www.cmu-edu.eu/jmte

Lp := **1250**

$$A := \frac{Lp - \frac{\pi \cdot (Dp1 + Dp2)}{2}}{2}$$

$$\gamma := 2 \cdot a\sin\left(\frac{Dp2 - Dp1}{2 \cdot A}\right)$$

$\beta 1 := \pi - \gamma$

$\beta 2 := \pi + \gamma$

$$v := \frac{\pi \cdot Dp1 \cdot n1}{60000}$$

$$\beta 1grade := \frac{\beta 1 \cdot 180}{\pi}$$

cβ := **1 - 0.003 x** (**180 -** β1grade)

$$z0 := \frac{PM \cdot cf}{cL \cdot c\beta \cdot P0}$$

z0 = **5.646**

$$zfinal := \frac{z0}{cz}$$

zfinal = **6.643**

z := **7**

$$f := \frac{1000 \cdot 2 \cdot v}{Lp}$$

$$F := \frac{1000 \cdot PM}{v}$$

F0 := **1.7**·F

B := (z – **1**)·e + **2**·f

REZULTS

itot = **2.87** [N/mm2]

iTCT = **1.435**

γprel = **0.138** [rad]

β1prel = **3.004** [rad]

β2prel = **3.279** [rad]

A = **385.454**

v = **18.784**

cβ = **0.975**

f = **30.055**

F = **1.597** × **10**^{3}

F0 = **2.715** × **10**^{3}

B = **150.109**

6. CONCLUSIONS

Making a machine is a complex process which, based on an accumulation of knowledge and previous achievements and a objective necessity (usually), passing through various stages, reaching final product.

The Mathcad interface allows users to combine a variety of different elements (mathematics, descriptive text, and supporting imagery) into the form of a worksheet, which is naturally readable. Because the mathematics are core to the program, the math is inherently live, dynamically recalculating as upstream values are altered. This allows for simple manipulation of input variables, assumptions, and expressions, which in turn update in real-time.

By introducing the Mathcad software in design of machine design is made interactive and easier data processing. In application created can be modified easily input data to obtain more rapid project results.

The present paper realise the design by using Mathcad program of V-belt drives for speed reducer with a spur wheel stage.

7. REFERENCES

[1] Ciortan S., Bologa O., Ioniță B., *Mathcad, proiectare interactivă*, Ed. Zigotto, Galați, 2003.
[2] Drăghici I. ș.a., *Îndrumar de proiectare în construcţia de maşini*, Vol. I,II Editura Tehnică,1982, 1983.
[2] Gafiţanu M. ș.a., *Organe de maşini*, Vol I,II, Ed. Tehnică, 1982, 1983.
[3] Pavelescu D. ș.a., *Organe de maşini*, Ed. Didactică şi Pedagogică Buc., 1986.
[4] Rădulescu Gh. ș.a., *Îndrumar de proiectare în construcţia de maşini*, Vol. III Editura Tehnică.
[5] Zidaru N., *Transmisii mecanice*, Ed. Printech, Bucureşti, 2004.
[6] T9-Maritime and Coastguard Agency (MCA), Code of Safe Working Practices for Merchant Seamen, London. The Stationery Office Publications Centre, Consolidated Edition, 2009 (ISBN 9780115530784)
[7] T13-Pritchard, R.T. Technician Workshop Processes and Materials. London, Hodder and Stoughton, 1979 (ISBN 0-34022-100-3) OUT OF PRINT, 1999
[8] Machines elements-CAD Induction/ Organe de Masini-Elemente de proiectare asistata de calculator/- Ediţie bilingva engleza-romana-2013-Editura Nautica-Ioan Calimanescu , Lucian Grigorescu, Viorica Popa.
[9] http://en.wikipedia.org/wiki/Matchcad

ISSN (Print): 1844-6116
ISSN (Online): 2501-8795 http://www.cmu-edu.eu/jmte

Journal of Marine technology and Environment Year 2017, Vol.1

DETERMINATION OF RELIABILITY FEATURES USING BAYES' THEOREM

Turof Mihaela

Constanta Maritime University, Faculty of Naval Electro-Mechanics, 104 Mircea cel Batran Street, 900663, Constanta, Romania, e-mail address:mihaela_turof@yahoo.com

Abstract: Bayes' theorem is one of the fundamental theorems of probability, which determines the probability of events and objects belonging to a certain group.

Reliability is considered in some sense a probability. To determine some characteristics of reliability, it is possible to use Bayes formula. Bayes' theorem can be used to review the likelihood of a specific event that already happened, it can be repeated again.

Some examples of application of Bayes' theorem in the technical field are presented in this paper, attempting to explain why this theorem is called the inverse probability law: we can use condiţional probability to make a prediction in reverse and to improve our prediction of events.

Key words : Bayes' theorem, characteristics of reability, conditional probabilities.

1. INTRODUCTION

In probability theory and statistics, Bayes' theorem (alternatively Bayes' law or Bayes' rule) describes the probability of an event, based on prior knowledge of conditions that might be related to the event.

One of the many applications of Bayes' theorem is Bayesian inference, a particular approach to statistical inference. When applied, the probabilities involved in Bayes' theorem may have different probability interpretations. With the Bayesian probability interpretation the theorem expresses how a subjective degree of belief should rationally change to account for availability of related evidence. Bayesian inference is fundamental to Bayesian statistics.

Bayes' theorem is named after Rev. Thomas Bayes (1701–1761), who first provided an equation that allows new evidence to update beliefs. It was further developed by Pierre-Simon Laplace, who first published the modern formulation in his 1812 "Théorie analytique des probabilités." Sir Harold Jeffreys put Bayes' algorithm and Laplace's formulation on an axiomatic basis. Jeffreys wrote that Bayes' theorem "is to the theory of probability what the Pythagorean theorem is to geometry.

If A and B are two events, Bayes' theorem allows us to calculate the probability of A given B if we knows the probability of B given A and the probabilities of each event alone.

The definition of condiţional probability:

Denoting by $P(A \mid B)$ *the probability of A given B,* $P(B \mid A)$ *the probability of B given A and by* $P(A \cap B)$ *or* $P(A, B)$ *the joint probability of A and B,*

$$P(B \mid A) \cdot P(B) = P(A \cap B) = P(B \mid A) \cdot P(A). \quad (1)$$

If, dividing left and righthand sides by $P(B)$ we obtain the Bayes' theorem:

$$P(A \mid B) = \frac{P(B \mid A) \cdot P(A)}{P(B)}. \quad (2)$$

Each term in Bayes' theorem has a convenţional name:

- → term $P(A)$ - is the prior probability of A
- → term $P(B)$ - is the prior or marginal probability of B
- → term $P(A \mid B)$ - is the posterior probability of A given B
- → term $P(B \mid A)$ - is the likelihood function for A

It is „prior" in the sense that it precedes any information about B.

It is „posterior" in the sense that it is derived from by the specified value of B.

ISSN (Print): 1844-6116
ISSN (Online): 2501-8795 http://www.cmu-edu.eu/jmte

More generally, if A_i and A_j are mutually exclusive events

$$P(A_i \mid B) = \frac{P(B \mid A_i) \cdot P(A_i)}{\sum P(B \mid A_j) \cdot P(A_j)}. \quad (3)$$

2. APPLYNG BAYES' THEOREM - NUMERICAL EXAMPLE

In the simplest case of only two hypotheses M_1 and M_2, we suppose we know that precisely one of two hypotheses must be true. If we know their „prior" probabilities $P(M_1)$ and $P(M_2)$ and the conditional probabilities, written as $P(D \mid M_1)$ and $P(D \mid M_2)$, we can to compute the posterior probabilities, if an event D is observed.

Let's suppose the case of a machine shafts failure, considering that:

- 30% of failures are generated by over loading (hypothesis M_1)
- 70% of failures are generated by execution errors and incorrect (hypothesis M_2)

We consider that:

- ⇨ 20% of overloading failures are broken shaft
- ⇨ 15% of other causes produce broken shafts

How probable is it that overloading generated the failure if we consider an event of broken shaft.

The prior probabilities of M_1 and M_2 events:

- $P(M_1) = 0{,}3$
- $P(M_2) = 0{,}7$

The data D consist in the observation of a broken shaft.

Conditioned probabilities are:

- $P(D \mid M_1) = 0{,}2$
- $P(D \mid M_2) = 0{,}15$

Then the Bayesian formula is:

$$P(M_1 \mid D) = \frac{P(M_1) \cdot P(D \mid M_1)}{P(M_1) \cdot P(D \mid M_1) + P(M_2) \cdot P(D \mid M_2)}, \quad (4)$$

$$P(M_1 \mid D) = \frac{0{,}3 \cdot 0{,}2}{0{,}3 \cdot 0{,}2 + 0.7 \cdot 0{,}15} = \frac{0{,}06}{0{,}165} = 0{,}363. \quad (5)$$

With Bayes' formula was determinate „posterior" probability of the hypothesis M_1, based on the „data" that the event „observation of a broken shaft" was occurred.

3. BAYES'S FORMULA – BASSICALY USE

We consider that we know the „prior" probabilities mutually excluding events occur, on the base that an event D has already happened, we notice that we can calculate the conditioned probability.

The events A_i is the „prior" probabilities (that are known beforehand) and are considered causes or hypotheses and their probabilities $P(M_1)$. They are known for other experiments or are approximately based on the observations of similar events, or are considered as known and by checking the correct approximation after their determination.

If an event D („data") has really occurred and was observed, we can determine the conditioned probability $P(H_i \mid D)$ that is „posterior" probability.

It is correctly considered in the initial phase of calculus, the Bayes' formula combines the information given by „priori" probabilities with the information given by the real occurrence of an event (that „conditioned the other probabilities") and result „posterior probability" (after the calculation).

Let's consider a new design that has functioned 8000 hours to the first failure and suppose that failures are an exponential model, with reliability:

$$R(t) = e^{-\alpha t}, \quad (6)$$

where:

$R(t)$ - is reability function

α - is failure rate ($\alpha = $ constant)

t - is the time

We propose the „prior" value for α:

- → $\alpha_1 = \frac{1}{1000}$ - for the very accurate design
- → $\alpha_2 = \frac{2}{1000}$ - for the approximate design

We consider the prior probability

- ⇨ $P(\alpha = \alpha_1) = 0{,}8$ - 80% of the previous causes the design was very accurate
- ⇨ $P(\alpha = \alpha_2) = 0{,}2$ - 20% approximate design

Reability function is:

$$R(t) = P(\alpha = \alpha_1) \cdot e^{-\alpha_1 t} + P(\alpha = \alpha_2) \cdot e^{-\alpha_2 t}, \quad (7)$$

$$R(t) = 0{,}8 \cdot e^{\frac{-t}{1000}} + 0{,}2 \cdot e^{\frac{-2t}{1000}}. \quad (8)$$

ISSN (Print): 1844-6116
ISSN (Online): 2501-8795 http://www.cmu-edu.eu/jmte

The conditioned probabilities are:

$$P(A|\alpha=\alpha_1)=1-e^{-\alpha_1 t_0}=1-e^{\frac{-t_0}{1000}}; \quad (9)$$

$$P(A|\alpha=\alpha_2)=1-e^{-\alpha_2 t_0}=1-e^{\frac{-2t_0}{1000}}. \quad (10)$$

The Bayes' formula is:

$$P(\alpha=\alpha_1|t_0=8000)= =\frac{P(\alpha=\alpha_1)\cdot P(A|\alpha=\alpha_1)}{P(\alpha=\alpha_1)\cdot P(A|\alpha=\alpha_1)+P(\alpha=\alpha_2)\cdot P(A|\alpha=\alpha_2)} \quad (11)$$

$$P(\alpha=\alpha_1|t_0=8000)= =\frac{0{,}8\cdot\left(1-e^{\frac{-8000}{1000}}\right)}{0{,}8\cdot\left(1-e^{\frac{-8000}{1000}}\right)+0{,}2\left(1-e^{\frac{-2\cdot 8000}{1000}}\right)}=q_1; \quad (12)$$

$$P(\alpha=\alpha_2|t_0=8000)=1-q_1, \quad (13)$$

$$R(t)=q_1\cdot e^{\frac{-t}{1000}}+(1-q_1)\cdot e^{\frac{-2t}{1000}}. \quad (14)$$

In the (14) relation we can consider many values for t and determine for reability for different times to the fist failure.

4. APPLYING BAYES' FORMULA IN RELIABILITY TESTS

Let's consider a new design, with failure rate $\alpha=10^{-4}$ failure per hour and 95% probability. The purpose is to realize a reability testing for 10.000 hours to the first failure.

This testing plan is considered expensive. For Bayesian approximation, we use the result of prior tests, applied to similar devices, but having some differences.

Denominate X, Y, Z three devices previously tested, for that we know:

- 2 failures in 60.000 hours for device X
- 1 failure in 60.000 hours for device Y
- 5 failures in 50.000 hours for device Z

We design 11 caracteristics (rotation per minute, wear, costs, etc.) to consider the similities and differences for X, Y and Z devices.

The similarity factors are defined as:

$$q_{X,Y,Z}=\frac{\sum q_i}{total\_number\_of\_caracteristics}. \quad (15)$$

where:

q_i - is the factor for identical characteristics

We have:

- 7 identical characteristics for device X
- 5 identical characteristics for device Y
- 5 identical characteristics for device Z

To calculate the factor:

→ $q_X=\frac{7}{11}$ for device X

→ $q_Y=\frac{5}{11}$ for device Y

→ $q_Z=\frac{5}{11}$ for device Z

The echivalent time are:

$$(T_0)_X=q_x\cdot 60000=\frac{7}{11}\cdot 60000=; \quad (16)$$
$$=38182 hours$$

$$(T_0)_Y=q_Y\cdot 60000=\frac{5}{11}\cdot 60000=; \quad (17)$$
$$=27273 hours$$

$$(T_0)_Z=q_Z\cdot 50000=\frac{5}{11}\cdot 50000=. \quad (18)$$
$$=22727 hours$$

The equivalent number of failures are:

$$(S_0)_X=q_x\cdot 2=\frac{7}{11}\cdot 2=1{,}27\ failures; \quad (19)$$

$$,(S_0)_Y=q_Y\cdot 1=\frac{5}{11}\cdot 1=0{,}46\ failures, \quad (20)$$

$$(S_0)_Z=q_Z\cdot 5=\frac{5}{11}\cdot 5=2{,}27\ failures. \quad (21)$$

The results of similarity factor application for the new design device are considered prior data:

ISSN (Print): 1844-6116
ISSN (Online): 2501-8795 http://www.cmu-edu.eu/jmte

❖ For total time for testing

$$T_0 = (T_0)_X + (T_0)_Y + (T_0)_Z = 88182 hours. \quad (22)$$

❖ For number of failures

$$S_0 = (S_0)_X + (S_0)_Y + (S_0)_Z = 4 \, failures \quad (23)$$

To simplify the application, we consider that failures are gamma model. This model is more general: exponential model is a particular case of gamma, with the parameter $p = 1$ and "chi squared" model (x^2) is a particular case of gamma, with $p = \frac{v}{2}$, where *v* is the number of liberty degrees.

For gamma failure rate, with the parameters:

- $a_0 = T_0 = 88181 hours$,
- $p_0 = S_0 + 1 = 4 + 1 = 5 \Rightarrow v = 2 \cdot p_0 = 10$.

We calculate for $\alpha = 10^{-4}$ failure/hour and probability 95%:

$$\alpha(0{,}95) = \frac{1}{a_1} \cdot \frac{x^2_{10}(0{,}95)}{2}. \quad (24)$$

Is given in tables of „chi squared" values $x^2_{10}(0{,}95) = 18{,}31$

$$a_1 = \frac{1}{\alpha(0{,}95)} \cdot \frac{x^2_{10}(0{,}95)}{2} = \frac{1}{10^{-4}} \cdot \frac{18{,}31}{2}. \quad (25)$$

$$\Rightarrow a_1 = 91550 hours$$

$$a_1 = T_0 + T$$

$$\Rightarrow T = a_1 - T_0 = 91550 - 88182 = 3368 hours. \quad (26)$$

5. CONCLUSIONS

a) Bayes' formula can be used in reliability studies of complex systems, with seria, parallel and compound components, to determine some reliability indices, when a priori probability can be estimated.

b) On the Bayesian approximation, a reliability testing plan providing 10.000 hours of test, is reduced at 3.300 hours. This is possible for „priori" data use(known for the similar devices).

c) For continous distributions we have a version of Bayes' theorem. If Y is a parameter whose exact values is unknown and y_i the possible values of Y, we denote as $g(y_i)$ the probabilities of this values. Supposing that X is a random variable whose values can be observed and $f(x \mid y)$ is probability density of X conditioned by Y.

„Posterior" function of probability is:

$$g(y_i \mid x) = \frac{f(x \mid y_i) \cdot g(y_i)}{\sum_{i=1}^{n} f(x \mid y_i) \cdot g(y_j)}. \quad (25)$$

The above relation is Bayes' theorem for continuous distribution and is used in particular cases when - one of random variable has a continous distribution.

6. REFERENCES

[1] Baron T ș.a., *Calitate și fiabilitate*, vol I, II, Editura Tehnică, București, 1988;

[2] Baron T., *Metode Statistice pentru Analiza și Controlul Calității Producţiei*, Editura Didactică și Pedagogică, Bucureşti, 1979.

[3] Baron T., *Statistică teoretică și economică,* Editura Didactică și Pedagogică, Bucureşti, 1996.

[4] Mihoc Gh. ș.a., *Bazele Matematice ale Teoriei Fiabilității*, Editura Dacia, Cluj Napoca, 1976.

[5] Tarcolea C. ș.a., *Tehnici Actuale în Teoria Fiabilității*, Editura Ştiinţifică și Enciclopedică, Bucureşti, 1989.

[6] Tudor A ș.a., *Durabilitatea și fiabilitatea transmisiilor mecanice*, Editura Tehnică, Bucureşti, 1988;

[7] http://links.math.rpi.edu/ - Bayes'Formula,

[8]http://www.zeus.roma1.infinit.it/~agostini/cern. - Bayes' theorem

[9] http://amoldkling.com - Bayes'Theorem, by Amold Kling,

[10] http://engineering.now.edu.au //Courses/ - Bayes' Theorem,

[11] http://en.wikipedia.org. - Wikipedia – The Free Encyclopedia - Bayes' theorem

ISSN (Print): 1844-6116
ISSN (Online): 2501-8795 http://www.cmu-edu.eu/jmte

Journal of Marine technology and Environment Year 2017, Vol.1

SAFE MOORING USING IMPROVED SHORE TENSION SYSTEM - ECONOMY OF ENERGY AND COSTS

Vasilescu Mihail – Vlad

Constanta Maritime University, Faculty of Naval Electro-Mechanics, 104 Mircea cel Batran Street, 900663, Constanţa, Romania, e-mail vladmihail_2005@yahoo.com

Abstract: The main focus of this article is the development and use safe, easy mooring system, with reduction of costs and energy. The operation of mooring a ship at port is extremely important and dangerous. It is very important to use a safe system for mooring, not to put people life's in danger or even the ship. By using an improved system like Shore Tension we can reduce the costs of mooring for charters and owners, save people energy, save time.

Quality of the lines used for mooring is very important, because with a damage one or a mooring line of poor quality, can appear accidents or even casualties. Improved Shore Tension System can be in future, the new system of mooring: safe, clean and easy.

Key words: Shore Tension, Improved, Energy; Mooring lines, Quality.

1. INTRODUCTION

The operation of mooring a ship at port can vary between haphazard to well organized. Off all the different types of berths, tankers terminals tend to have the safest set-up, but there can still be problems.

In March 2015 a second officer in charge of the forward mooring station of the LNG carrier Zarga was send to hospital, by helicopter, with serious head injuries. The accident took place at South Hook LNG terminal at Milford Haven in United Kingdom.

In this case UK`s Marine Accident Investigation Branch –MAIB, said in a safety bulletin that the line failed at well below its certificated minimum breaking load and well before its anticipated lifetime prediction.

This is one unfortunately event from several in the last years, which cause injury or even casualties.

Even if tanker terminals try to offer the safest mooring set-ups, accident still happen.

All efficient terminals try to have a weather factor, berthing criterion, which will vary at each terminal.

2. QUALITY AND QUANTITY

Before each maneuvering, there must be done by the Master a risk assessment, which should include:

- The quality of the lines;
- The wind force and direction;
- The position of the berth, if it is open or protected;
- The tug availability;
- The current and draft;
- The under kill clearance;
- The availability of the deck ratings;
- The manning of the shore mooring gang;
- The tiredness of the deck crew.

Figure 1 Damage line

In a situation where the wind is blowing strongly off the berth, or is expected to be bad weather, a minimum of two lines should be put out together both forward and aft. If two lines fore and aft are to be put out at the same time this will require two crew to each line and two winch operators, making a total of 12 crew and two officers.

If we read IMO resolution no A.890(21) we will see that is stated that the Principle of Safe Manning, should

ISSN (Print): 1844-6116
ISSN (Online): 2501-8795 http://www.cmu-edu.eu/jmte

be such as to meet "peak workload situations" and conditions, but many owners ignore this.

Too often only one line can be put out at a time with all the heaving strain placed on this line.

There are also a lot of cases documented where the officer in charge had been assisting with the line handling instead of supervising.

Finally to compound the problem many owners are using untrained engine crew to supplement deck ratings. This is a recipe for an accident. If there are insufficient deck crew available for a correct and safe mooring operation, then it is essential that the pilot is advised of the situation because further tug assistance may be required.

The shore berth also has responsibility for its mooring gang. Frequently there are too few personnel to take both the fore and aft lines simultaneously; instead of trying to use the same personnel moving between the two ends of the ship causing delays in the securing of the lines, they should find solution like hiring more people or use a different mooring system.

In windy conditions, difficulty can be experienced in holding the position of the ship with only lines secured at one end. The offside anchor should be considered in difficult mooring conditions.

3. SNAP – BACK ZONES

Figure 2 Snap-Back Zone

Synthetic rope has a considerable degree of flexibility, which means that when it breaks there is a considerable snap-back.

While the intention of snap-back zones is good they lead to a false impression that there are safe areas on the mooring station.

In addition, when a mix ropes is used, predicting a snap-back area, is further complicated. Under these circumstances consideration should be given to the removal of such zone markings.

The strength and capability of mooring lines have improved over recent years.

While tanker berths are normally well-suited to the type of ships using the berth, an occasion, ship have to make do with existing bollards for the lines, which may govern how many lines can be put out and the length of lead.

All this factors are influencing the movement of the ship while alongside.

There is also a tendency to lead the head and stern lines out as far as possible, whereas the best place for these are slightly ahead and astern of the breast lines.

Leading them out too far increases their elasticity, especially with synthetic lines.

4. LOAD DISTRIBUTION

The standard rule for load distribution is that the mooring lines should be arranged as evenly as possible based around the mid-section of the ship. All the lines should be made on the same construction and material.

5. SHORE TENSION

To avoid all this problem, we can try a new innovating system called Shore Tension. This system does not require so many resources, so many crew members and is much more easy to use and safer.

Figure 3 Shore Tension system

Shore Tension is a system for safer mooring of sea-going ships that is as convenient as it is revolutionary. Shore Tension, a cylindrical device, can be flexibly used in any port at terminals where containers, general cargo and/or bulk are handled. With Shore Tension, ships of any size can be firmly anchored to the quay. Shore Tension significantly reduces movement caused by strong winds, currents, swell or passing ships. With the traditional mooring method using mooring lines on bollards, this movement is always present. In extreme conditions, the tremendous pressure this exerts on the ship can cause the mooring lines to snap with potentially serious consequences. As ports have experienced in the past, this is definitely a realistic risk. Shore Tension mitigates this risk significantly.

Ships are moored to the quay much sturdier and therefore much safer. In addition, the flexibly deployable Shore Tension aims to allow terminals to operate more efficiently. Because ships are moored alongside the quay with greater stability,

ISSN (Print): 1844-6116
ISSN (Online): 2501-8795 http://www.cmu-edu.eu/jmte

Shore Tension promotes unhindered quay crane operations and significantly reduces therisk of damage during unloading and loading. Furthermore, operations can continue formuch longer in bad weather. Visiting ships can be handled more quickly.

Energy saving, lower costs and co2 reduction

Making use of Shore Tension also results in energy savings, lower costs and a substantial reduction in CO2 emissions. Ships no longer need to use tension winches for exerting the constant tension on their mooring lines. These tension winches consume megawatts of power and are not nearly as effective. Shore Tension can bear the tension of the largest cargo and passenger vessels available and requiring hardly any external energy.

5.1 How it works

Figure 4 Shore Tension System securing the ships

The cylindrically shaped Shore Tension exerts the same, constant tension to the ship's mooring lines which are fastened to the bollards on the quay. This requires no electricity except for an external hydraulic system which only needs to be used once to get Shore Tension at the correct setting. After that, the cylinder of Shore Tension hydraulically moves along with the forces which the mooring line is exposed to. This process continues perpetually without the need for additional energy. Shore Tension aims to keep all mooring lines at the same, constant tension, also in case of swell, waves, wind and passing vessels - particularly crucial for the safe and stable mooring of vessels. It is the differences in tension between the different mooring lines which cause a ship to move and potentially cause the mooring lines to snap.

Because of the exceptional demands of Shore Tension and requirements for safe mooring and efficient operations, Dyneema mooring lines are used. These specially designed mooring lines are known for their strength, lightweight and durability, and provide extraordinary performance even in the most extreme conditions.

Because of the exceptional demands of Shore Tension and requirements for safe mooring and efficient operations, Dyneema mooring lines are used. These specially designed mooring lines are known for their strength, lightweight and durability, and provide extraordinary performance even in the most extreme conditions.

5.2 Wireless control unit

Every Shore Tension has its own wireless controller that works on solar energy. This enables the captain of the ship, the terminal operator and other parties to remotely monitor the tension on the mooring lines in real-time. Through SMS, all parties involved will be automatically notified if the safe working load (SWL) of a mooring line approaches the pre-established limits and if additional measures are required.

For almost any ship in virtually any situation depending on the ship size, weather conditions and local conditions, two to four Shore Tension devices are necessary for the optimal operation of Shore Tension. Shore Tension has been developed for all loads and is adjustable, ensuring compatibility with all other mooring devices such as bollards, fairleads, etc. Furthermore, Shore Tension is able to withstand extreme environmental conditions. Shore Tension has been certified by Lloyds Register in London with a safe working load (SWL) up to150 metric tons. Shore Tension can conveniently be used on a stand-alone basis horizontally on quay walls and aboard ships.

4.3 Dynamic mooring system

During heavy swell conditions, the fast inward and outward movements of a Shore Tension system causes high temperatures - especially - in the inner core of the mooring lines.

With this innovative new snatch block we have created a friction free operation hence all systems are sold with this block.

4.4 Improving shore tension system

Figure 5 Making fast the line on the bollard- dangerous movement

ISSN (Print): 1844-6116
ISSN (Online): 2501-8795 http://www.cmu-edu.eu/jmte

Journal of Marine technology and Environment Year 2017, Vol.1

t

Figure 6 Handcuffs for making fast the line on bollard, excluding the human factor

Shore Tension system is very effective, but should be improved. In the moment when the line is made fast on the bollard, I suggest to use a pair of handcuffs, with the role of keeping the line, excluding using the human factor, which is difficult and very dangerous.

5. CONCLUSIONS

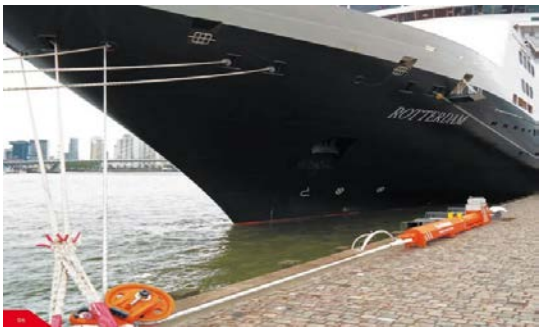

Figure 7 Shore Tension System

Specification of the Shore Tension system:

- Safe working load - Up to 150 metric tons (1500 kN) in fully extended condition
- Vessel motion reduction - Up to 90% compared to conventional mooring systems
- Reduces the problem of swell
- Application - For all types of vessels
- Wireless control - Sensors register the loads in the ropesData is available for the ship's master, port and terminal operatorsData will be logged for review of berthA warning system monitors when limits are exceededGPS data provide an overview of where warnings are issuedin ports across the globe
- Mooring lines - Special mooring lines made with Dyneema
- Certified by - Pressure Equipment (PED)
- Lloyd's register for - Lifting appliance (Heavy lifting)
- - Use in explosive atmospheres (ATEX).

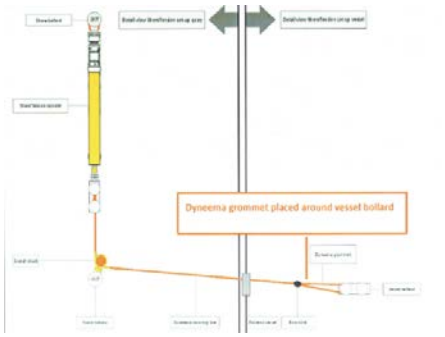

Figure 8 Bosslink shackle outside fairlead

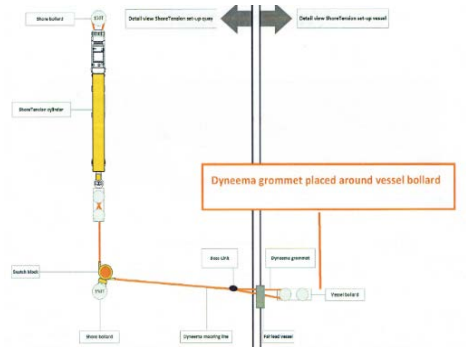

Figure 9 Bosslink shackle inside fairlead

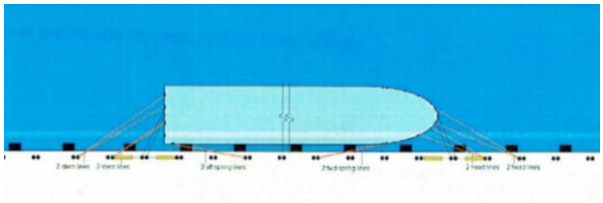

Figure 10 Shore Tension mooring arrangement – 4 St units breast

6. REFERENCES

[1] CHROLENKO, MICHAEL OLIVIER, *Dynamic Analysis and Design of Mooring Lines*, Marine Technology, June 2013.
[2] *The Hazards of Snap-back Initial learnings from a serious incident of mooring line failure*, OCIMF, September 2015
[3] http://www.safety4sea.com
[4] https://shoretension.com/
[5] https://www.ukpandi.com

PUBLISHED SINCE 2008
ISSN:1844-6116
ON LINE SINCE: 2008
PUBLISHED BY: Editura Nautica/ Constanta Maritime University